Chem Soc Rev

REVIEW ARTICLE

View Article Online
View Journal | View Issue

Cite this: *Chem. Soc. Rev.*, 2016, **45**, 5358

Polyferrocenylsilanes: synthesis, properties, and applications

Rebekah L. N. Hailes,† Alex M. Oliver,† Jessica Gwyther,‡ George R. Whittell‡ and Ian Manners*

This in-depth review covers progress in the area of polyferrocenylsilanes (PFS), a well-established, readily accessible class of main chain organosilicon metallopolymer consisting of alternating ferrocene and organosilane units. Soluble, high molar mass samples of these materials were first prepared in the early 1990s by ring-opening polymerisation (ROP) of silicon-bridged [1]ferrocenophanes (sila[1]ferrocenophanes). Thermal, transition metal-catalysed, and also two different living anionic ROP methodologies have been developed: the latter permit access to controlled polymer architectures, such as monodisperse PFS homopolymers and block copolymers. Depending on the substituents, PFS homopolymers can be amorphous or crystalline, and soluble in organic solvents or aqueous media. PFS materials have attracted widespread attention as high refractive index materials, electroactuated redox-active gels, fibres, films, and nanoporous membranes, as precursors to nanostructured magnetic ceramics, and as etch resists to plasmas and other radiation. PFS block copolymers form phase-separated iron-rich, redox-active and preceramic nanodomains in the solid state with applications in nanolithography, nanotemplating, and nanocatalysis. In selective solvents functional micelles with core–shell structures are formed. Block copolymers with a crystallisable PFS core-forming block were the first to be found to undergo "living crystallisation-driven self-assembly" in solution, a controlled method of assembling block copolymers into 1D or 2D structures that resembles a living covalent polymerisation, but on a longer length scale of 10 nm–10 μm.

Received 26th February 2016

DOI: 10.1039/c6cs00155f

www.rsc.org/chemsocrev

1. Introduction

Metal centres play a crucial role in the functions of biological polymers and many solid state compounds, such as state of the art magnetic materials used in data storage, electrical conductors and superconductors, electrochromics, and catalysts. Metal-containing polymers (metallopolymers), in which the facile processing typical of organic polymers is combined with the worthwhile properties of the metal centre, have therefore been long regarded as a desirable target. However, synthetic access to soluble, well-characterised metallopolymers with a molar mass above the critical entanglement molecular weight has proven to be a significant challenge. Although pioneering studies in the metallopolymer field were initiated shortly after the 2nd World War, examples of well-characterised truly macromolecular materials (with molar masses above 10 000 g mol^{-1}) that exhibit chain entanglement, and thereby useful mechanical properties, were not reported until the 1970s. However, only since the mid 1990s has much more rapid progress has been made and metallopolymers now play an increasingly important role in terms of complementing the vast and impressive array of functional organic polymers that are currently available.[1]

Polyferrocenylsilanes (PFSs) represent one of the most well-developed classes of metallopolymer and possess a main chain consisting of alternating ferrocene and organosilane units. Poorly characterised examples were first described in patents in the 1960s as discoloured, very low molecular weight materials formed in step-growth polycondensation reactions.[2,3] The use of ring-opening polymerisation (ROP) of strained silicon-bridged [1]ferrocenophane precursors was first described in 1992 and represents a chain-growth route.[4] The ROP method affords amber, high molar mass, soluble PFS materials that have been well-characterised by a wide range of techniques (Scheme 1). The initial ROP approach involved thermal treatment of the monomer (*ca.* 130–150 °C) but the synthetic toolbox has rapidly

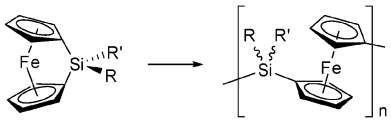

Scheme 1 Synthesis of PFSs by the ROP of silicon-bridged [1]ferrocenophanes.

School of Chemistry, University of Bristol, Bristol, BS8 1TS, UK.
E-mail: ian.manners@bristol.ac.uk
† These authors contributed equally.
‡ These authors contributed equally to this work.

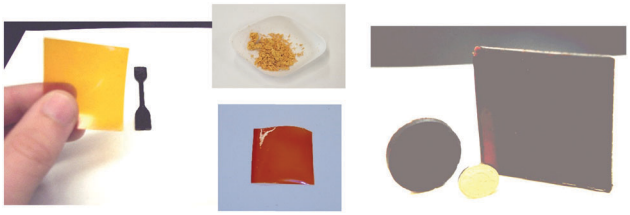

Fig. 1 PFSs isolated as a powder and after fabrication into films and shapes by solution- or melt-processing. Adapted with permission from ref. 8. Copyright 2004 John Wiley & Sons Inc.

expanded with the development of alternative, more convenient ambient temperature routes and also "living" polymerisation approaches. This has permitted molar mass control, access to materials with narrow molecular weight distributions and desired end-group functionalisation, and also the formation of PFS block copolymers and other controlled architectures. PFS materials are readily processed from solution or the melt (see Fig. 1) and studies of their properties and applications by numerous workers over the past 25 years have created a field that continues to flourish.[5,6]

Developments concerning PFS homopolymers and/or block copolymers and their properties and applications have been previously reviewed.[4–8] This article, while aiming to be comprehensive, has a particular focus on more recent developments over the past decade although key work from earlier is also discussed.

2. Synthetic routes to polyferrocenylsilane homopolymers

2.1. Monomer synthesis

Silicon-bridged [1]ferrocenophanes were first prepared in the mid 1970s by Osborne *et al.*,[9] and are now readily available on a significant scale. In solution, each of the cyclopentadienyl (Cp) rings of ferrocene can be lithiated by a strong Li-containing base such as *n*-butyllithium, catalysed by *N*,*N*,*N*′,*N*′-tetramethylethylenediamine (TMEDA).[10] The orange crystalline solid isolated after work up has been shown to have the bulk formula of $(\eta^5\text{-}C_5H_4Li)_2Fe{\cdot}TMEDA$, although single crystal X-ray analysis has shown that other compositions are possible.[11,12] Reactions between the dilithioferrocene–TMEDA complex and dichloroorganosilanes give a wide range of sila[1]ferrocenophanes with symmetrically and unsymmetrically substituted silicon atoms bearing alkyl or aryl groups (Scheme 2(A)).[13–15] Alternatively, chlorine

Rebekah L. N. Hailes (centre), Alex M. Oliver (middle right), Jessica Gwyther (middle left), George R. Whittell (far left) and Ian Manners (far right)

Rebekah L. N. Hailes (centre) studied at the University of Bristol, graduating in 2015 with an MSci (First Class) in Chemistry. She spent her final year working with Dr Chris Russell on coinage metal acetylides. Currently, she is a PhD student in Prof. Ian Manners' group focussing on the synthesis, structure, and reactivity of [n]metallocenophanes and transition metal pincer complexes.

Alex M. Oliver (middle right) grew up in Leamington Spa, a small town in the heart of England. He graduated in 2012 with an MSci (Honours) in Chemistry from the University of Bristol, spending his final year working under the supervision of Prof. Ian Manners. Now continuing his work in the Manners group, Alex is working towards his PhD on the subject of synthesis and self-assembly of functional triblock terpolymers by crystallization-driven processes.

Jessica Gwyther (middle left) studied at the University of Bristol, graduating with an MSci in Chemistry in 2007. After her degree, she obtained a PhD in 2011 under the supervision of Prof. Ian Manners focusing on the synthesis, characterisation and thin film self-assembly of metal-containing polymers. She is now a Research Associate in the same group working on crystallisation-driven self-assembly of block copolymers.

George R. Whittell (far left) obtained his BSc degree in Chemistry from the University of Bristol in 1996 and PhD from the same institution in 2000. The latter focused on the synthesis, structure and reactivity of transition metal boryl complexes in the group of Prof. Nick Norman. He was then awarded a Royal Society postdoctoral fellowship to work with Prof. Warren Roper on the synthesis of osmium stannyl and distannyl complexes, before returning to work on transition metal boron chemistry in the group of Prof. Holger Braunschweig. In 2005 he joined the group of Prof. Ian Manners as Senior Research Associate where he works on projects ranging from catalytic dehydrogenation to block copolymer self-assembly.

Ian Manners (far right) received his PhD from the University of Bristol, conducted postdoctoral work in Germany and then in the USA, and joined the University of Toronto, Canada as an Assistant Professor in 1990. He was made Full Professor in 1995 and a Canada Research Chair in 2001. In 2006 he returned to Bristol to take up a Chair in Inorganic, Macromolecular and Materials Chemistry and an EU Marie Curie Chair. His awards include a Sloan Fellowship (from the US), the Steacie Prize (from Canada), the RSC Award in Main Group Chemistry, the RSC Peter Day Award for Soft Matter Materials Chemistry, and a Humboldt Research Award from Germany. He is an elected member of both the Canadian and the British National Academies of Science. His work is documented in >600 papers and 4 books and has been presented in ca. 500 invited lectures worldwide.

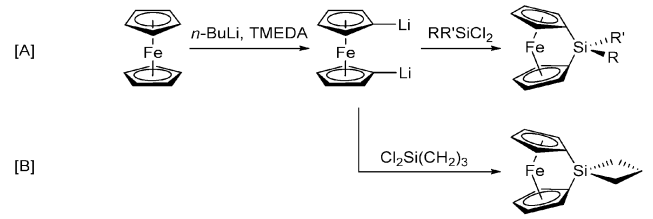

Scheme 2 Synthesis of sila[1]ferrocenophanes from ferrocene.

has been introduced as a substituent through the reaction of $Fe(\eta^5\text{-}C_5H_4Li)_2\cdot$TMEDA with $SiCl_4$ or $RSiCl_3$, which, *via* subsequent nucleophilic substitution reactions at the $SiCl_2$- or SiClR-bridge, provides a facile route to [1]ferrocenophanes with alkoxy, aryloxy, and amino substituents at silicon.[16] Hypercoordinate silicon-bridged [1]ferrocenophanes can also be synthesised from chlorosila[1]ferrocenophanes $Fe(\eta^5\text{-}C_5H_4)_2SiRR'$ (R = R′ = Cl or R = Me, R′ = Cl) and $Li[2\text{-}C_6H_4CH_2NMe_2]$ or $Fe(\eta^5\text{-}C_5H_4)_2SiCl(CH_2Cl)$ and *N*-methyl-*N*-(trimethylsilyl)acetamide.[17,18] These pentacoordinate species show a pronounced Si–N or Si–O interaction with a pseudo trigonal bipyramidal geometry at the bridging silicon atom in the solid state.[18,19] In addition, spirocyclic sila[1]ferrocenophanes can be prepared in a similar manner to that already described: for example the reaction of $Fe(\eta^5\text{-}C_5H_4Li)_2\cdot$TMEDA with $Cl_2Si(CH_2)_3$ gives silacyclobutyl[1]ferrocenophane (Scheme 2(B)).[20] These species are of importance in the preparation of PFS materials as they function as crosslinkers during polymerisation reactions.

The introduction of an *ansa*-bridge can result in a loss of the coplanar cyclopentadienyl ring arrangement of ferrocene. The angle, α, measured between the two tilted cyclopentadienyl rings relative to when they are parallel ($\alpha = 0^\circ$), can be taken as an indication of the strain present. Typical values of α for sila[1]ferrocenophanes lie between 16–21°.[13,21–23] For example, the cyclopentadienyl rings in dimethylsila[1]ferrocenophane are tilted by 20.8(5)° with respect to one another, and the corresponding strain energy for the complex was measured to be 80 kJ mol^{-1}.[22] Increasing methylation of the Cp rings leads to a decreased ring tilt, increased angles between the Cp ring planes and the exocyclic Cp–Si bonds (β), and decreased Fe–Si distances: the permethylated analogue of dimethylsila[1]ferrocenophane has an α angle of 16.1(3)°,[23] due to the greater energetic penalty in deforming the octamethylferrocenediyl unit, the potential energy of the ferrocenediyl unit is increased compared to the unsubstituted case.[24] Other angles that are used to describe the structure of [1]metallocenophanes include: δ, the $Cp_{centroid}$–M–$Cp_{centroid}'$ angle; and θ, the C_{ipso}–E–C_{ipso}' angle (Fig. 2).

In addition to loss of Cp ligand coplanarity, another consequence of the *ansa* bridge in [1]ferrocenophanes is that the iron centre lies in closer proximity to the Cp *ipso*-carbons than to the two carbons that lie on the opposite side of the ring. Thus, the C–C bond opposite the *ipso*-carbons is shortened relative to ferrocene. Furthermore, the angle θ is far smaller than is expected compared to that of ideal hybridisation at the bridging atom, E.[13,24]

Silicon-bridged [1]ferrocenophanes are isolated as red, crystalline solids or liquids. As a result of their ring strain, they can readily undergo ring-opening polymerisation (ROP) reactions to give polyferrocenylsilanes (PFSs). It is noteworthy that even sila[1]ferrocenophanes with highly sterically-demanding substituents at silicon such as $Si(SiMe_3)_3$ still undergo ROP.[15] Reported synthetic methods to prepare high molecular weight PFSs involve: thermal, transition metal-catalysed, γ-irradiation-induced, cationic, and living anionic and photocontrolled living anionic ROP, and these methods are now discussed.

2.2. ROP routes to PFS homopolymers

2.2.1. Thermal ring-opening polymerisation. A thermal method of synthesising high-molecular weight PFSs from silicon-bridged [1]ferrocenophanes was first reported in 1992,[22] with the release of ring-strain (60–80 kJ mol^{-1}) driving the reaction. Due to its relatively high functional group tolerance, a wide range of strained ferrocenophanes have been used to access alkyl, alkoxy, aryl, aryloxy, amino, and chloro functionalised PFSs (Scheme 3) *via* this route.[4,7,15,25,26] Interestingly, a cyclic dimer in addition to high molecular weight polymer was isolated from dichlorosila[1]ferrocenophane when attempting thermal ROP.[27,28] The thermal ROP reactions can be performed in either high boiling point solvents or the melt, and although high molecular weight polymers are formed, there is no control over the molecular weight and the molecular weight distributions are broad (PDI > 1.5).

Thermal ROP of silicon-bridged [1]ferrocenophanes has been shown to proceed *via* cleavage of the Cp–Si bond; in the case of Cp rings with different degrees of methylation, non-selective cleavage of the Si–Cp bonds occurs.[29] Increasing the degree of methylation of the Cp rings resulted in increasing onset temperatures for the polymerisation but did not appreciably affect the enthalpy of polymerisation, ΔH_p, as measured

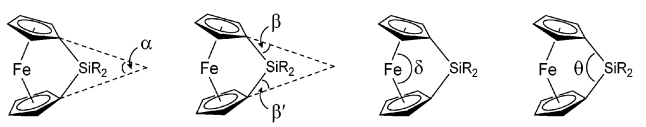

Fig. 2 Geometric parameters used to describe the structure of [1]ferrocenophanes.

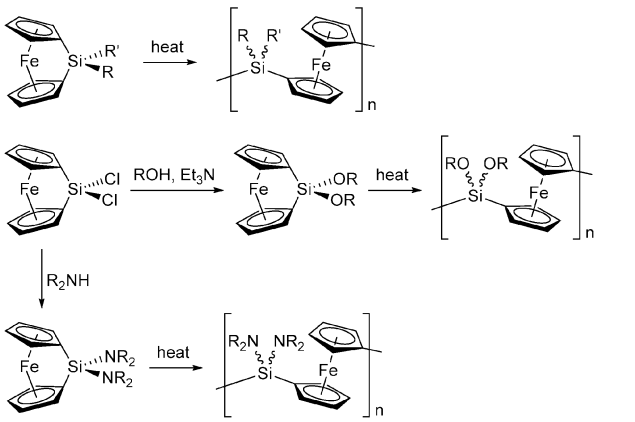

Scheme 3 Thermal ring-opening polymerisation of sila[1]ferrocenophanes to give PFSs.

by DSC.[30] Although attempts have been made to deduce the mechanism of thermal polymerisation, neither this nor the nature of the propagating species is known with certainty. A carbanionic mechanism appears unlikely however, because the ROP of monomers bearing Si–Cl substituents results in high molecular weight polymers.[28] Radicals also do not seem to be involved, and the most likely mechanism appears to be a nucleophilically-assisted process.[31,32]

2.2.2. Catalytic ROP. In 1995 it was discovered that a variety of late transition metal complexes catalysed the ROP of sila[1]ferrocenophanes, to yield high molecular weight PFSs both in solution and at room temperature.[33,34] Complexes used as precatalysts feature platinum (Pt^0, Pt^{II}),[33–36] for example Karstedt's catalyst (platinum divinyltetramethyldisiloxane complex),[36] palladium (Pd^0, Pd^{II}),[33,34] and rhodium (Rh^I).[37] Catalytic amounts of $[Rh(1,5\text{-cod})_2]A$ (cod = 1,5-cyclooctadiene, A = $[OTf]^-$, $[PF_6]^-$) initiated the ROP of sila[1]ferrocenophanes with quantitative conversion within 2 minutes.[37] In the case of Pt, it has been reported that heterogeneous metal colloids form as the active catalysts, and postulated that oxidative-addition and reductive-elimination reactions at the metal surface resulted in formation of the polymer.[38] For silicon-bridged ferrocenophanes in which one Cp ring is methylated, Pt^{II}-catalysed ROP proceeds solely by selective cleavage of the Si–Cp^H ($Cp^H = C_5H_4$) bond to yield a regioregular, crystalline PFS, unlike thermal ROP which affords a regioirregular amorphous material.[39]

Transition metal-catalysed ROP is advantageous in that it does not require high monomer and solvent purity unlike anionic ROP (Section 2.2.4), or the high temperatures used in thermal ROP.[40] The method therefore allows the use of many monomers that would otherwise decompose under more aggressive reaction conditions. However, in contrast to PFS prepared by anionic ROP, polydispersities typically remain in excess of 1.4. When transition metal-catalysed ROP of sila[1]ferrocenophanes is carried out in the presence of a terminating agent containing an Si–H bond, the molecular weight of PFS can be controlled by variation of the initial ratio of the monomer to the silane. The mechanism is believed to involve competition between the Si–H and strained Si–C bonds for oxidative-addition at the metal centre.[38,41] Use of end-capping materials with Si–H groups has allowed the preparation of regioregular, comb-shaped graft copolymers, star-shaped polymers, and block copolymer architectures.[39] Chlorosilanes such as ClMePhSiH are more effective terminating agents than Et_3SiH due to steric and electronic considerations, and also introduce a Si–Cl end functionality to telechelic polyferrocenylsilanes. These can then be used in a variety of post-polymerisation reactions to yield block copolymers.[41] Alternatively, if PFS is synthesised from a monomer containing chlorine at silicon, a wide range of substitution reactions on the polymer backbone can be performed (Scheme 4).[28,36,42] However, broad molecular weight distributions result with all terminating agents.

2.2.3. ROP induced by γ-irradiation and cationic initiators. PFDMS (PFDMS: poly(ferrocenyldimethylsilane)) can be synthesised from the crystalline monomer in the solid state, with the use of γ-irradiation at elevated temperature (60 °C). It was reported that as the dose of initiating radiation rose, the weight average molar mass increased, indicating a greater degree of polymerisation.[43] Higher radiation rates are expected to yield more reaction centres, which typically, and contrary to the observations, would be expected to afford lower molar mass polymers. Solid state polymerisation of crystalline $[Fe(\eta^5\text{-}C_5H_4)_2SiMePh]$ yielded stereoregular PFMPS (PFMPS: poly(ferrocenylmethylphenylsilane)), in a topotactic process based on NMR analysis.[44] Thus, the tacticity of the polymer was inherited from the arrangement of substituents in the crystal of the monomer. However, as sources of γ-radiation are inconvenient to access, this is not a commonly used method.

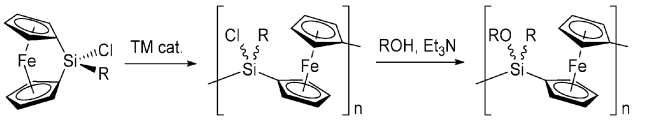

Scheme 4 Transition metal-catalysed ROP of a strained sila[1]ferrocenophane, and subsequent main chain functionalisation.

Cationic ROP of a hypercoordinate [1]silaferrocenophane has been reported in the presence of a silyl cation as an initiator.[18] The resulting PFS appeared to retain the pentacoordinate Si centres but the molar mass was low (M_w = *ca.* 9000 Da).

2.2.4. Living anionic ROP routes to homopolymers

2.2.4.1. Living anionic ROP involving cleavage of the Cp–Si bond. Living anionic ROP of sila[1]ferrocenophanes was developed in the mid 1990s,[45,46] and allows access to PFSs with molecular weight control and predetermined chain end function, provided that low levels of impurity are present.[46,47] For this reason, high purity monomer is required and this is generally achieved by multiple recrystallisation and sublimation steps to remove ring-opened or cyclic and linear oligomeric contaminants. Induced by nucleophilic attack of an anionic initiator at the bridging silicon atom, ROP proceeds *via* Si–Cp bond cleavage generating a basic iron-coordinated cyclopentadienyl anion. Fast initiation is followed by rapid chain propagation, which occurs with minimal chain transfer or termination, and therefore yields polymers of controlled molecular weight (Fig. 3) and with narrow molecular weight distributions (PDI < 1.2 and often < 1.05). Thus, this process is an example of a living polymerisation which, when discovered, represented the first of its kind to afford polymers with transition metal atoms in the main chain. Since the initial report, the living anionic ROP of sila[1]ferrocenophanes has been extended to other monomers with both symmetrical (R = R′ = Me)[46] and unsymmetrical (R, R′ = Me, Et; Me, Ph; Me, iPr)[48–51] substitution at silicon (Scheme 5). Studies on silicon-bridged [1]ferrocenophanes $Fe(\eta^5\text{-}C_5H_4)_2SiRR'$ with bulky substituents have shown that if R = H, R′ = $N(SiMe_3)_2$ the monomer does not undergo anionic ROP, despite forming polymer under thermal ROP conditions. It was proposed that this was due to a lack of chain propagation at the Cp-based sp^2 carbanion, presumably due to steric protection of the silicon centre by the bulky $N(SiMe_3)_2$ substituent.[15] Generally the rate of living anionic ROP decreases as the size of the substituents on silicon increases.[51]

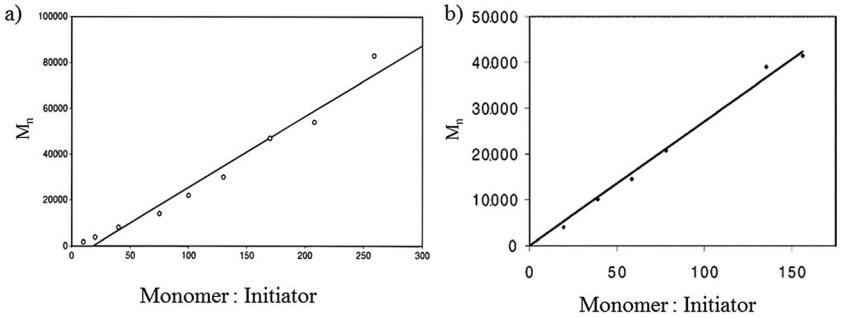

Fig. 3 A plot of the mole ratio of monomer: initiator *versus* M_n for (a) the *n*-BuLi initiated synthesis of PFDMS (R = *n*-Bu, E = H, Scheme 5); (b) the *n*-BuLi initiated synthesis of PFEMS (PFEMS: poly(ferrocenylethylmethylsilane)). Reproduced with permission from ref. 46 (copyright 1996 American Chemical Society) and ref. 49 (copyright 2005 American Chemical Society).

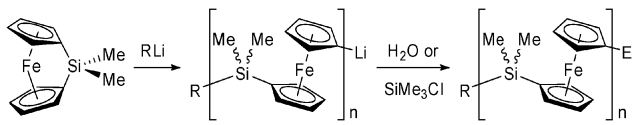

Scheme 5 Living anionic ring opening polymerisation of sila[1]ferrocenophanes. R = Fc, Ph, or *n*-Bu; E = H or $SiMe_3$.

Subsequent end functionalisation can occur at the lithiated site on the polymer using a variety of reagents to modify the polymer properties or yield block and graft copolymers.[52,53] In addition, sequential polymerisation of different monomers can occur to produce a range of block copolymers.[46,54] If in the case of post-polymerisation, 4-[(trimethylsilyl)ethynyl]-benzaldehyde is used to trap the living chain, a terminal alkyne is generated. Diblock copolymers can then be constructed *via* a Cu(I)-catalysed alkyne/azide cycloaddition with azide end-capped polymers.[55] Anionic initiators used comprise alkyl, aryl, and ferrocenyl lithiates, and can include other polymers prepared by anionic polymerisation.[46] *tert*-Butyldimethylsilyloxy-1-propyllithium has also been used as an initiator for the polymerisation of dimethylsila[1]ferrocenophane, as this provides a convenient route to hydroxyl-terminated PFSs.[56] Unfortunately, monomers with base sensitive side groups are incompatible with this method of polymerisation.

2.2.4.2. Living "Photocontrolled" anionic ROP involving Cp–Fe bond cleavage. An alternative living anionic polymerisation method was reported in the mid 2000s, involving the photoactivation of sila[1]ferrocenophanes.[57,58] In this case, ROP proceeds with irradiation of the monomer by the Pyrex-filtered emission from a mercury lamp ($\lambda > 310$ nm) in a donor solvent, such as THF. The subsequent, presumably solvated, ring-slipped structure reacts with the anionic initiator, sodium cyclopentadienide ($Na[C_5H_5]$).[57] Cleavage of the Fe–η^1-cyclopentadienyl bond in the photoexcited monomer affords a ring-opened species possessing a free silyl-substituted Cp anion that can propagate *via* attack on another ring-slipped monomer. The living polymer chain can then be capped with, for example, methanol to give PFSs (Scheme 6).[57,58] This method contrasts with the previously reported living anionic ROP, which proceeds in the absence of UV irradiation and uses organolithium initiators to induce Si–Cp(*ipso*) bond cleavage.[57] Nevertheless, both anionic ROPs generate polymers of controlled molecular weight and with narrow molecular weight distributions. Crucially for "photocontrolled" anionic ROP, the delocalised free cyclopentadienyl initiating and propagating sites are far less basic than the charge localised iron-coordinated alternative that occurs in the classical anionic ROP.[58–64] This reaction is therefore more tolerant of sensitive functional monomers; for example, it has allowed the preparation of PFSs with pendant alkynyl,[61] amino,[62] and fluoroalkyl groups.[60] Also, PFS with a pendant ruthenocenyl group was prepared *via* "photocontrolled" anionic ROP to give monodisperse, soluble polymers, where the use of thermal ROP had failed.[63] As this polymerisation can be controlled by switching the light source on and off, sequential addition of different monomers is facile. Diblock copolymers have also been produced by the use of PS (PS: polystyrene) homopolymers end-capped with a cyclopentadienyl group, and used as macroinitiators for the PROP of sila[1]ferrocenophanes.[64] tBu$_3$terpy (4,4′,4″-tri-*tert*-butyl-2,2′:6′,2″-terpyridine) was evaluated as another initiator, but displayed far less molecular weight control and gave lower polymer yields than $Na[C_5H_5]$.[59] Remarkably, photolysis of a solution containing dimethylsila[1]ferrocenophane, $Na[C_5H_5]$, and tBu$_3$terpy resulted in dissociation of both ferrocenophane Cp rings.

Irradiation of $[Fe(\eta^5\text{-}C_5H_4)_2SiMe_2]$ in the presence of 4,4′-dimethyl-2,2′-bipyridine, a substitutionally more labile ligand

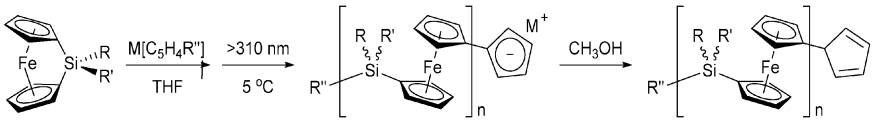

Scheme 6 Photocontrolled living anionic ring-opening polymerisation of sila[1]ferrocenophanes.

than Cp, initiated ROP to give a distribution of cyclic PFSs and linear oligomers.[65] Temperature and concentration were reported to influence the molecular weight distribution and the ratio of cyclic to linear products, thus enabling the formation of cyclic PFSs with molecular weights greater than 100 kDa.[66]

Although the mechanism of photocontrolled anionic ROP has not been completely elucidated, the presence of a sila-bridge in a [1]ferrocenophane causes the cyclopentadienyl rings to tilt, and, presumably as a consequence, weakens the Fe–Cp bond. Metal–ligand charge transfer occurs due to photoirradiation, and is suggested to further weaken this bond and to increase the electrophilicity at iron and, probably, to induce Cp ring-slippage in the presence of a donor solvent (such as THF).[58] These effects all combine to favour polymerisation when an anionic initiator is present. Kinetic studies of the photopolymerisation at various temperatures demonstrated that the reaction was a living process (PDI < 1.1).[58] While the photoactivation of the monomer is independent of temperature, deactivation of the photoexcited system, or the subsequently formed ring-slipped product (M*) to the ground state monomer (M) is favoured at higher temperatures (Scheme 7). As a consequence, at elevated temperatures the rates of initiation and propagation are decreased, and ROP is slower. Moreover, the polymers obtained have a broader molecular weight distribution (PDI = 1.2–1.3).[58]

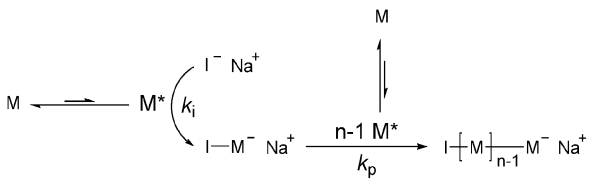

Scheme 7 Upon irradiation some monomers (M) are promoted to a photoexcited state (M*). The photoexcited monomer M* reacts with the initiator (I) with rate constant k_i to form a ring-opened monomer, which undergoes chain propagation (with rate constant k_p) in the presence of more photoexcited monomer.[58] The photoexcited monomer M* is presumed to possess a ring-slipped structure.[67]

2.2.5. Post-polymerisation functionalisation. Modification of the properties of PFS materials is most commonly achieved by varying the substituents on the silicon atom of the organosilyl spacer. This can be performed either on the monomer, as described in Scheme 3, or with post-polymerisation reactions on the PFS backbone (Scheme 8). Certain reaction conditions, such as the presence of low pH, should be avoided generally, as PFS can be sensitive towards chain cleavage by acid.

PFSs with chlorine substituents at silicon undergo nucleophilic substitution reactions to give a variety of products, including hydrophilic PFSs with organic substituents that promote water solubility.[28,36,68] The first of these was reported in 2000, through the treatment of poly(ferrocenylchloromethylsilane) with oligo(ethylene glycol) monomethylether or $Me_2NCH_2CH_2OH$.[36] Cationic polyelectrolytes were subsequently prepared *via* quaternisation of the dimethylamino groups in the latter. Further water-soluble polyelectrolytes were synthesised from PFS (R = Me, R′ = C≡CCN$(Me_2SiCH_2)_2$), which itself was readily obtained *via* a substitution reaction from poly(ferrocenylchloromethylsilane).[69] These polyelectrolytes remained stable in water even after a period of several months. The PFS, $[Fe(\eta^5\text{-}C_5H_4)_2SiMe(N(CH_2)_3SiMe_2(CH_2)_2SiMe_2)]_n$ was prepared by the ROP of a ferrocenophane precursor with a cyclic silylamino substituent *via* an unexpected rearrangement/ring expansion process.[69] Alternatively, the water-soluble cation, poly(ferrocenyl(3-ammoniumpropyl)methylsilane) was produced by the ROP of $[Fe(\eta^5\text{-}C_5H_4)_2SiCH_3(CH_2)_3Cl]$ and subsequent amination of the chloropropyl moieties using potassium 1,1,3,3-tetramethylsilazide followed by protonation (Scheme 8).[70]

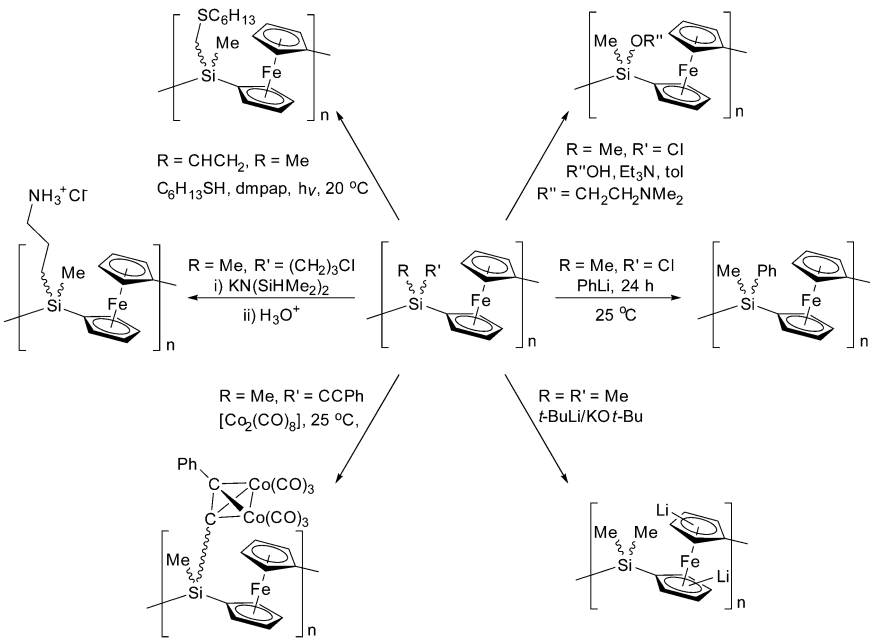

Scheme 8 Examples of post-polymerisation functionalisation methods for polyferrocenylsilanes.

Water-soluble PFS polyanions and polycations have also been synthesised by reaction of poly(ferrocenyl(3-halopropyl)methylsilanes) (halo = Cl, Br, or I) with a variety of nucleophiles, including alkali metal amides, neutral amines, and ester enolate anions.[70–72]

With a hydrogen or olefinic substituent at silicon, hydrosilation chemistry is possible. Reaction of poly(ferrocenylmethylvinylsilane) with Et_3SiH allowed for facile functionalisation, giving an example of a hexane-soluble PFS material.[73] Hydrosilylation reactions have also proved useful in attaching mesogenic groups to PFSs containing Si–H functionalities, which allow access to thermotropic side chain liquid crystalline (LC) materials.[74]

Thiol–ene click chemistry provides a versatile approach to PFS functionalisation. The reaction of a range of thiols with vinyl-containing PFS scaffolds gave hydrothiolated PFSs, which displayed interesting solubility and functionality.[75] As a diverse range of thiols are available, and the thiol–ene reaction is tolerant to most functional groups, this post-polymerisation route is useful for the preparation of PFS materials with a range of properties from the same homopolymer precursor.

Highly metallised PFSs: $[Fe(\eta^5\text{-}C_5H_4)_2Si(Me)(Co_2(CO)_6C_2Ph)]_n$ (Co-PFS), $[Fe(\eta^5\text{-}C_5H_4)_2Si(Me)(Mo_2Cp_2(CO)_4C_2Ph)]_n$ (Mo-PFS), and $[Fe(\eta^5\text{-}C_5H_4)_2Si(Me)(Ni_2Cp_2C_2Ph)]_n$ (Ni-PFS), were synthesised by the clusterisation of carbon–carbon triple bonds in an acetylide substituted PFS.[76,77] By varying the chain length of the parent acetylide-substituted PFS or by changing the extent of clusterisation, the molecular weight and metal content of the PFS, respectively, could be controlled.[77] The materials were all air- and moisture-stable and they have been shown to serve as resists for electron-beam and UV photolithography (Section 3.9).

Another distinct route to PFS modification involves ROP of Cp-substituted sila[1]ferrocenophane monomers, but the syntheses of such species are multi-step and often low yielding.[78] Functional groups directly attached to the cyclopentadienyl rings are appealing as the redox properties of the iron centres can be directly influenced. In response to aforementioned synthetic problems, successful functionalisation of the Cp groups of PFDMS was reported using low temperature metalation with *t*-BuLi/KO*t*-Bu in THF, followed by reaction with Me_3SiCl (Scheme 8). The degree of substitution varied between 0.59 and 1.82 per ferrocendiyl, the maximum of which was achieved with a mixture of polymer and KO*t*-Bu (8 equivalents), and *t*-BuLi (16.5 equivalents). Notably, lithiation occurred regioselectively on the β-carbon.[79] The substitution of the Cp ring led to a loss of crystallinity, solubility in alkanes, and a large increase in glass transition temperatures.

3. Polyferrocenylsilane homopolymers: properties and applications

3.1. Solution characterisation

Multiple methods for determining the molecular weights and molecular weight distributions have been used for soluble PFSs, the most common of which is gel permeation chromatography (GPC). To characterise the solution behaviour of PFS in tetrahydrofuran (THF), PFDMSs spanning a molecular weight range of *ca.* 10 000–100 000 g mol^{-1}, with narrow polydispersities, were synthesised by anionic polymerisation. The molecular weight was determined by GPC *versus* monodisperse polystyrene standards, GPC with a triple detection system (refractive index, viscometry, and light-scattering), and static light scattering.[80] Whilst the latter two techniques produced molecular weights that were in good agreement, conventional GPC *versus* PS standards gave a 30% underestimation. In THF, PFDMS retains a more compact random coil conformation than for PS of the same molecular weight, due to less favourable PFDMS–solvent interactions. The Mark–Houwink parameter for high molar mass PFDMS in THF at 23 °C, $a = 0.62$ ($k = 2.5 \times 10^{-4}$), is typical of flexible chains in a fairly marginal solvent.[80] Earlier studies of other PFSs by low angle laser light scattering in THF revealed that conventional GPC with PS standards for column calibration also gave a substantial molar mass underestimation.[81,82]

The solubility parameter of a polymer (δ) is often estimated by measuring the degree of swelling of a lightly crosslinked polymer network in different solvents. Thus, from the swelling characteristics of a PFDMS network containing 4 mol% of a spirocyclic crosslinker, a δ value of 18.7 $MPa^{1/2}$ was established.[83] Maximum swelling of the gel is therefore observed for solvents with δ values of 18.0 to 19.4 $MPa^{1/2}$ (xylenes (18.0), toluene (18.2), THF (18.6), dichloromethane (18.6), chloroform (19.0), methyl ethyl ketone (19.0)).

Small-angle neutron scattering (SANS) in solution has also been employed to calculate the radius of gyration, weight-averaged molecular weight, and polydispersity index of PFSs, but in the absence of the column effects present in GPC.[84] Fitting the scattered intensity to a model based on a Schultz–Zimm distribution of isolated chains with excluded volume yielded molecular weight and size data that was in acceptable agreement with values determined by GPC. However, the assumed shape of the molecular weight distribution had a small influence on the polydispersity index values.

Solution state ^1H, ^{13}C, and ^{29}Si NMR spectroscopy is readily applicable for structural characterisation of PFSs, due to the presence of these NMR active nuclei in the polymer backbone or side-group structure. For example, NMR analysis has been used to investigate the tacticity of PFSs: ethylmethylsila[1]ferrocenophane underwent living anionic ROP to give an atactic PFS as determined from the integration of the triad methyl peaks (mm, mr/rm, and rr) in the ^1H NMR spectrum.[49] Thermal ROP also appears to give atactic materials and this has been evidenced by ^{29}Si NMR spectroscopy.[28] In addition, post-polymerisation functionalisation can be monitored by NMR spectroscopy. A LC PFS with a mesogenic phenyl benzoate group was characterised by ^1H and ^{13}C NMR spectroscopy, and compared to the spectra of the poly[6-(4′-butyloxyphenyl 4″-benzoyl)hexyl acrylate] to determine when side chain grafting was complete.[85]

3.2. Morphology in the solid state: crystalline and amorphous materials

In the case of PFSs, their physical properties are modified by the substituents on silicon and the Cp rings. PFSs symmetrically substituted at silicon with small alkyl groups (Me, Et, *n*-Pr, *n*-Bu, and *n*-pentyl)

are able to crystallise, as evidenced by a variety of analytical methods.[7] The degree of crystallinity has been observed to increase with time, particularly once the selected polymer has been annealed above its T_g. With longer substituents such as di(*n*-hexyl), or unsymmetrical side groups at silicon, however, PFSs are usually amorphous. One exception to this is atactic PFMS (PFMS: poly(ferrocenylmethylsilane)) which has Me and H substituents at silicon and was found to be semicrystalline in nature.[86] Apparently the reduced steric demand of hydrogen compared to methyl still enables the ordered packing of polymer chains even in this unsymmetrically-substituted case, despite the irregular arrangement of substituents along the backbone. The presence of two melting points (87 and 102 °C) for PFMS were assigned to reorganisation of the crystals during the heating process.[86] PFSs with very long flexible substituents at silicon (*e.g.* $OC_{18}H_{37}$) have been found to undergo side-chain crystallisation.[16]

Generally, for PFSs with hydrogen substituents on the Cp rings, T_g values can range from −51 °C with long, flexible substituents at silicon, such as R = R′ = OC_6H_{13}, to 99 °C for materials with ferrocenyl and methyl substituents, demonstrating the substantial influence of the side group structure. For a comprehensive illustration, Table 1 contains thermal transition and molecular weight data for PFS homopolymers determined by differential scanning calorimetry (DSC) and gel permeation chromatography (GPC), respectively.[6,7,51,60,68,71,75,78] A significant increase in T_g also occurs when the hydrogens on the cyclopentadienyl ligands are replaced with more sterically demanding alkyl groups.[30,78]

Table 1 Thermal transition and gel permeation chromatography (GPC) molecular weight data for PFS homopolymers, $[Fe(\eta^5\text{-}C_5H_4)_2SiRR']_n$

R	R′	$T_g(T_m)^b$/°C	$M_n{}^a$	PDI[c]	Ref.
H	H	16(165)	[d]	[d]	6
Me	Me	33(122–143)	3.4×10^5	1.5	6
Et	Et	22(108)	4.8×10^5	1.6	6
Pr^n	Pr^n	24(98)	8.5×10^5	2.7	6
Bu^n	Bu^n	3(116, 129)	3.4×10^5	2.6	6
n-C_5H_{11}	*n*-C_5H_{11}	−11 (80–105)	3.0×10^5	1.6	6
n-C_6H_{13}	*n*-C_6H_{13}	−26	7.6×10^5	1.5	6
Me	H	9(87, 102)	4.2×10^5	2.0	6, 86
Me	Et	15	2.9×10^5	1.7	6
Me	$CH_2CH_2CF_3$	59	8.1×10^5	3.3	6
Me	$CH{=}CH_2$	28	7.7×10^5	2.1	6
Me	$CH_2CH{=}CH_2$	7	1.1×10^5	1.2	6
Me	*n*-$C_{18}H_{37}$	1(16)	5.6×10^5	2.5	6
Me	Ph	90	1.5×10^5	2.0	6
Me	$(\eta^5\text{-}C_5H_4)Fe(\eta^5\text{-}C_5H_5)$	99	7.1×10^5	2.3	6
Me	5-Norbornyl	81	1.1×10^5	1.5	6
OMe	OMe	19	1.5×10^5	1.9	6
OEt	OEt	0	3.8×10^5	2.1	6
OCH_2CF_3	OCH_2CF_3	16	2.2×10^5	1.2	6
OBu	OBu	−43	3.9×10^5	2.1	6
OC_6H_{13}	OC_6H_{13}	−51	0.9×10^5	2.4	6
$O(CH_2)_{11}CH_3$	$O(CH_2)_{11}CH_3$	(−30)	1.9×10^5	2.5	6
$O(CH_2)_{17}CH_3$	$O(CH_2)_{17}CH_3$	(32)	2.3×10^5	2.2	6
OPh	OPh	54	2.3×10^5	2.0	6
$OC_6H_4Bu^t$-*p*	$OC_6H_4Bu^t$-*p*	89	1.9×10^5	1.9	6
OC_6H_4Ph-*p*	OC_6H_4Ph-*p*	97	5.4×10^5	2.4	6
Me	$OCH_2CH{=}CH_2$	8	2.8×10^5	2.1	6
Me	$OCH_2CH_2OCOC{=}CH_2(Me)$	16	3.0×10^5	2.7	6
Me	iPr	60	2.9×10^4	1.3	51
Me	$(CH_2)_3Cl$	38	1.9×10^5	1.6	71
Me	$(CH_2)_3I$	45	1.9×10^5	1.6	71
Me	$(CH_2)_3Br$	41	1.5×10^5	1.9	71
Me	$(CH_2)_2SC_6H_{13}$	−28	1.5×10^4	1.0	75
Me	$(CH_2)_2SC_9H_{19}$	−36	1.7×10^4	1.0	75
Me	$(CH_2)_2SC_{12}H_{25}$	−43	1.9×10^4	1.0	75
Me	$(CH_2)_2SC_{18}H_{37}$	(42)	2.1×10^4	1.0	75
Me	$CH_2CH_2(CF_2)_7CF_3$	16	1.8×10^4	1.0	60
Me	$CH_2CH_2CH_2C_6F_5$	35	1.8×10^4	1.1	60
Me	$CH_2CH_2CF_3$	56	1.5×10^4	1.0	60
Me	$OCH_2CH_2NMe_3COOC_6H_2(O(CH_2)_{12}CH_3)_3$	16(64)	[e]	[e]	68
Me	$OCH_2CH_2NMe_3COOC_6H_2(O(CH_2)_{14}CH_3)_3$	15(78)	[e]	[e]	68
Me	$OCH_2CH_2NMe_3COOC_6H_2(O(CH_2)_{16}CH_3)_3$	13(85)	[e]	[e]	68
Me[f]	Me[f]	73	7.3×10^4	1.9	78
Ph[g]	Ph[g]	212	1.7×10^6	1.4	30

[a] GPC data obtained from the analysis of THF polymer solutions which contained 0.1% $[Bu_4N]Br$ and molecular weight values are relative to polystyrene standards. Although in this case GPC provides only molecular weight estimates, absolute determinations of M_w by static light scattering for several polymers have indicated that GPC underestimates the real values by 30%. [b] DSC data collected at a heating rate of at 10 °C min^{-1}. [c] PDI = M_w/M_n. [d] Insoluble polymer. [e] Not reported. [f] $[Fe(\eta^5\text{-}C_5H_3Me)_2SiMe_2]_n$. [g] $[Fe(\eta^5\text{-}C_5H_3tBu)_2SiPh_2]_n$.

One notable property of these materials is their high thermal stabilities to weight loss; for example, PFS with two hydrogen substituents retained 90% of its initial mass when heated to 600 °C.[87] PFDMS, is an amber thermoplastic with a glass transition temperature (T_g) of 33 °C, and a melt transition temperature (T_m) between 122–145 °C depending on the thermal history of the polymer.[47] The experimental T_m comprises a range of values as each of the varying sizes of crystallite present melt at minutely different temperatures.[88] O'Driscoll's equation: $T_g = T_{g,\infty} - KM_n^{-2/3}$,[89] describes the relationship between the glass transition temperature at infinite chain length, $T_{g,\infty}$, and T_g which reaches a maximum value when the polymer comprises *ca.* 90 repeat units. A detailed study of the crystallisation behaviour of PFDMS attributed the slow rate of crystallisation to the low melt enthalpy.[90] Moreover, using the Gibbs–Thomson approach resulted in the prediction of an equilibrium melting temperature of *ca.* 215 °C.[90] This value corresponds to a 100% perfect crystallite of infinite size, which cannot be obtained experimentally.

A LC PFS with poly[6-(4′-butyloxyphenyl-4″-benzoyl)hexyl acrylate] side chains (Fig. 4) was synthesised by atom transfer radical polymerisation.[85] It was demonstrated to form a thermotropic nematic phase in the high temperature region and smectic A phase in the low temperature region. When compared to poly[6-(4′-butyloxyphenyl-4′-benzoyl)hexyl acrylate], the PFS brush material exhibited a lower glass transition temperature (46 °C *vs.* 48 °C) and clearing point (118 °C *vs.* 125 °C).

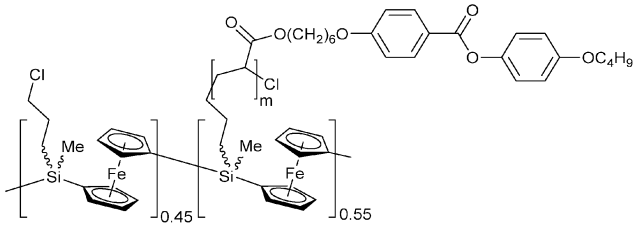

Fig. 4 A LC PFS with poly[6-(4′-butyloxyphenyl-4″-benzoyl)hexyl acrylate] side chains.

An understanding of the conformations of PFS polymer chains in the solid state is primarily based again on the study of PFDMS. Molecular mechanics calculations of the possible conformations of well-defined oligomeric species, both as isolated molecules and in the solid state, have been compared to single crystal X-ray diffraction data.[91–93] The diffraction pattern of the pentamer was found to display a broad peak with a similar *d*-spacing to that of high molecular weight PFDMS, thus providing evidence of a close relationship between the two structures. With reference to the pentamer, a single-crystal X-ray diffraction study showed parallel packing of *trans*-planar zig-zag polymer chains, with the terminal ferrocene twisted approximately perpendicular to the plane (Fig. 5).[93] Calculations showed the polymer chains in PFDMS to be conformationally flexible. Intermolecular interactions were found to be significant and the lowest energy conformation displayed twisted ferrocene units with favourable Fe–Cp electrostatic interactions between neighbouring polymer chains.[91]

Studies of films and fibres using X-ray diffraction revealed that crystalline PFDMS contains coexisting 2-D mesophases, crystals with a hexagonal or tetragonal packing of macromolecules, and 3-D monoclinic crystalline phases.[94] The formation of partially disordered crystalline phases was attributed to small energy differences between the various polymer conformations. Electrospun nanofibres of PFDMS have also been studied and in this case using electron diffraction.[95] The data obtained were consistent with the assignment of a monoclinic unit cell for the crystals in the nanofibre. Furthermore, the *c*-axes of the crystals were found to lie along the fibre axis but both the *a*- and *b*-axes of a multitude of crystals were found to be randomly distributed in the azimuthal directions. Studies of other PFSs, including amorphous materials that were unsymmetrically substituted at silicon, have also been reported.[96] In comparison to the semi-crystallinity of PFDMS and symmetrically substituted analogs

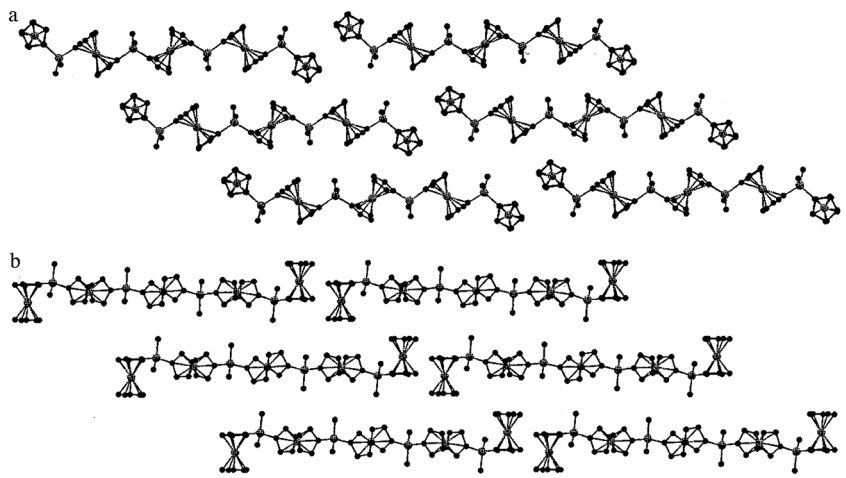

Fig. 5 The crystal packing arrangement of the PFDMS pentamer, showing three pairs of molecules. The terminal ferrocenyl groups are twisted in opposite directions, perpendicular to the interior, trans-planar, zig-zag units. Reproduced with permission from ref. 93. Copyright 1996 American Chemical Society.

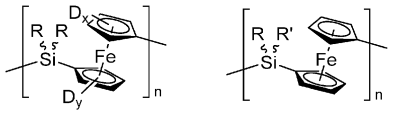

R = CH_3, x+y = 2
R = OCH_3, x+y = 4
R = OC_6H_{13}, x+y = 4

R_1=CD_3, R_2 = CH_3
R_1 = R_2 = OCD_3

Fig. 6 Polyferrocenylsilanes studied by solid-state ^{2}H NMR spectroscopy.

with small alkyl groups at silicon, *n*-hexyl substituted PFS has been isolated as an amorphous gum with a T_g of −26 °C. Apparently, for these materials once the length of the alkyl chain exceeds five carbon atoms regular packing of the polymer chains cannot be achieved.[7] Alkoxy-substituted PFSs are also generally amorphous, however, the incorporation of long alkoxy chains at silicon, such as *n*-octadecyloxy, yields PFSs that exhibit side-chain crystallisation to form lamellar structures with interdigitated side groups.[16]

The polymer backbone motions of deuterium-labelled PFSs over a range of temperatures were studied by solid-state ^{2}H NMR spectroscopy, and the nature and rates of molecular motions were determined from the shape of the spectral line and the spin–lattice relaxation time (T_1). Symmetrically substituted PFSs with methyl, methoxy, hexyloxy substituents at silicon were studied where the Cp rings were fully deuterated (Fig. 6). Interestingly, when the Cp rings were deuterium-labelled, a lack of motion in the backbone was observed below the T_g.[97] This was unexpected because Cp ligand rotation in ferrocene is facile due to the low barrier of rotation about the iron–Cp bonds (3.34 kJ mol^{-1}).[98] At temperatures just above the T_g, small-angle oscillations of the Cp groups were noted which increased in rate with temperature. Above 50–70 °C, the spectra indicated the presence of rapid isotropic movements. Studies of PFSs with –CD_3 or –OCD_3 groups at silicon provided insight into the motions of side groups as a function of temperature. For example, deuterated PFDMS side groups showed fast methyl rotation about the Si–CD_3 bond even at temperatures below the glass transition.[99] With methoxy substituents, fast methyl rotation was observed about the O–CD_3 bond alongside a discrete jumping motion displayed by the Si–O bond.[99] In a separate study, solid state ^{13}C NMR spectra of PFDMS and poly(ferrocenyldibutylsilane) allowed the structure and segmental motions of these semi-crystalline polymers to be examined. Polymer main chain rigidity on the time scale of the cross-polarisation time between protons and carbons, T_{CH}, was confirmed at room temperature although some libration of ferrocenyl groups was possible in the latter case.[100] In addition, the butyl substituents were found to be significantly disordered.

3.3. High refractive index materials

Organic polymers possess a relatively narrow range of refractive indices (RIs), commonly between 1.35 and 1.65,[101] which limits their application.[102] To resolve this, RIs can be increased through molecular tailoring of polymers with functional groups that vary in electronic polarisation, such as incorporating conjugated double bonds or aromatic heterocyclic rings directly on the polymer backbone.[103] However, the device applications of these highly conjugated, organic polymers are often limited by unfavourable optical properties and insolubility.[104] An alternative approach incorporates high refractive index inorganic clusters into a polymer matrix.[105] For example, RIs reported for nanocomposites containing PEO (PEO: poly(ethylene oxide)) and PbS range between 2.9 and 3.4.[106] These polymers, however, suffer from optical inhomogeneities, poor processability, and increased Rayleigh scattering at critical diameters.[105] Notably, the inclusion of highly polarisable atoms (Si, Ge, Sn, S), substituents with low molar volumes and high molar refractions (aromatic rings, halogens excluding F), or metallic elements into macromolecules increases the RI exhibited by the material without significantly increasing the optical dispersion.[107,108]

Table 2 The refractive indices at λ = 589 nm of PFS homopolymers [Fe(η^5-C_5H_4)$_2$SiRR′]$_n$ with various substituents[109,110]

R	R′	n (589 nm)
CH_3	$CH_2CH_2CF_3$	1.599
CH_3	CH_2CH_3	1.663
CH_3	CH_3	1.678
CH_3	C_6H_5	1.681
CH_3	*p*-OC_6H_4Br	1.682
CH_3	Ferrocenyl	1.696
CH_3	Thienyl	1.691

High molecular weight PFSs have been found to possess relatively high RI values (up to *ca.* 1.70), as expected from the high concentration of polarisable iron and silicon atoms in the polymer backbone.[109] The refractive indices at λ = 589 nm of PFSs with various substituents are displayed in Table 2. These PFSs also possess significantly lower optical dispersion than organic polymers for the same values of refractive index.[110]

Tapered optical fibres coated with PFMPS have been explored as gas sensing devices for NH_3 and CO_2. When a gas interacted with the polymer coating, the resulting small variations in refractive index caused significant changes in the transmitted optical signal.[111] However, while the device was highly sensitive to other changes in environment, the magnitude of the response was (qualitatively) not concentration dependent.

3.4. Redox and charge transport properties

Unlike ferrocene containing side-chain polymers, which generally only exhibit a single oxidation wave for the Fe(II)/Fe(III) redox couple, PFSs display cyclic voltammograms with two reversible oxidation waves of equal intensity.[7,93,112–114] This is indicative of a stepwise process where initial oxidation at alternating iron centres occurs, because as one iron centre is oxidised ($^1E_{1/2}$), the neighbouring sites become more difficult to oxidise (Scheme 9). Thus a higher potential is required ($^2E_{1/2}$), resulting in the two oxidation waves with redox coupling, $\Delta E_{1/2} = {}^2E_{1/2} - {}^1E_{1/2}$ ($\approx$250 mV for PFSs).[93] When identical experimental conditions are used for the electrochemical experiments (including the use of the same solvent and supporting electrolyte) the separation of the two waves, $\Delta E_{1/2}$, provides an approximate measure of the electronic interaction between iron centres along the polymer backbone.[115] Studies of isolated

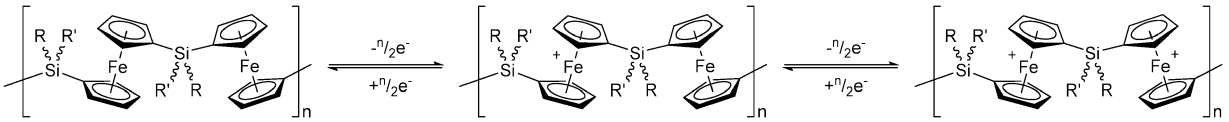

Scheme 9 The stepwise oxidation and reduction of PFS.

linear and cyclic oligomers has shown that the equal intensity, two redox-wave pattern characteristic of PFS materials corresponds to the limiting case of an infinite chain.[66,93] Functionalisation of the Cp rings with electron donating groups lowers the oxidation potential of the ferrocene center in the neutral species. For example, the cyclic voltammetric halfwave oxidation potentials of PFS are reduced by *ca.* 55 mV per Cp methyl substituent relative to the non-methylated polymer.[30]

The redox properties of PFSs have been exploited for a wide range of studies and applications. PFS homopolymers with a thiol end group have been self-assembled as monolayers on a gold surface, and probed to determine the morphology and volume changes upon oxidation and reduction.[116] Surface plasmon resonance spectroscopy and spectroscopic ellipsometry measurements showed a reversible 15% increase in thickness of the polymer monolayers upon electrochemical oxidation, confirmed by X-ray reflectivity measurements. The authors attributed this change to both stretching of the polymer backbone upon oxidation, as a result of an increase in charge density, and the attraction of counter-ions and associated solvent molecules. These processes were reversed when the polymer monolayer was reduced to a neutral state. Furthermore, in a separate study, changes in elasticity of individual PFS chains on a surface was also induced by a change in oxidation state,[117] such that the oxidised polymer had an increased segment elasticity (45 nN nm^{-1}) and Kuhn length (0.65 nm) compared to its neutral analogue (30 nN nm^{-1} and 0.38 nm, respectively).[118] This change was reversible and has been used as the basis for a single (macro)-molecular motor. PFS was operated in a controlled cyclic fashion to perform mechanical movement (output) as a consequence of an electrochemical potential (input) (Fig. 7).[118] For PFS homopolymers (degree of polymerisation = 80) 3.4×10^{-19} J of work was achieved at an efficiency of 5%, as estimated from the experimental data. Closed mechanoelectrochemical cycles of individual PFS chains have also been studied using electrochemical AFM-based single-molecule force spectroscopy, and a quantitative analysis of the efficiency of the closed cycles has been performed as a function of extension. A maximum value of 26% was observed experimentally.[119] Atomic force microscopy (AFM) was used to study the force interactions between the tip and a PFS grafted gold surface subjected to external potential in $NaClO_4$ solution.[120] The physisorption of the PFS chains to the tip dominated the total interaction force, regardless of a subsequently applied surface charge, if the tip was in contact with the polymer surface prior to electrochemically induced redox chemistry.

Although neutral PFSs are classed as insulators, with an intrinsic conductance (σ) of 10^{-14} Ω^{-1} cm^{-1}, oxidative doping can increase this by several orders of magnitude to values in

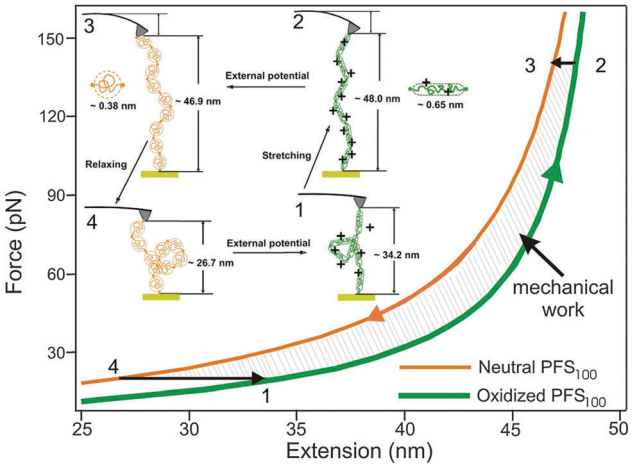

Fig. 7 Single molecule operating cycle of PFS macromolecules (degree of polymerisation = 80) powered by an electrochemical potential; (inset) schematic illustration of a single molecule operating cycle with redox-active macromolecules. Reproduced with permission from ref. 118. Copyright 2006 Elsevier.

the range of 10^{-8} to 10^{-4} Ω^{-1} cm^{-1}, typical of p-type semiconductors.[121] The hole transport properties have been shown to be appreciable.[121] Vapour-phase chemical oxidation of PFS thin films was achieved using iodine, *via* irreversible electron transfer to form ferrocenium ion centres with $[I_3]^-$ counter-ions.[122,123] Further doping with I_2 saw the reversible formation of $[I_5]^-$ ions.[124] Treatment of the iodine-doped films with NH_3 resulted in reformation of the insulating material. Significantly, chemical oxidation under these conditions resulted in considerable cleavage of the polymer backbone. Oxidation can also occur with ferric chloride, tris(4-bromophenyl)ammoniumyl hexachloroantimonate,[125,126] tetracyanoethylene, or 2,3-dichloro-5,6-dicyanoquinone.[42] Tris(4-bromophenyl)ammoniumyl hexachloroantimonate, however, can also act as an oxidant in radical cation chemistry and a Lewis acid in carbocation mediated transformations, as aminium hexachloroantimonates can release antimony pentachloride.[127] On the other hand, tris(4-bromophenyl)aminium hexafluorophosphate, and hexafluoroantimonate, cleanly oxidise ferrocene derivatives as the counterions are relatively inert.[128] Decamethylferrocene was found to be a good reducing agent for oxidised PFS.[78,126,128]

Photo-oxidation of amorphous PFMPS thin films either cast from chloroform solution or in the presence of chloroform vapour, was achieved by irradiation with near-UV light.[129] The photo-oxidised films displayed a significant increase in conductivity in the absence of light relative to pristine samples; moreover, a significant photoconductive response was also measured under illumination. However, a substantial reduction

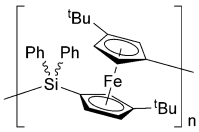

Fig. 8 Poly(ferrocenyldiphenylsilane) with two *tert*-butyl substituents per ferrocenediyl.

in the molecular weight of the polymer was detected after the photo-oxidation/reduction process which is believed to be caused by the highly reactive chlorinated photoproducts derived from $CHCl_3$.

Significant chain cleavage has been noted to be facile when the degree of oxidation of PFS exceeded 10%, even with mildly nucleophilic species, as the highly labile ferrocenium centres readily undergo Fe–Cp bond cleavage.[78] As oxidised PFSs are generally insoluble in non-nucleophilic organic solvents these materials are difficult to process and study. Introducing bulky electron-donating substituents to the Cp rings has been used in an attempt to resolve these issues. Thus, the oxidation potentials of poly(di*tert*-butylferrocenyldiphenylsilane) (Fig. 8) were more negative than those of the methylated or non-methylated analogues due to the electron donating effect of the *tert*-butyl group on the iron centre.[78] Substantial redox coupling ($\Delta E_{1/2}$ = 0.33 V) was also detected. Significantly, the presence of *tert*-butyl groups markedly decreased the propensity for the polymer to undergo chain cleavage on oxidation. Furthermore, soluble (*e.g.* in CH_2Cl_2) PFS salts were achieved up to high degrees of oxidation (*ca.* 50%).[78]

PFSs have also been investigated as host materials for CdSe nanocrystals.[130] It was noted that PFS caused quenching of the band edge photoluminescence of the quantum dots in films and in solution, although in the latter case the quenching effects were solvent dependent. As the emission properties of the CdSe nanocrystals can be controlled *via* the oxidation of PFS, there are potential applications in electrochromics or optical switching in which the response of the nanocrystal is altered by the redox chemistry of the polymer.

PFDMS and PFMPS have also shown potential as charge dissipation coatings for dielectric poly(ethylene terephthalate) (Mylar) films.[131] In this study, a 50 mm thick Mylar layer was coated with PFS and then exposed to an electron beam. It was noted that the PFSs imparted a high degree of immunity to the dielectric films with respect to high energy arc discharges brought about by negative charge accumulation. This was rationalised by the explanation that the PFSs were acting as a semiconductor: the charge formed at the surface of the coated sample was drained slowly to the ground.

PFS nanocontainers prepared by a miniemulsion/solvent evaporation protocol were found to release hydrophobic material over a period of time when oxidised by H_2O_2.[132] The release was also coupled to the enzymatic oxidation of glucose with oxygen by the enzyme glucose oxidase.

3.5. Redox-active gels

Stimuli responsive materials rapidly alter their structure and properties in response to changes in environment, such as pH, temperature, applied stress, and electromagnetic fields.[133] While responses to such traditional stimuli have been well documented, redox responsive gels are much less studied.[134] Organic solvent swellable gels based on crosslinked PFS were reported in 1996 and their preparation involved thermal copolymerisation of dimethylsila[1]ferrocenophane with a small quantity of spirocyclic [1]ferrocenophane.[20,135] As noted earlier (Section 3.1), the best solvents for PFDMS are tetrahydrofuran, chloroform, and dichloromethane; these resulted in the maximum degree of swelling.[83] Analogous crosslinked PFS materials have also been produced *via* photo-crosslinking of pendant methacrylate groups,[35] hydrolysis of PFS with ethoxy side groups,[136] and thiol–ene addition reactions.[137]

As a result of the low polarity of PFS in the neutral Fe(II) state and the higher polarity of oxidised Fe(III) materials, PFS gels show tunable swelling based on the degree of oxidation in the selected solvent. Based on this concept, a redox-responsive colloidal photonic crystal was reported that consisted of an unconnected but ordered array of silica spheres embedded in a swellable crosslinked PFS matrix. Monodisperse silica microspheres were organised into planar silica colloidal crystals by evaporative deposition, surface-modified with chloromethylsila[1]ferrocenophane, and infiltrated with ethylmethylsila[1]ferrocenophane (an unsymmetrically substituted monomer was used to prevent microcrystallisation of the resulting PFS within the network) and a silacyclobutyl-substituted [1]ferrocenophane crosslinker.[128] Thermal polymerisation then yielded a silica–PFS composite colloidal crystal film (Fig. 9). A later study investigated the effect of exposing a similar photonic crystal to solvent vapour, deducing that the subsequent swelling changed the refractive index and increased the lattice spacing of the photonic crystal at higher vapour pressures.[138] The degree of swelling of the PFS chains in the photonic crystal was noted to depend on the oxidation state of the iron centres, and the solvent system used. This response was used to develop a device in which the reflected colour was voltage tunable through the

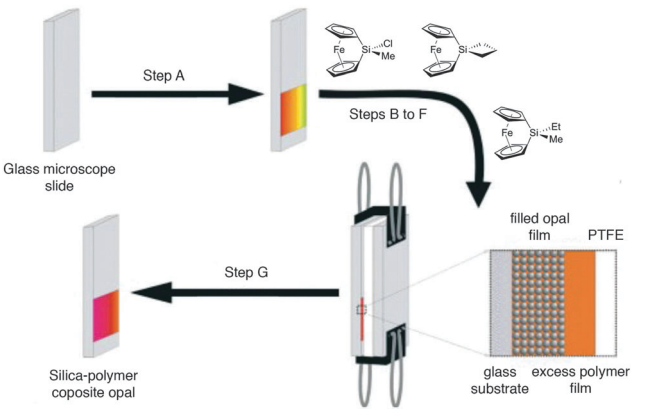

Fig. 9 Schematic of steps in fabrication of a silica–PFS composite opal. (A) Evaporation deposition of silica colloids. (B) 200 °C, 12 h, vacuum. (C) Treatment with capping agent (chloromethylsila[1]ferrocenophane). (D) Infiltration of ethylmethylsila[1]ferrocenophane and a cyclobutyl-substituted [1]ferrocenophane crosslinker, solvent removal. (E) Sample covered with PTFE sheet, glass slide, and bound. (F) 190 °C, 13 h, N_2. (G) Removal of clips, PTFE, and glass cover. Reproduced with permission from ref. 128. Copyright 2007 John Wiley & Sons Inc.

whole visible range, *via* reversible expansion and contraction of the photonic lattice.[139] Thin films of monodisperse silica spheres were deposited onto glass plates coated with indium tin oxide. The voids between the spheres were infiltrated by low molecular weight PFMVS (PFMVS: poly(ferrocenylmethylvinylsilane)), a small amount of multifunctional thiol, and a radical photo-initiator, and were then irradiated with ultra-violet light to give a PFS polymeric network *via* a thiol–ene addition reaction. However, it was noted that electrolyte diffusion through the silica packed polymer matrix impeded electron and ion transport, slowed switching times, and increased the voltage required to power the device.[139]

Electroactive inverse polymer gel opals based on PFS were reported in 2009. Silica spheres were deposited on glass and infiltrated as before with well-defined PFMVS or PFDVS (PFDVS: poly(ferrocenyldivinylsilane)), however after crosslinking and removal of the polymer over-layer, the spheres were removed with hydrofluoric acid.[137] This yielded a free-standing inverse polymer–gel opal in which electrolyte could freely infuse the nanoporous lattice. When an oxidative potential was applied, the reflected optical diffraction peak was red-shifted, as the influx of ions and solvent caused the polymer to swell. When a reducing potential was applied the reverse occurred. Thus, full colour was afforded at low drive voltages with wavelength shifts across the ultraviolet, visible, and near infrared spectral range (Fig. 10).

Hydrogels based on water soluble PFSs have also been developed.[140] The incorporation of ionic side groups into the PFS, or the linking the polymer chains with water-soluble polymers such as PEG (PEG: poly(ethyleneglycol)), has allowed for hydrogel formation.[141] For example, two distinct types of PFS polyelectrolyte networks with either permanently positively or negatively charged side groups have been prepared (Fig. 11).[142] The reaction of poly[ferrocenyl(3-iodopropyl)methylsilane] with *N*,*N*,*N*′,*N*″,*N*″-pentamethyldiethylenetriamine gave a lightly crosslinked network. The remaining iodopropyl side groups were then converted into positively charged moieties by quaternisation using *N*,*N*-dimethylethylamine, which resulted in a permanently charged cationic network. An anionic PFS hydrogel was obtained from poly(ferrocenyl(3-iodopropyl)methylsilane) and α-lithio isobutyl methanesulfonate *via* intermolecular alkylation, followed by cleavage of the isobutylsulfonate side groups using tetrabutylammonium iodide, and exchange of counterions. The PFS hydrogels showed reversible hydration and dehydration in water, the extent of which was controlled by the redox voltage. An obvious change in mechanical behaviour occurred upon the oxidation of the anionic hydrogel: the elastic nature was lost and the gel collapsed. However, the network reswelled and regained its elasticity upon subsequent reduction and reestablishment of charge balance.[142] Water-solubility was also achieved by crosslinking PFS containing acrylic side groups with PEG–dithiol using the thiol–ene addition click reaction.[143] The redox state, and hence swelling and mechanical properties of the PFS, could be reversibly tuned. The PFS–PEG hydrogel was proposed to have potential use as a redox controlled drug release carrier where release is based on hydrophobic–hydrophilic switching. A dual thermo- and redox-responsive poly(*N*-isopropylacrylamide)–PFS based hydrogel was synthesised as a precursor for the redox-induced formation of hydrogel silver composites.[144] These composites were reported to have a good biocompatibility with cells and display high antimicrobial activity. Dual-responsive PFS bottlebrushes with poly(*N*-isopropylacrylamide) side chains have also been studied.[145]

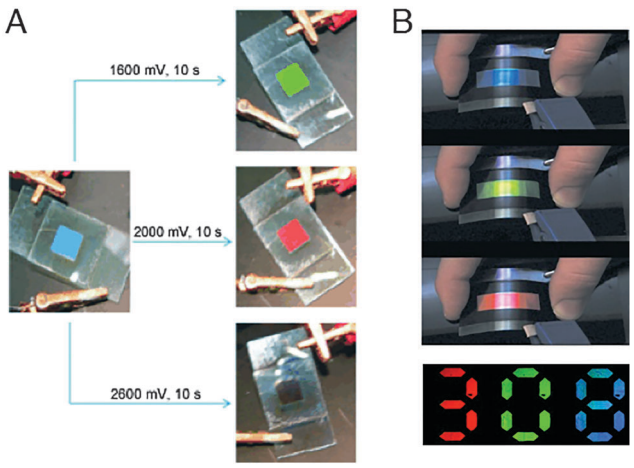

Fig. 10 (A) Proof of full colour tuning by photographs of the first electroactive inverse polymer–gel opal. The cross-linker concentration in this sample was 10 mol%. (B) Extracted frames from a video taken when a flexible P-Ink device was simultaneously switched and flexed. Reproduced with permission of ref. 137. Copyright 2009 John Wiley & Sons Inc.

Redox-responsive PFS-based poly(ionic liquids) (PILs) have been reported to form water swellable, redox-active gels. Poly[ferrocenyl(3-iodopropyl)methylsilane] was reacted with 1-vinylimidazole, before the iodide counterions were exchanged for chloride to improve solubility.[146] At low concentrations, the PIL self-cross-linked into nanogels, and at higher concentrations macroscopic hydrogel networks were formed. Chemical oxidation of the iron centres in PFS by H_2O_2 was accompanied by a distinct colour change from amber to blue/green.[140] Upon oxidation the hydrogel collapsed, while subsequent reduction allowed the PFS chains to reswell. A possible use of PFS–PIL is as a stabiliser for micro-emulsion polymerisation, due to the amphiphilic nature of the polymer chain. Redox-responsive porous membranes have been formed by electrostatic complexation between PFS-based PILs with vinylimidazolium bis(trifluoromethylsulfonyl)imide side groups ($VImTf_2N$), and PAA (PAA: poly(acrylic acid)).[147] The PFS–$VImTf_2N$/PAA membrane displayed redox responsive behaviour, which enabled reversible switching between open and closed porous structures with associated changes in permeability (Fig. 12). The authors noted that such a system could have uses in selective filtration, the preparation of enzyme-entrapped membranes for bio-sensing, controlled loading and release, and catalysis in microfluidic reactors.

A comb copolymer consisting of a PFS backbone with *N*-dimethylethyl and *N*-dimethyldecyl ammonium substituents (Fig. 13) was reported for use in the redox triggered release of molecular payloads. The amphiphilic behaviour of the comb polymer allowed the formation of micellar assemblies with

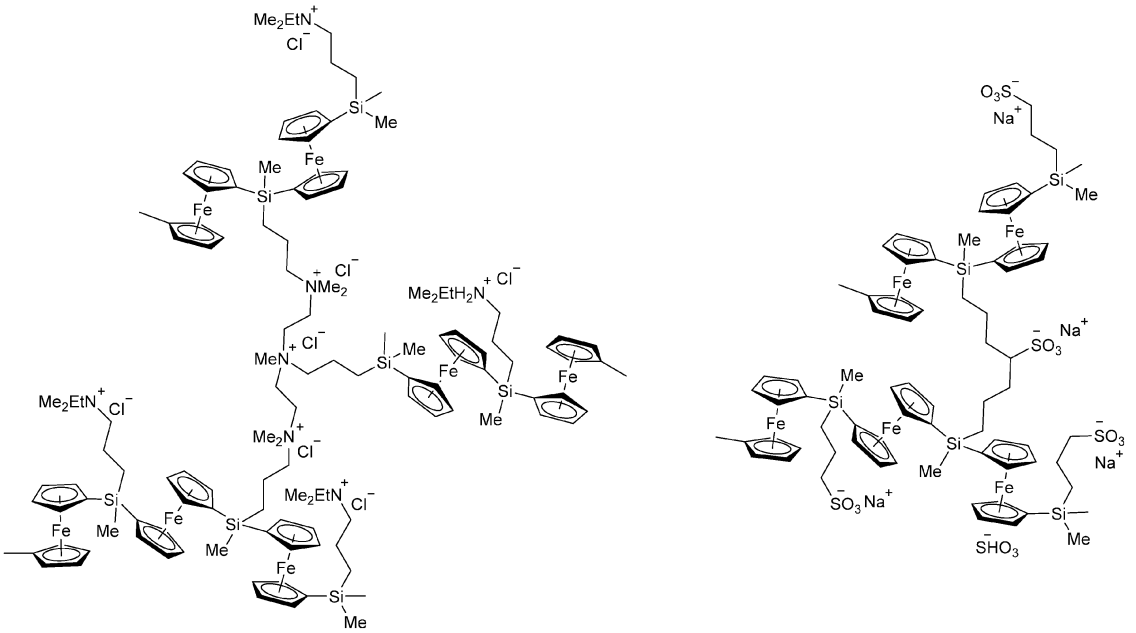

Fig. 11 Permanently charged cationic and anionic PFS networks.

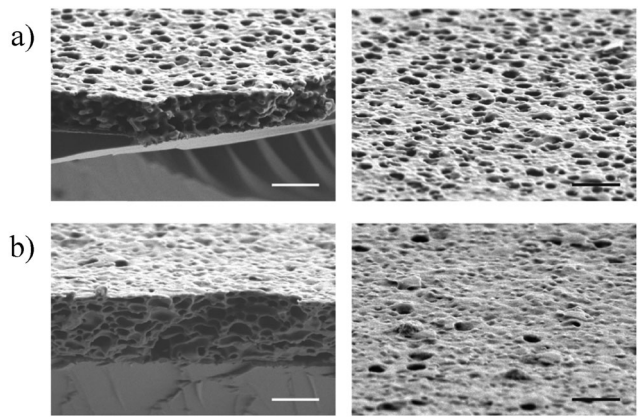

Fig. 12 Cross-sectional and surface SEM images of PFS-VImTf$_2$N/PAA porous membranes after oxidation at 0.6 V for 10 min (a), and then reduction at −0.2 V for 10 min (b). Scale bars are 1 μm. Reproduced with permission from ref. 147. Copyright 2014 John Wiley & Sons Inc.

hydrophobic pockets that displayed redox-induced morphology changes in water.[148] When Paclitaxel and Nile Red were encapsulated in the micelles, oxidation of the polymer chains caused a shift to a less compact structure that allowed their controlled release.

3.6. Magnetic ceramic precursors

Ceramic materials have traditionally been prepared from powders in a sequence of synthesis, processing, shaping, and sintering steps that require exact stoichiometries and afford little control over ceramic morphology.[149] Moreover, the very high temperatures (>1500 °C) required mean that processing is both difficult and expensive. Synthesis from polymers has been explored as it allows for homogeneous ceramics, better control over morphology, and enhanced physical properties, in

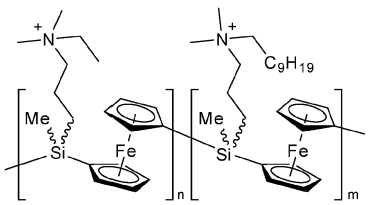

Fig. 13 A comb-copolymer consisting of a PFS backbone with *N*-dimethylethyl and *N*-dimethyldecyl ammonium substituents.

addition to easy fabrication into fibers, films and shaped objects.[150] The incorporation of iron into polymer precursors has the potential to introduce magnetic, conductive, and catalytic properties.[151] PFSs are a well-studied class of organometallic polymers for the preparation of Fe/Si/C ceramics with the first studies reported in 1993.[152]

Pyrolysis of PFSs at temperatures above 500 °C under a flow of nitrogen yielded α-Fe crystallites embedded in a C/SiC/Si_3N_4 matrix.[152–154] Various substituents on silicon were investigated and PFSs with Si–H and vinyl groups gave the highest ceramic yields at 600 °C, whilst a 1 : 1 blend of both was highest at 1000 °C. Nonetheless, these ceramic yields (17–56%) were still too low to afford good shape retention.[153] Subsequent work demonstrated that a crosslinked matrix obtained from the thermal ROP of dimethylsila[1]ferrocenophane with a spirocyclic crosslinker formed well-defined ceramics when pyrolysed at 600–1000 °C, in greater than 90% ceramic yield (Scheme 10).[155] Within this temperature range it was found that the magnetic properties of the ceramics could be tuned. When prepared at temperatures below 900 °C small, single domain iron nanoclusters were formed that displayed virtually no hysteresis at 100 or 300 K, characteristic of superparamagnetic ceramics (Young's modulus = 29.4 GPa). Ceramics prepared at higher temperatures

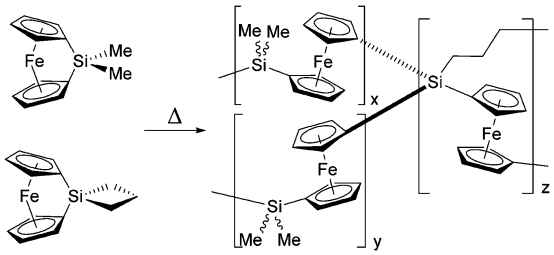

Scheme 10 Thermal ROP of PFDMS with a spirocyclic crosslinker to give a crosslinked matrix.

(Young's modulus = 15.4 GPa), however, contained larger ferromagnetic, multi-domain iron nanoparticles. This crosslinked PFS system enabled the shape retention of monolithic shaped objects and formation of micron-scale patterned materials (Fig. 14).[151] A possible mechanism for ceramic formation from the PFS network involved the controlled release of Fe atoms from the matrix, and nucleation and growth of iron nanoparticles.

The pyrolysis of hyperbranched PFDMS has also been studied and this yielded conductive, magnetic ceramics that exhibited a negligibly small hysteresis loss.[156] A 3-D mesoporous network of nanoclusters was generated *via* simultaneous evaporation of volatile organics and agglomeration of inorganic elements during pyrolysis. These hyperbranched polymers were determined to be superior to the linear analogues in terms of ceramic yield and retention of iron in the product (respectively 48–62% and 36–43%, *vs.* 36% and 11% for the linear polymer).[156] The high ceramic yield for magnetic Fe nanoclusters with high magnetic susceptibilities was corroborated by further work on a hyperbranched PFS polymer from ferrocenyl dilithium and silicon tetrachloride ($SiCl_4$).[157] However, the solubility of the resulting polymers was remarkably reduced. Similarly, hyperbranched polymers were produced from dilithioferrocene with trichlorosilanes.[158] It was noted that the polymers with small substituents at silicon were partially soluble, while those with long alkyl chains were completely soluble and readily formed films, which were then pyrolysed to give ferromagnetic ceramics. The roles of atmosphere and heating rate on the composition and magnetic properties of Fe/Si/C ceramics formed from hyperbranched PFS has also been investigated. The iron present in the ceramics sintered at 900 °C under N_2 and NH_3 atmospheres

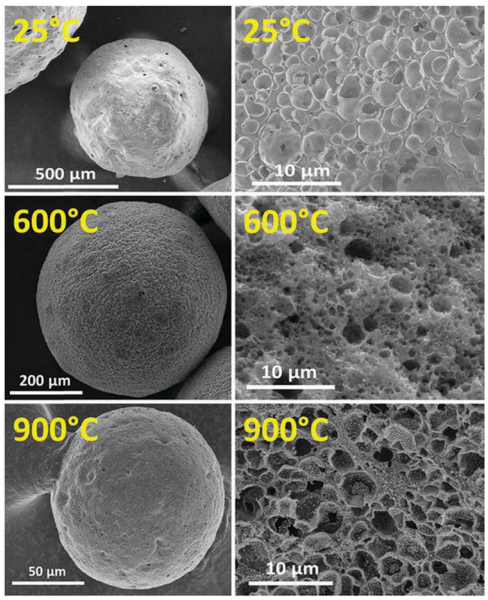

Fig. 15 SEM images of hyperbranched PFS microspheres (25 °C) and ceramic microspheres after pyrolysis at 600 and 900 °C: the overall appearance (left) and cross-section morphology (right). Reproduced with permission from ref. 160. Copyright 2015 Springer Publishing Company.

appeared as α-Fe, while those sintered under air contained γ-Fe_2O_3 and carbon.[159] Ceramics sintered under all three atmospheres were ferromagnetic with low remnant magnetisation and coercivity; however, those sintered under NH_3 displayed the largest saturation magnetisation. This was increased further when ceramics were prepared at a slow heating rate. The pyrolysis of the hyperbranched PFS at different temperatures was used to obtain ceramic microspheres with porous structures by solvent extraction/evaporation-based microencapsulation methods (Fig. 15).[160] Fe nanoparticles were also produced on the internal surface of the pores, giving the ceramic microspheres catalytic properties.

A bimetallic system was developed to combine the processability of linear high molecular weight polymers, the high ceramic yields achieved by thermally crosslinked systems, and the presence of a high concentration of two different metal atoms. An acetylene-substituted PFS was functionalised in a high yield post polymerisation by reaction with $Co_2(CO)_8$.[161] Ceramics prepared from $[Fe(\eta^5\text{-}C_5H_4)_2Si(Me)C_2PhCo_2(CO)_6]_n$ (Co-PFS) at

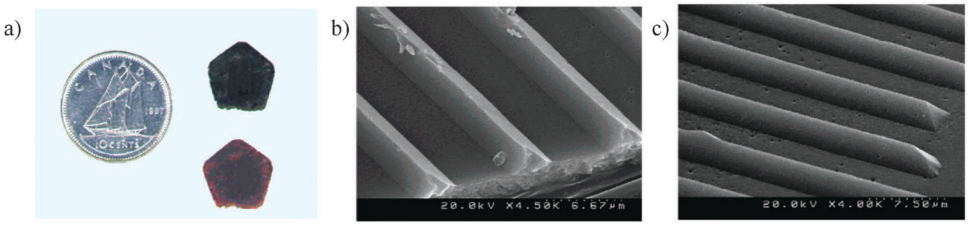

Fig. 14 (A) Pentagon-shaped polymer (bottom) and the resulting pentagon-shaped ceramic after pyrolysis (top). (B) SEM images of a patterned polymer film, it is evident that the polymer film replicated the triangular grooves patterned on the Si wafer. (C) SEM image of the resulting ceramic film, illustrating the shape retention of the polymer without the presence of a mould during pyrolysis. Reproduced with permission from ref. 151. Copyright 2002 American Chemical Society.

600 °C were superparamagnetic, and those prepared at 900 °C ferromagnetic or superparamagnetic with a $T_b > 355$ K. It was also reported that at 500 °C pyrolysis, smaller NPs were formed in the underlying layer of the ceramic film, while partially embedded uniform and larger CoFe alloy nanoparticles formed on the film surface.[162] Pyrolysis of Co-PFS at higher temperatures yielded larger nanoparticles with a broad size distribution at the film surface (800 °C: 36.5 ± 12.5 nm, 900 °C: 40.5 ± 14.8 nm). Moreover, surface nanoparticles were found to be oxidised upon exposure to air.

Fabrication of patterned arrays of magnetic ceramics on the sub-micron scale was achieved by electron-beam lithography and pyrolysis of thin films with Co-PFS acting as a negative resist. Co-PFS was also found to act as a negative-tone UV-photoresist.[163] Furthermore, reactive ion etching of a thin film of Co-PFS with either a hydrogen or an oxygen plasma in a secondary magnetic field, afforded ferromagnetic ceramic films in a viable alternative to pyrolysis.[164a] PFEMS was doped with palladium(II)acetylacetonate either by sublimation of $Pd(acac)_2$ which formed Pd nanoparticles in the PFEMS films, or by mixing $Pd(acac)_2$ with the PFEMS polymer precursor prior to film deposition.[164b] The magnetic susceptibility of the resultant soft processable paramagnetic polymer films increased with palladium content. Upon pyrolysis of the precursors, ferromagnetic ceramics were formed. Unusually, FePd alloys were observed for ceramics formed by pyrolysis under argon at 1000 °C, which resulted in their enhanced coercivity, remnant magnetisation, and saturation magnetisation.

Composite materials of mesoporous silica and PFDMS have been prepared using a vapour-phase impregnation technique, where ROP occurs *in situ* inside the channels of silica. The pyrolysis of the resultant materials gave composites with Fe nanoparticles (20 ± 5 Å) confined to the channels of the mesoporous silica.[165] In a later report, $Fe(\eta^5\text{-}C_5H_4)_2SiMe_2$ and $Fe(\eta^5\text{-}C_5H_4)_2Si(CH_2)_3$ were incorporated into the hexagonal channels of mesoporous silica. However, in the latter case the ferrocenophane ring was completely opened, whilst the silacyclobutane ring remained mostly intact. When pyrolysed, the composites containing PFDMS formed Fe nanoparticles in the 30–40 Å channels of mesoporous silica. Characterisation indicated that the nanostructured ceramic was superparamagnetic.[166]

PFS materials have also been investigated as burning rate promotors. The formation of iron oxide nanoparticles has been advanced as an explanation for the observed behaviour.[167] Thermolysis of PFS precursors in the presence of Au and acetylene gas has also been explored and is reported to give Au–carbon nanotube composites.[168]

3.7. Redox-active and preceramic microspheres

Solid PFS-microspheres with diameter of *ca.* 2 μm have been prepared by precipitation polymerisation of dimethyl[1]silaferrocenophane with a spirocyclic crosslinker.[169,170] Chemical oxidation with iodine gave positively charged particles. These then underwent electrostatic self-assembly with negatively charged silica spheres to form composite superstructures in which the larger organometallic core was surrounded by the smaller silica particles (Fig. 16).

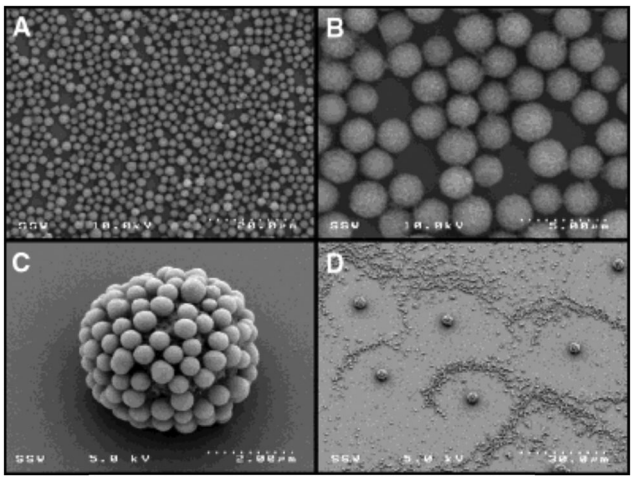

Fig. 16 SEM micrographs of: (A) PFS microsphere monolayer. (B) Higher magnification of a close packed region. (C) Negatively charged silica microspheres electrostatically bound to the surface of oxidised poly-ferrocenylsilane microspheres. (D) Surface patterns of core–corona oxidised PFS microsphere–silica assemblies circumscribed by regions of silica spheres. Reproduced with permission from ref. 169. Copyright 2001 American Chemical Society.

Thermal treatment proceeded with shape retention to give ceramic microspheres containing α-Fe nanoclusters embedded within a silicon carbide–carbon matrix. The magnetic properties of the ceramics could be tuned from the superparamagnetic to the ferromagnetic state by varying the pyrolysis conditions.[169] Moreover, the ceramics formed into organised 2-D arrays at the air–water interface under the influence of an externally applied magnetic field.

PFSs with acrylate and vinyl imidazole side groups have been used as microgel precursors.[171] Microfluidic processing enabled a liquid jet of the two immiscible monomers to form monodisperse PFS macro-crosslinker droplets. Cross-linked microgel particles were then obtained *via* UV-induced cross-linking of the colloids (Fig. 17). The redox-active microspheres could act as a reducing agent for the formation of silver nanoparticles from $AgPF_6$, as well as directing the growth of the resulting Ag structures. Moreover, the loading and release of guest molecules such as rhodamine 6G, a fluorescent dye, was demonstrated.

3.8. Layer-by-layer assembly of water-soluble polyferrocenylsilane polyelectroytes

Electrostatic superlattices formed by layer-by-layer (LbL) self-assembly of oppositely charged polymers have been of interest since the technique was first reported in 1991 by Decher.[172,173] The LbL self-assembly method is based on electrostatic intermolecular forces; it involves the sequential adsorption of polyanions and polycations from aqueous electrolyte solutions onto a substrate surface, forming multilayer films and hollow nanostructures with defined structure and function. The formation of organic–organometallic PFS-based superlattices by the layer-by-layer deposition process involved anionic poly(styrene-sulfonate) and the a cationic water-soluble PFS on primed

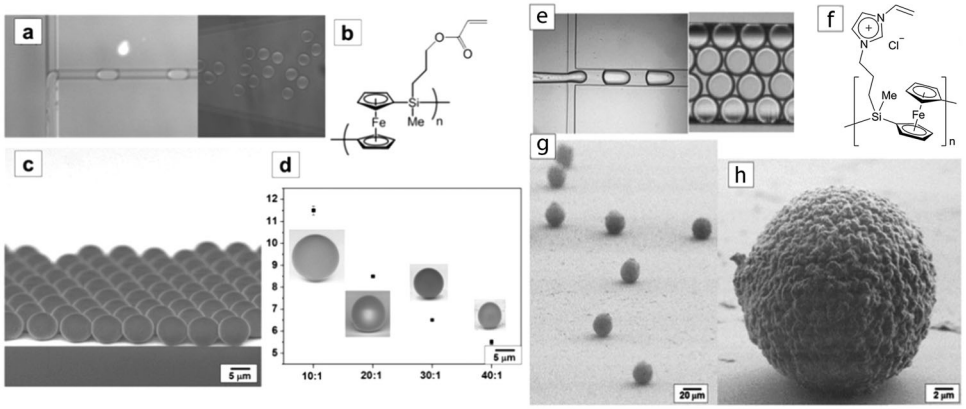

Fig. 17 (a) Images of head-on forming droplets of PFS (b). (c) SEM images of the microgels formed from (b). (d) The diameter of PFS (b) microspheres produced at increasing water-to-oil flow rate ratios, *e.g.* 10: 1 Q_w = 1 mL min^{-1}, Q_{PFS} = 0.1 mL min^{-1}. (e) Hydrogel precursor droplets of PFS (f) formed in a flow focusing microfluidic device. (g) SEM images of PFS (f) microgels, and (h) SEM image of a single PFS (f) microgel particle. Reproduced with permission from ref. 171. Copyright 2014 Royal Society of Chemistry.

Au, Si, and quartz substrates. This yielded regularly stacked, homogeneous electrostatic superlattices.[174] In another study, poly(ferrocenyl(3-ammoniumpropyl)methylsilane) was used in conjunction with poly(sodium vinylsulfonate) to form a multilayer film on quartz.[70] It was noted that a linear relationship between optical absorbance and the number of bilayers was indicative of the formation of well-defined multilayers.

Transition metal catalysed ROP and nucleophilic substitution methodologies allowed the production of both water soluble PFS polycations and polyanions, compounds with charges on the polymer side groups which made them suitable for fabrication of all-organometallic multilayer thin films using a LbL method.[175,176] The polyions were deposited electrostatically onto a variety of substrates, such as silicon, gold, and hydrophilic/hydrophobically patterned substrates, the latter of which led to the formation of laterally structured PFS multilayers.[177] It was reported that hydroxyl-terminated monolayer alkanethiol regions prevented deposition of the polyions due to hydrogen-bonding interactions with the solvent.

The syntheses of PFS polyelectrolytes *via* photolytic ROP gave well-controlled architectures with desired molecular weight and low polydispersity, which are not accessible by transition metal catalysed ROP.[62] Furthermore, such control was not possible using *n*-BuLi-initiated anionic ROP due to its intolerance towards the necessary functional groups. Preliminary studies on LbL assembly indicated that films made from monodisperse low molecular-weight PFSs possessed a considerably thinner bilayer thickness and higher refractive index than those made from polydisperse PFSs.[62] Subsequent findings determined that the number of deposited bilayers primarily controlled bilayer thickness, though ionic strength had a significant influence.[178,179] The refractive index of films of thickness up to 55 nm were considerably higher than those of other common polyelectrolytes, and values varied over the spectral range from 1.53 (near-infrared) to 1.8 (ultraviolet). Multilayer films have also been fabricated from LbL deposition of PFS and a redox-inert polymer, PEI (PEI: poly(ethylene imine)), onto various

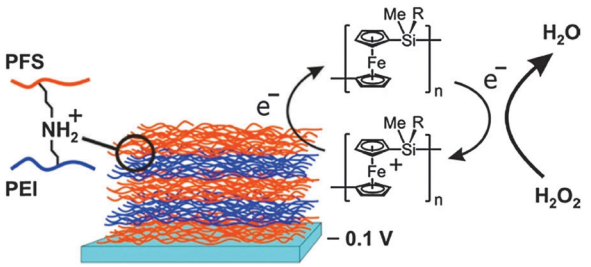

Fig. 18 Poly[ferrocenyl(3-bromopropyl)methylsilane] and PEI were employed in a layer-by-layer deposition process to form covalently connected, redox-active multilayer thin films. Upon oxidation and reduction, these covalently interconnected layers do not disassemble, in contrast to PFS layers featuring similar backbone structures that are held together by electrostatic forces. Reproduced with permission from ref. 180. Copyright 2009 American Chemical Society.

substrates (Fig. 18).[180] Interconnected by a covalent linker, the PFS/PEI multilayers were effective for the electrochemical sensing of ascorbic acid and hydrogen peroxide *via* an amperometric response, and showed improved sensing performance at higher bilayer numbers.

In 2014 a new technique was reported to allow the quantitative visualisation of subnanometer height changes occurring in thin films of PFSs upon reversible electrochemical oxidation/reduction *in situ* and in real-time, electrochemistry imaging ellipsometry (EC-IE).[181] For example, a height change of 6 ± 1 Å was deduced from imaging ellipsometry data on the two step oxidation of surface grafted PFS on a patterned area of 600 × 400 μm^2. The layer-by-layer self-assembly of high molar mass, double stranded DNA and PFS polycations into thin films and microcapsules with three-dimensional macroporous structures was also demonstrated.[182] It was noted that the formation of the porous architecture was likely due to the persistence length and chain-length mismatch of the two components, as well as the hydrophobicity of the PFS backbone.

The disassembly of polyferrocenylsilane LbL assembled thin films has been electrochemically controlled by prolonged

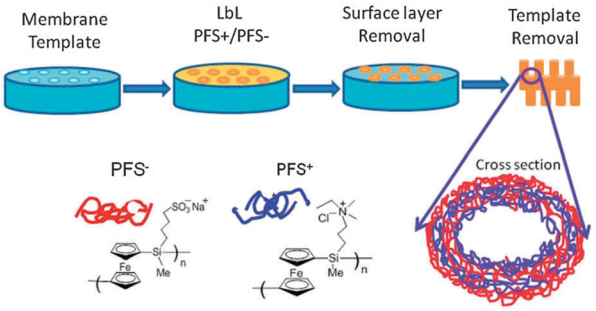

Fig. 19 LbL assembly of redox polyelectrolyte nanotubes. Reproduced with permission from ref. 185. Copyright 2013 Royal Society of Chemistry.

exposure to a low potential. The kinetics and profile of the multilayer release were controlled by blocking layers, surface charge, and the type of supporting electrolyte solution.[183] The driving force for this release of PFS was proposed to be electrostatic polyion binding and electrostatic repulsion. A high degree of control over the release of a fluorescent dye labelled Dextran positioned within the multilayer structure was achieved by varying the electrode potential.[184] The application potential of the PFS system in controlled molecular delivery, such as dosing in microfluidics, was also demonstrated with nanotubes. A template assisted layer-by-layer technique was used to fabricate redox-responsive nanotubes from composite mixtures of PFS and PAA. Multilayers of the polyions were deposited onto the inner pores of either anodised porous alumina or track-etched polycarbonate membranes, followed by subsequent removal of the template (Fig. 19).[185] Electrochemically controlled release of dye labelled dextran molecules and negatively charged quantum dots were achieved upon electrochemical stimulation of the nanotubes.

Various approaches have been reported for introducing redox-active molecules onto metallic electrodes. One of the first methods involved the insertion of PFSs into preformed self-assembled monolayers of hydroxyl-terminated alkane thiols on gold from toluene solution.[186] Very low surface coverages were achieved by inserting from very dilute PFS solutions. Alternatively, PFS with a thiol end-group was end-grafted onto gold substrates, forming redox-active monolayers.[187] In aqueous $NaClO_4$, two reversible redox peaks were observed, as expected for the stepwise oxidation of PFSs (Section 3.4). It was determined that the oxidation process in the first step was controlled by the diffusion of counter-ions into the polymer film, while the second displayed greater reversibility. This was attributed to the swelling of the partially oxidised PFS films in the aqueous electrolyte solutions, leading to a higher segmental mobility of the polymer chains and a much increased counter-ion mobility within the film. In a similar manner, sulfur end-functionalised PFDMS was grafted onto gold surfaces to form a redox responsive monolayer. The adherence and friction of the films were reversibly controlled from an oxidised state (high adhesion, high friction) to a reduced neutral state (low adhesion, low friction), with the gold substrate an electrode.[188] This electrode rectification behaviour could be useful in applications in thin film devices based on PFS films. Gold electrodes have also been modified by cathodic reduction of the Au substrates, immersed in a solution of imidazolium-functionalised PFS chains in the poly(ionic liquid), 1-ethyl-3-methylimidazolium ethyl sulfate.[189] The polymer films were employed as an ascorbic acid sensor, exhibiting high sensitivity, stability, and reproducibility. A high sensitivity to ascorbic acid was also exhibited by PFS films formed by an alkylation reaction of an amine monolayer on silicon or gold surfaces with PFS chains featuring iodopropyl side groups.[190] Also, as the anchored PFS chains possessed unreacted iodopropyl side groups they could be derivatised into a range of functionalities including cationic, anionic, hydrophilic, or hydrophobic moieties. This system constituted a highly versatile platform for facile chemical modification of electrodes. In addition to a PFS with iodopropyl side groups (PFS-I), undecylsulfonate-substituted thin films ($PFS–SO_3^-$) were immobilised on electrode surfaces (Fig. 20).[191] The authors reported that the surface characteristics of the two films could be reversibly switched between hydrophobic and hydrophilic states under electrochemical control: the water contact angle for PFS-I varied between 80° (reduced state) to 70° (oxidised state) over repeated cycles. However, an opposite change in wettability was observed for $PFS–SO_3^-$, where the values observed varied from 59° (reduced state) to 77° (oxidised state). Unfortunately, the observed switching of the $PFS–SO_3^-$ films was not possible with water as a solvent, which would restrict the potential *in situ* application of this system in aqueous solutions, for example in microchannels for flow control.[191]

Layer-by-layer assembly has also been used to tune the photonic stop band of colloidal photonic crystals, which were

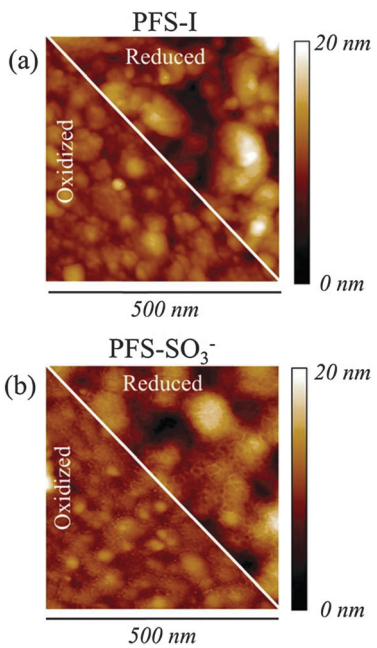

Fig. 20 Tapping-mode AFM images in air of (a) PFS-I and (b) $PFS-SO_3^-$ films upon redox at a scan size of 500 nm and a *z* scale of 20 nm. Reproduced with permission from ref. 191. Copyright 2015 American Chemical Society.

discussed in depth earlier (Section 3.5). Silica colloidal photonic crystals with embedded redox-active PFS polyelectrolyte multilayer planar defects were prepared by growing a PFS polyelectrolyte in a LbL fashion onto a polydimethylsiloxane sheet. This multilayer was transfer-printed onto the surface of a colloidal photonic crystal before a second colloidal photonic crystal was grown on top of the defect.[192] The structural defect allowed for reversible tuning of the transmitting state when subjected to redox cycling. Controlled infiltration and LbL assembly of low molecular weight PFS electrolytes into the interstitial voids of colloidal photonic crystals allowed for nanometre-scale fine optical tuning in a cost-effective manner.[193] Low molecular weight and low PDI samples were used to ensure uniform coating across the photonic lattice. As this method could be applied to vary the optical response of any porous structure, amorphous photonic media would benefit as multiple or resonant scattering could be accurately modulated by deposition of a dielectric thin coating on the inner pore or cavity walls.

The redox-controllable permeability of PFS-based polyelectrolyte microcapsules has also been studied. Polyelectrolyte capsules were prepared *via* layer deposition for polyanion/polycation pairs in the sequence of $(PSS^-/PAH^+)_2$ $(PFS^-/PFS^+)_3$ (PSS^-: poly(styrene sulfonate), PAH^+: poly(allylamine hydrochloride)) on melamine formaldehyde (MF) cores.[194] Once the capsules were assembled, the ferrocene units were chemically oxidised, which triggered capsule swelling, thus increasing shell wall permeability, consistent with the electrostatic repulsion within the polyelectrolyte shell due to the excess positive charge on the chains, which would increase the distance between segments. The substantial swelling could be suppressed by the application of an additional coating bearing common redox-inert species of PSS^- and PAH^+ on the outer wall of the capsules.[194]

3.9. Plasma and electron beam etch resists

The constant demand for smaller, faster, and more energy efficient electronic devices has necessitated increased component density, and thus smaller component sizes. The use of lithography has been integral to the progress of integrated circuit technology. PFS homopolymers and also block copolymers (see Section 5.2.2) have attracted significant attention for lithographic applications as a result of impressive etch resistance of the organometallic component which enables pattern transfer to a substrate. Thus, large-area PFS patterns have been fabricated by using various soft lithographic techniques, and subsequently transferred into the underlying substrate by reactive ion etching (RIE).

PFMPS has been reported as a high-contrast etch mask material,[195] for example in the fabrication of uniform, nanoporous polyethersulfone membranes.[196,197] Under RIE PFS was remarkably stable compared to organic polymers, due to the presence of iron and silicon in the main chain. For example, when exposed to an oxygen plasma a thin, non-volatile oxide layer was formed at the surface which gave rise to relatively low etching rates.[198] Low etching rates of PFMPS were also obtained when fluorocarbon plasmas were applied. With the oxide layer mask possessing such a high etching barrier, access to structures with high aspect ratios was possible, with potential use also in very thin resist layer applications.

PFSs bearing pendant photo-crosslinkable methacrylate groups were used as negative-tone photoresists for photolithographic patterning.[35] Although a low-cost method for the controlled two dimensional patterning of PFS networks over large areas, crosslinking of methacrylate side groups by free radicals that propagated beyond the edges of the exposure pattern did not allow for reproducible features below a 3 μm scale. A PFS bearing metal carbonyl moieties has also been used as a negative-tone photoresist and an electron-beam resist. $[Fe(\eta^5\text{-}C_5H_4)_2Si(Me)\{Co_2(CO)_6C_2Ph\}]_n$ (Co-PFS), $[Fe(\eta^5\text{-}C_5H_4)_2Si(Me)\{Mo_2Cp_2(CO)_4C_2Ph\}]_n$ (Mo-PFS), and $[Fe(\eta^5\text{-}C_5H_4)_2Si(Me)(Ni_2Cp_2C_2Ph)]_n$ (Ni-PFS) were synthesised by the clusterisation of carbon–carbon triple bonds in an acetylide substituted PFS.[76,77] All three polymers functioned as negative-tone resists in electron-beam lithography to give well formed microbars and microdots (Fig. 21). Co-PFS and Mo-PFS were also found to function well as a photoresist for UV-photolithography, giving sharp micron-sized features after UV exposure. On the other hand, Ni-PFS was not able to act as a photoresist due to the absence of carbonyl ligands, which prevented decarbonylation and crosslinking of the polymer, the proposed cause of the reduced solubility of exposed regions of Co-PFS and Mo-PFS.[77]

Capillary force lithography (CFL) is a non-photolithographic technique in which a polymer, above its glass transition temperature but initially confined in a thin film, is squeezed out from areas of contact between a PFDMS stamp and silicon substrate. It diffuses into the grooves where structures are formed along the vertical walls of the stamp due to capillary rise.[199] The molar mass of a polymer, processing temperature, and initial polymer film thickness all have a direct impact on the quality of the CFL polymer patterns and so must be controlled. Unsymmetrically substituted PFSs have been demonstrated to be ideal polymers for CFL as they will not crystallise.[200] If the polymer resist lines have a uniform thickness, the resulting patterns can then be used as lithographic masks.

Although PFSs have seen use and photoresists for photolithographic patterning, conventional lithographic techniques

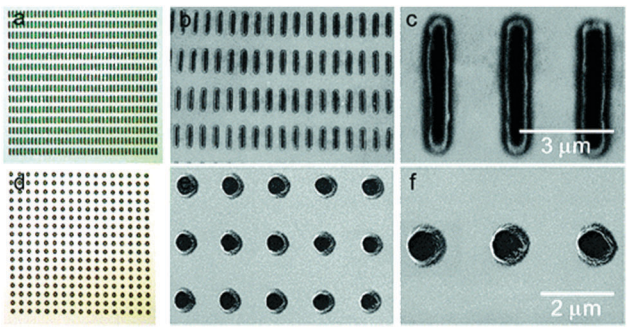

Fig. 21 (a) Optical micrograph and (b and c) scanning electron micrographs of Mo-PFS microbars (0.5 × 4.0 μm^2), (d) optical micrograph, and (e and f) scanning electron micrographs of Ni-PFS microdots (diameter = 1.0 μm). Reproduced with permission from ref. 77. Copyright 2005 American Chemical Society.

have become increasingly difficult to use for the formation of features with dimensions smaller than 50 nm.[54] Block copolymers have offered an alternative approach for the fabrication of structures on the nanometer scale, as they can self-assemble into a variety of nanoscale morphologies (see Section 5.1).

4. Synthetic routes to polyferrocenylsilane block copolymers (PFS BCPs)

4.1. ROP routes to PFS BCPs

Synthetic methods that allow the preparation of well-defined BCPs have been available for all-organic materials since the 1950s. Living anionic polymerisation, and more recently ring-opening metathesis polymerisation and "controlled" radical polymerisation, have played a key role in the development of BCP science.[201–216] Synthetic routes to PFS-containing BCPs were first developed in the mid 1990s and, depending on the method, provide either moderate or excellent control over the resulting segmented structures.

4.1.1. Metal-catalysed ROP routes to PFS BCPs. Transition metal-catalysed ring-opening polymerisation of dimethylsila[1]ferrocenophane, has been shown to proceed in solution at room temperature using Pt, Pd and Rh catalysts.[34,38,39,211] The addition of termination agents bearing a Si–H bond (*e.g.* Et_3SiH) can be used to control the molecular weight of the polymer by controlling the initial monomer-to-silane ratio.[39,41,212] This method can easily be extended to the use of polymers bearing a terminal Si–H group to allow the formation of PFS-containing BCPs.[39] For example, the preparation of a PFDMS-*b*-PEO (PFDMS: polyferrocenyldimethylsilane, PEO: polyethylene oxide) amphiphilic BCP was achieved through this method starting from a hydroxyl-terminated PEO.[41] First, a terminal Si–H functionality was incorporated by a condensation reaction between the polymer and methylphenylchlorosilane. Reaction of the hydrosilyl-terminated PEO with dimethylsila[1]ferrocenophane in the presence of Karstedt's catalyst under ambient conditions yielded the desired PFDMS-*b*-PEO diblock copolymer. A PFDMS-*b*-PDMS-*b*-PFDMS (PDMS: polydimethylsiloxane) triblock copolymer has also been prepared *via* this method by using a difunctional PDMS polymer with terminal Si–H bonds at either end of the polymer chain.[213] As transition metal-catalysed ROP of ferrocenophanes is characterised by random chain termination events involving reductive-elimination at the metal centre[38] it is not a living process and the PFS segments in the resulting BCPs therefore have relatively high polydispersities (PDI > 1.5).

4.1.2. Living anionic ROP routes to PFS BCPs. Living polymerisations can allow the synthesis of polymeric materials with excellent control over molecular weights, permit end-group functionalisation and BCP synthesis, and access to materials with low polydispersities (PDI < 1.1) as both chain transfer and chain termination reactions are either absent or minimal.[214–216] These processes are therefore the method of choice for the preparation of tailored, well-defined BCPs. Two mechanistically distinct living anionic polymerisation methods have been developed for the synthesis of PFS BCPs using silicon-bridged [1]ferrocenophane monomers and these are discussed in turn.

4.1.2.1. Living anionic ROP involving Cp–Si bond cleavage. The use aryl- and alkyllithium reagents, such as phenyllithium (PhLi) and *n*-butyllithium (*n*BuLi), as initiators for the synthesis of PFS homopolymers and BCPs was reported over the 1994–1996 period.[45,46] This allowed the preparation of well-defined materials with controlled molecular weights and narrow polydispersities (PDI < 1.2). The proposed mechanism involves nucleophilic attack of the initiator at the bridging silicon centre followed by Cp–Si cleavage to generate an anionic propagating site based on the iron-coordinated Cp ring.[2] The method has been applied to silicon-bridged [1]ferrocenophanes with a variety of substituents at silicon, allowing access to PFS homopolymers and segments in BCPs that are able to crystallise (*e.g.* PFDMS,[46] PFDES[217]) or which are amorphous (*e.g.* PFEMS,[48,49] PFMPS,[48,218] PFiPMS[51]). Degrees of polymerisation of 300 and higher have been reported and, although obtaining the high molar masses required to realise PFS-rich BCPs is a challenge, it is achievable.[49,219] The 'living' nature of this polymerisation allows different monomers to be added sequentially in order of descending propagating site reactivity to form well-defined BCPs. The reactivity of living anionic-chain end groups for a number of common monomers has been found to follow the sequence PI ≥ PS > PFDMS > P2VP ≥ PDMS ≈ PMVS (PI: polyisoprene, PS: polystyrene, P2VP: poly-2-vinylpyridine, PMVS: polymethylvinylsiloxane).[46] Following this reactivity series allowed the synthesis of organic–organometallic BCPs such as PS-*b*-PFDMS (see Scheme 11A; R = R′ = Me) and organometallic–inorganic BCPs such as PFDMS-*b*-PDMS (see Scheme 11B; R = R′ = Me).[46,220] The use of this method was subsequently extended to other polymerisable monomers, which has allowed the preparation of PI-*b*-PFDMS[221] and PFDMS-*b*-PMVS.[222] Phosphorus-bridged [1]ferrocenophanes also undergo living anionic ROP in the presence of aryl- and alkyllithium reagents[223] and this has allowed the preparation of PFPP-*b*-PFDMS-*b*-PDMS (PFPP: poly(ferrocenylphenylphosphine)).[224]

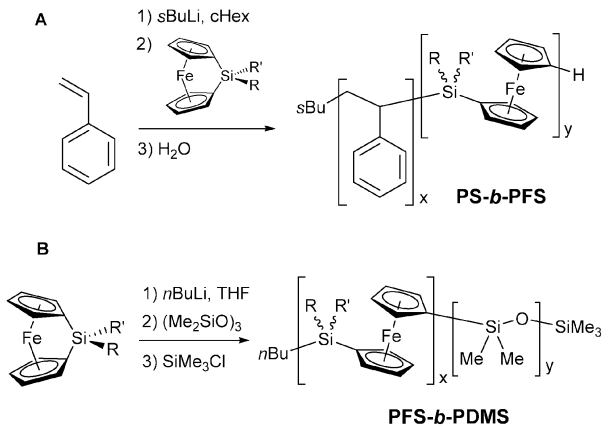

Scheme 11 Sequential living anionic polymerisation of (A) styrene in cyclohexane (cHex) and sila[1]ferrocenophane for the formation of PS-*b*-PFS, and (B) sila[1]ferrocenophane and hexamethylcyclotrisiloxane for the formation of PFS-*b*-PDMS (R = R′ = Me).

The use of difunctional initiators, such as 1,1′-dilithioferrocene and lithium napthalide, has allowed the formation of symmetrical PFS-containing triblock copolymers and pentablock copolymers.[46] The difunctional initiator forms propagating anionic sites at both ends of the resulting polymer chain. This can allow further polymerisation to create a secondary block at both ends of the polymer chain, therefore allowing the formation of symmetric triblock and pentablock copolymers by sequential addition of monomers. A range of PFS-containing materials have been prepared by this method, such as PDMS-*b*-PFDMS-*b*-PDMS, PFDMS-*b*-PS-*b*-PFDMS and PDMS-*b*-PFDMS-*b*-PS-*b*-PFDMS-*b*-PDMS.[46]

In principle, this method can be extrapolated to any monomer that can undergo living anionic polymerisation. However, many monomers require modifications to the procedure due to the presence of side reactions with basic carbanionic initiators and propagating sites. For example, PFDMS-*b*-PDMAEMA (PDMAEMA: poly(dimethylaminoethylmethacrylate)) BCPs have been prepared by a two-step anionic polymerisation (see Scheme 12).[56] PFDMS was end-functionalised with a hydroxyl group by using *tert*-butyldimethylsilyloxy-1-propyllithium as an initiator followed by deprotection of the alcohol functionality under ambient conditions. The deprotected PFDMS-OH was then deprotonated using KH to give an alkoxyanion, which can initiate the anionic polymerisation of DMAEMA monomer, giving the PFDMS-*b*-PDMAEMA BCP with well-defined block lengths and fairly low dispersities (M_n = 11 000, PDI = 1.3).

An alternative method to yield PFDMS-*b*-PMMA (PMMA: poly(methylmethacrylate)) BCPs involved the preparation of a PFS-based atom transfer radical polymerisation (ATRP) macroinitiator.[225] Firstly, PFDMS was prepared by anionic polymerisation and capped with a siloxypropylchlorosilane which was followed by deprotection and isolation to give a PFDMS-OH polymer. The material was subsequently reacted with 2-bromoisobutyric acid to give the desired PFDMS macroinitiator. MMA monomer was then polymerised using the PFS macroinitiator and an ATRP-active Ru-based catalyst to give the PFDMS-*b*-PMMA BCP. The PFDMS content and molecular weights of these materials was easily controlled through varying the macroinitiator-to-monomer ratio, whilst maintaining materials with relatively narrow molecular weight distributions (PDI < 1.2).

PFDMS-*b*-PMMA has also been synthesised through moderation of the reactivity of the propagating anion site (see Scheme 13).[53]

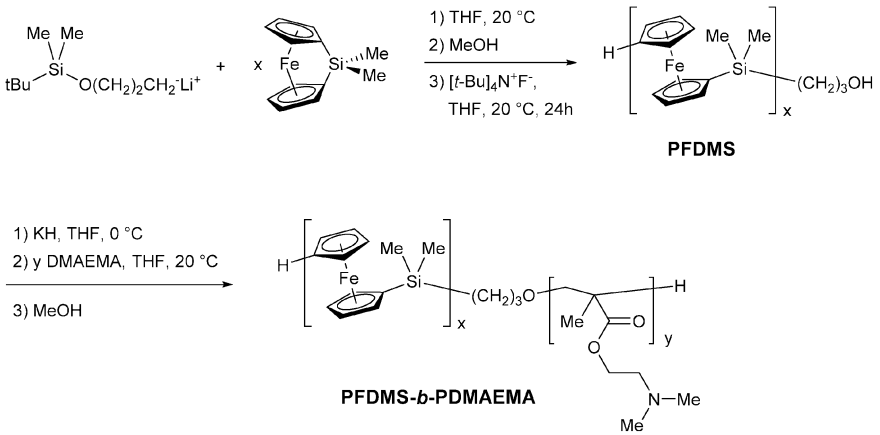

Scheme 12 Synthesis of poly(ferrocenyldimethylsilane)-*block*-polydimethylaminoethylmethacrylate (PFDMS-*b*-PDMAEMA).

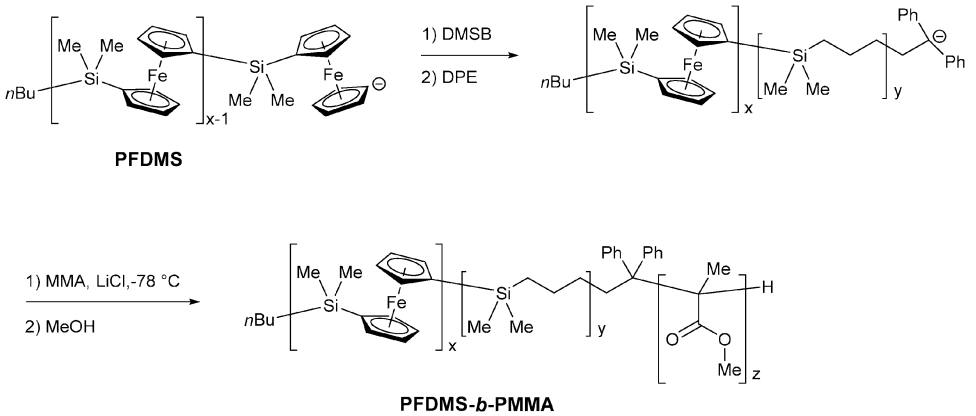

Scheme 13 Synthesis of polyferrocenyldimethylsilane-*block*-polymethylmethacrylate (PFDMS-*b*-PMMA) *via* reactivity mediation method using DMSB and DPE.

This is necessary in order to hinder side reactions involving nucleophilic attack at the carbonyl functionality of the MMA. This was achieved using two additional steps that were performed *in situ* and involved the use of dimethylsilacyclobutane (DMSB) and diphenylethylene (DPE). DMSB was used as a "carbanion pump" to ensure efficient coupling of the DPE at the PFDMS chain terminus. MALDI-TOF analysis of model systems suggested the level of DMSB incorporation was 1–3 repeat units. Significantly, the increased steric bulk associated with the anionic DPE-capped chain end promotes attack at the alkenyl double bond in MMA instead of the carbonyl group. This allowed successful formation of PFDMS-*b*-PMMA BCPs of controlled molecular weights (M_n = 27 000–84 500) and low polydispersities (PDI < 1.1). This approach for reactivity mediation has allowed the synthesis of a number of other PFS BCPs previously unavailable by anionic polymerisation such as, for example, PFDMS-*b*-P2VP,[226] PFDMS-*b*-P*t*BMA (PtBMA: poly-*tert*-butylmethacrylate),[227] PFDMS-*b*-PEO diblock copolymers,[228] PS-*b*-PFDMS-*b*-PMMA[229] and PS-*b*-PFEMS-*b*-P2VP triblock terpolymers,[230] and PMMA-*b*-PFDMS-*b*-PS-*b*-PFDMS-*b*-PMMA pentablock terpolymers.[231]

A number of PFS-*b*-polypeptide BCPs have been prepared by different methods for self-assembly studies and for their potential in biological applications.[232,233] PFDMS-*b*-PBLG (PBLG: poly(γ-benzyl-L-glutamate)) was prepared by a two-step route.[232] Firstly, the PFS segment was synthesised by anionic polymerisation and capped with a protected amine group (see Scheme 14), which was subsequently deprotected upon precipitation into MeOH due to the lability of the protecting group in lower alcohols to give PFDMS–NH_2. This telechelic polymer was used to induce the ROP of γ-benzyl-L-glutamate to afford PFDMS-*b*-PBLG BCPs with controlled molecular weights (M_n = 15 300–30 200) and narrow molecular weight distributions (PDI = 1.13–1.21). This method has also been used for the formation of PFDMS-*b*-PZLys (PZLys: poly(ε-benzyloxycarbonyl-L-lysine))[234] and a range of PFS-*b*-tetrapeptide materials.[235,236] Use of hydroxyl-functionalised PFDMS as an initiator for the ROP of D/L-lactide has allowed the preparation of PFDMS-*b*-PLA (PLA: poly-D/L-lactide).[237]

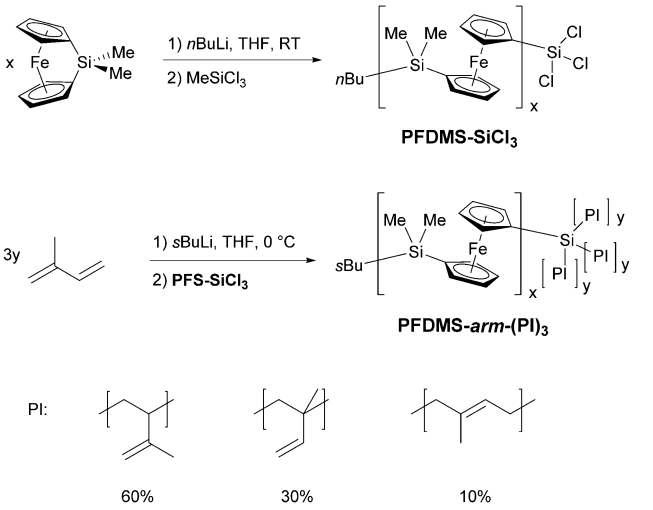

Scheme 15 Synthesis of polyferrocenyldimethylsilane-*arm*-(polyisoprene)$_3$ (PFDMS-*arm*-(PI)$_3$) heteroarm star polymer.

A further strategy to access PFS-*b*-polypeptide BCPs involves the conjugation of two independent homopolymers through a Diels–Alder cycloaddition mechanism to form PFDMS-*b*-PBLG.[233]

Organometallic–organic heteroarm star polymers have also been prepared.[238] A PFDMS-*arm*-(PI)$_3$ was synthesised in a two-step method (see Scheme 15); firstly PFS was prepared by anionic polymerisation and was quenched by dropwise addition to an excess of tetrachlorosilane to give a PFDMS–$SiCl_3$. This was to ensure that only one polymeric chain was grafted onto each silane capping agent. After purification, the PFDMS–$SiCl_3$ was added to an excess of polyisoprenyllithium as a capping agent, which ensured complete substitution of all 3 Cl groups to afford the desired star polymer. Linear-dendritic PFS-containing BCPs have been synthesised by quenching living PFDMS chain ends with chlorine-functionalised PBE (PBE: poly(benzyl ether)) first- or second-generation dendrons.[239,240]

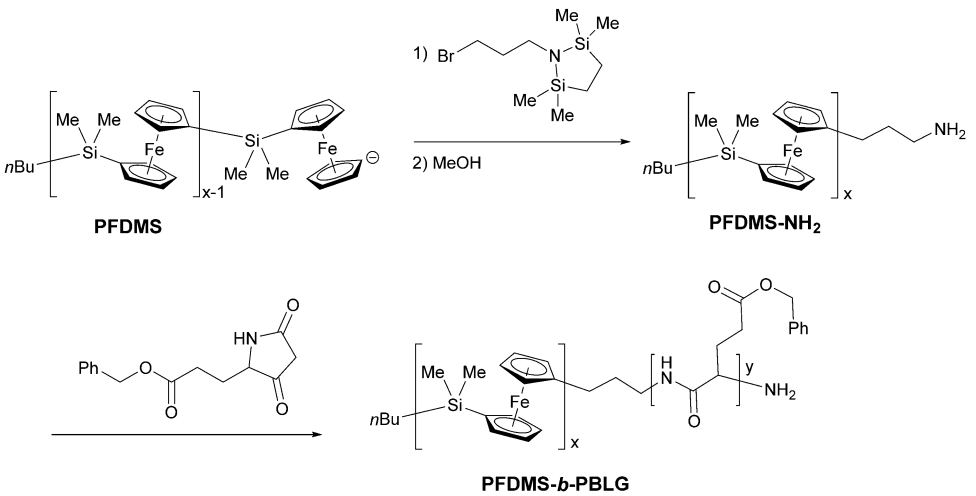

Scheme 14 Synthesis of polyferrocenyldimethylsilane-*block*-poly(γ-benzyl-L-glutamate) (PFDMS-*b*-PBLG).

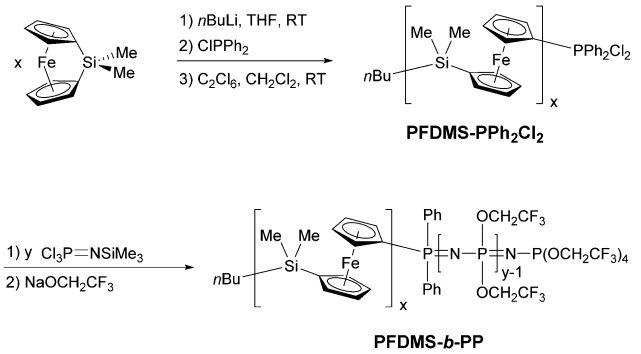

Scheme 16 Synthesis of polyferrocenyldimethylsilane-*block*-polyphosphazene (PFDMS-*b*-PP).

A PS-*b*-PFDMS-*b*-PS triblock copolymer with unsymmetrical PS blocks was prepared *via* a similar method in a "universal methodology" for the preparation of BCPs using chemoselective stepwise coupling between living polymer chains and a heterobifunctional linking agent.[241] PS-*b*-PFDMS was prepared by living sequential anionic polymerisation and the living chains were quenched with chloro(3-chloropropyl)dimethylsilane to yield a Cl end-functionalised BCP. The PS-*b*-PFDMS was subsequently used to quench living PS anions to yield the desired triblock copolymer. This system could essentially allow the preparation of BCPs with block sequences that are unobtainable for materials exclusively prepared by sequential living anionic polymerisation methods.

The formation of the organometallic–inorganic BCP, PFDMS-*b*-PP (PP: polyphosphazene) was reported[242] by combining the living anionic ROP route to PFS with the living cationic polymerisation of phosphoranimines[243–245] (see Scheme 16). This was achieved by capping living PFDMS anions with an excess of chlorodiphenylphosphine to give PFS–PPh_2 after purification. The homopolymer end group was then chlorinated using hexachloroethane to give the dichlorodiphenylphosphino-functionalised PFS derivative. The telechelic PFS–PPh_2Cl_2 reacted with different amount of phosphoranimine monomer and finally the material was treated with an excess of $NaOCH_2CF_3$ to make the materials air- and moisture-stable. Materials were prepared with a range of molecular weights (M_n = 27 170–84 490) and block ratios with narrow molecular weight distributions (PDI = 1.09–1.19).

The combination of living anionic polymerisation techniques with copper-catalysed azide–alkyne Huisgen cycloaddition (CuAAC) "click" chemistry has facilitated the rapid expansion of accessible functional macromolecular materials.[246] This type of approach has been used for the convenient preparation of a range of PFS-containing diblock copolymers (see Scheme 17),[55] of which several have not been previously possible to access through sequential anionic methods. Alkyne-functionalised PFDMS was synthesised by quenching living PFDMS chains with the protected alkyne, 4-[(trimethylsily)ethynyl]lbenzaldehyde (TSEBA). The polymer was deprotected, reacted with a small excess of the relevant azide-functionalised polymer with a Cu(I) catalyst and subsequently purified to give the targeted BCP in high yield. This method has been effective in the preparation of PFS three-armed miktoarm star materials by sequential click reactions of azide-terminated polymers to a central functional core molecule.[247]

4.1.2.2. "Photocontrolled" living anionic ROP involving Fe–Cp bond cleavage. In the presence of light, silicon-bridged [1]ferrocenophanes can also be polymerised by anionic reagents which are insufficiently reactive to attack the bridging silicon atom. The unusual and interesting mechanism has been shown to involve Fe–Cp bond cleavage and therefore differs from the aryl- or alkyllithium-initiated living anionic polymerisation in which Cp–Si bonds are broken.[248]

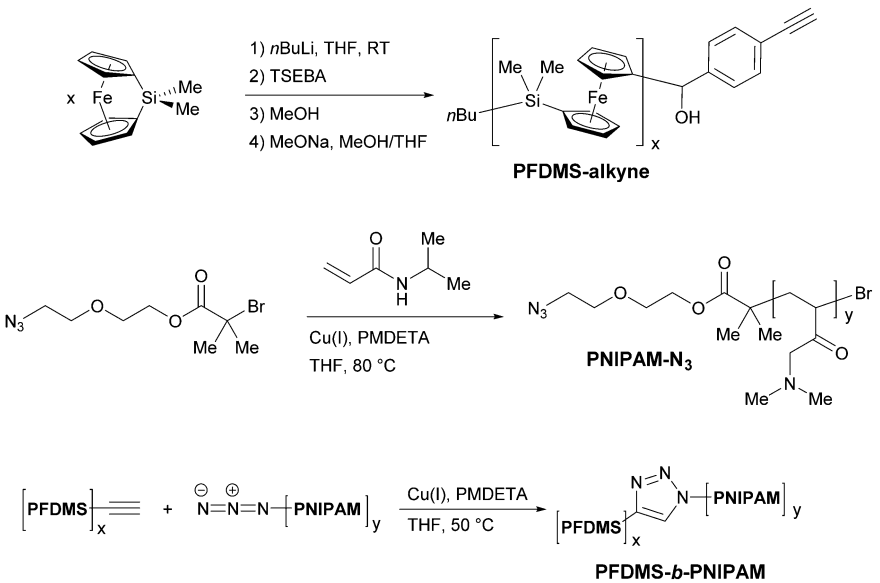

Scheme 17 Synthesis of polyferrocenyldimethylsilane-*block*-poly(*N*-isopropylacrylamide) (PFS-*b*-PNIPAM) *via* an azide–alkyne Huisgen cycloaddition (CuAAC) "click" reaction (TSEBA: 4-[(trimethylsilyl)ethynyl]benzaldehyde; PMDETA: *N*,*N*,*N*′,*N*″,*N*″-pentamethyldiethylenetriamine)).

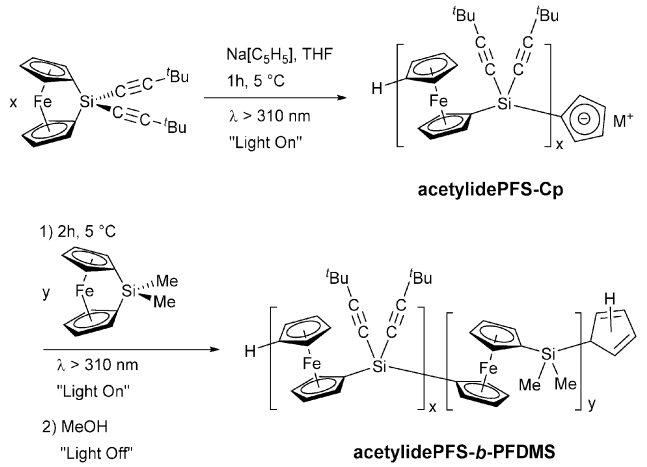

Scheme 18 Synthesis of polyferrocenyldi(*t*-butylacetylidyl)silane-*block*-polyferrocenyldimethylsilane (acetylide PFS-*b*-PFDMS) *via* photolytic living anionic polymerisation.

The detailed role of light has not been fully elucidated but it appears to involve enhancement of electrophilicity of the Fe centre *via* the population of excited states with some ligand character, presumably accompanied by solvent co-ordination at iron and a haptotropic shift of the Cp ring.[67] Mildly basic cyclopentadienyl anions $[C_5H_4R]^-$ (R = H/Me), rather than highly basic reagents such as *n*BuLi, have been used as the anionic initiators. This leads to a relatively mild protocol that is functional group tolerant and a useful method for the synthesis of PFS BCPs with substituents that are inaccessible by the aryl- or alkyllithium-initiated route due to side reactions.

An example of such a BCP prepared through the ''photo-controlled'' living anionic ROP method is acetylide PFS-*b*-PFDMS (see Scheme 18) which possesses acetylide groups attached to silicon.[248] Initially, an acetylide-substituted monomer in THF was irradiated with UV light in the presence of $Na[C_5H_5]$ initiator to yield living PFS with pendant acetylide groups. After turning off the irradiation source, dimethylsila[1]ferrocenophane was added and the reaction mixture was irradiated again. The acetylide PFS-*b*-PFDMS was isolated after addition of methanol to quench the reaction giving BCPs with predictable molecular weights (based on the monomer to $M[C_5H_5]$ ratio) and low polydispersities. This method has also allowed the formation of a range of BCPs, including PFE-*b*-PFDMS (PFE: polyferrocenylethylene),[249] PFPP-*b*-PFDMS,[250] PFPP-*b*-PFS_F[60] (PFS_F: PFS with fluorinated side groups), PFEMS-*b*-PFS_A[251] (PFS_A: PFS with aminoalkyl side groups) and PFS-*b*-PCE[252] (PCE: poly(cobaltoceniumethylene)) materials to be synthesised.

Organic–organometallic PS-*b*-PFS BCPs have been prepared by a combination of conventional and photocontrolled anionic polymerisation.[253] Firstly, PS was prepared using an alkyllithium initiator and the living anionic chain ends were capped with dichlorodimethylsilane. The resulting PS–$SiMe_2Cl$ homopolymer was subsequently reacted with magnesocene and then chlorotrimethylsilane to give a PS–Cp macroinitiator. The telechelic polymer was irradiated with UV light in the presence of acetylide-functionalised sila[1]ferrocenophane monomer to give the targeted PS-*b*-PFS diblock copolymer. Materials were prepared with excellent molecular weight control and narrow distributions (PDI < 1.2). This synthetic approach has been extended to use with ferrocenophane monomers with pendant ruthenocene units.[63]

4.1.3. Post-polymerisation functionalisation of PFS BCPs. A further route to targeted PFS-based BCPs involves post-polymerisation functionalisation using side groups introduced during living anionic ROP. For example, PFDMS-*b*-PBLG BCPs were prepared by hydrogenative cleavage of the benzyl group in the PBLG block with H_2/Pd.[232] This yielded amphiphilic PFDMS-*b*-PGA (PGA: poly-L-glutamic acid) BCPs which were soluble in 0.1 M NaOH.

A highly metallised PFS-based BCP has been prepared by post-functionalisation of acetylide PFS-*b*-PFDMS.[248] The pendant acetylide groups were reacted with a nickel-based cluster reagent $[NiCp(CO)]_2$ (Cp = η^5-C_5H_5) (see Scheme 19), forming NiPFS-*b*-PFDMS materials which can form novel bulk-state morphologies with Ni/Fe and Fe only domains. Similar methods have been used to functionalise organic–organometallic PS-*b*-PFS BCPs with cobalt and gold complexes.[253]

Recently, a general route for the controlled functionalisation of PFS-*b*-PMVS *via* a thiol–ene ''click'' reaction has been reported (see Scheme 20).[254] Firstly, PFDMS-*b*-PMVS was synthesised by sequential living anionic polymerisation. This was followed by functionalisation of the pendant vinyl groups along the PMVS block backbone with a range of thiols using UV irradiation and a photoinitiator. However, due to the localised density of vinyl groups within the block, significant cross-linking occurred along the PMVS block. Copolymerisation of the PMVS block with PDMS to reduce the number of vinyl groups and decrease unintended cross-linking was performed,

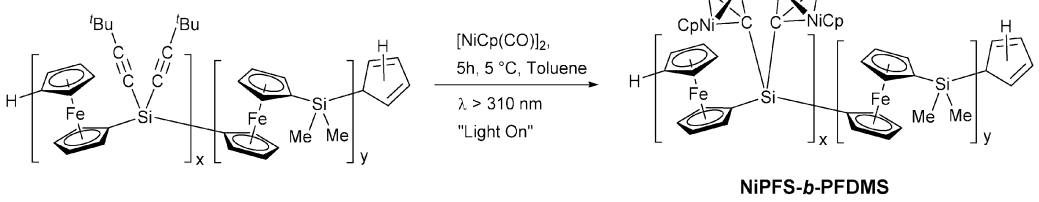

Scheme 19 Synthesis of highly metallised NiPFS-*b*-PFDMS through post-polymerisation functionalisation of acetylide PFS-*b*-PFDMS with $[NiCp(CO)]_2$.

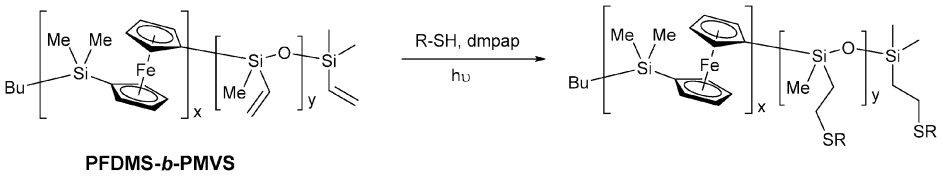

PFDMS-*b*-PMVS

Scheme 20 Functionalisation of polyferrocenyldimethylsilane-*block*-polymethylvinylsiloxane (PFDMS-*b*-PMVS) *via* a UV initiated thiol–ene "click" reaction (dmpap = the photoinitiator 2,2-dimethoxy-2-phenylacetophenone).

which increased the efficiency of thiol functionalisation. This approach is particularly effective for tuning the solubility of the resulting material or for incorporation of complex functionality for specific applications.

Linear-hyperbranched PFS BCPs have been prepared by post-polymerisation functionalization.[255] First, a linear diblock copolymer was prepared by sequential photocontrolled anionic ROP of dimethyl[1]silaferrocenophane and methylvinyl[1]-silaferrocenophane. The second block was then functionalised by the hydrosilylation polyaddition of different silane-based AB_2 monomers.

5. PFS BCPs: properties and applications

5.1. PFS BCP self-assembly in bulk and thin films

5.1.1. Self-assembly of PFS diblock copolymers to form phase-separated materials. PFS BCPs phase-separate on the nanoscale due to the immiscibility of the PFS block with a wide range of organic or inorganic coblocks. This allows the formation of a variety of interesting nanostructured materials with periodic iron-rich domains and varied morphologies.[256] Following initial reports in the mid 1990s,[46] bulk and thin film self-assembly has been studied in detail for a variety of PFS-containing BCPs including PFDMS-*b*-PMMA,[53,257] PI-*b*-PFDMS,[258] PS-*b*-PFDMS,[259,260] PS-*b*-PFEMS[49,219,261] and PS-*b*-PFiPMS.[51] TEM micrographs of different solid state bulk morphologies for PS-*b*-PFEMS,[49] PFDMS-*b*-PMMA (blended with homopolymer),[257] and PMMA-*b*-PFDMS-*b*-PS-*b*-PFDMS-*b*-PMMA BCPs are shown in Fig. 22.[231] Phase diagrams[262] for both PS-*b*-PFDMS[259] and PS-*b*-PFEMS[49,219] BCPs have been reported previously. In the bulk, microtomed sections of these materials can be observed by TEM without the need of staining due to the increased scattering ability of the electron-rich PFS domains compared to those of organic polymers.[46] Complications can arise during the solid-state self-assembly of PFS BCPs with symmetrical *n*-alkyl substituents at the silicon centre (*e.g.* poly(ferrocenyldimethylsilane), PFDMS) due to the semi-crystallinity of the PFS block; this is because crystal break-out competes with the incompatibility of the blocks as the driving force for self-assembly.[263] Formation of self-assembled structures with a high volume fraction of the organometallic PFS block has also proved challenging, however examples of these have now been reported.[51,219] In the case of lamellae-forming PS-*b*-PFDMS, crystallisation of the PFDMS can be confined by the higher T_g organic domains.[264] The effect of crystallisation

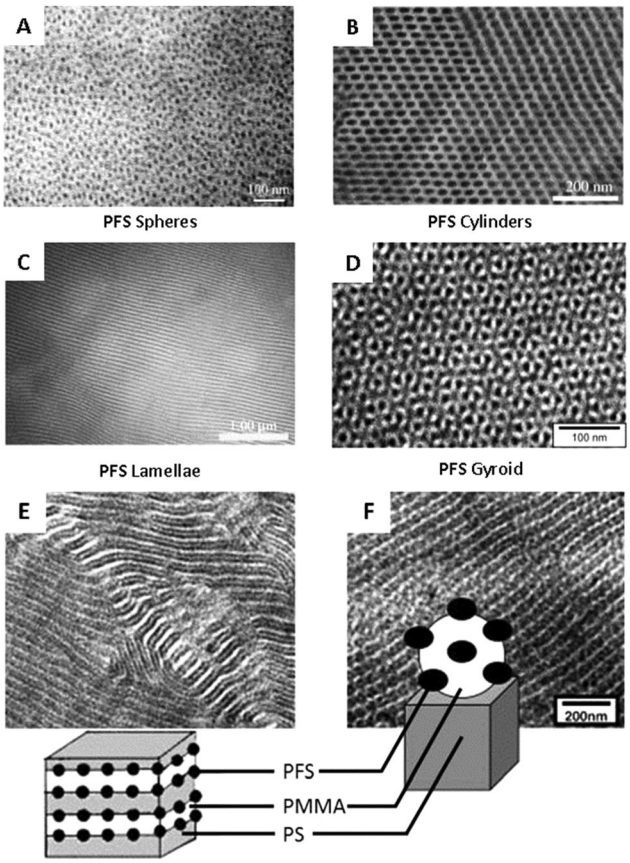

Fig. 22 TEM micrographs for morphologies in the bulk state of PS-*b*-PFEMS (a–c), PFDMS-*b*-PMMA (blended with homopolymer) (d) and PMMA-*b*-PFDMS-*b*-PS-*b*-PFDMS-*b*-PMMA. (e and f) Reproduced with permission from ref. 49 (copyright 2005 American Chemical Society), ref. 231 (copyright 2004 John Wiley & Sons Inc.), and ref. 257 (copyright 2004 American Chemical Society).

can be avoided by using unsymmetrically substituted PFSs (*e.g.* poly(ferrocenylethylmethylsilane), PFEMS) which do not crystallise.[49] It has been shown that, for the PS-*b*-PFDMS and PI-*b*-PFDMS systems, oxidation of the PFDMS block influences the order–disorder transition temperature of the phase-separated morphologies.[265,266] Moreover, in depth studies of the thermodynamic interactions in PS-*b*-PFDMS by birefringence, SAXS, and SANS allowed the determination of the Flory Huggins interaction parameter χ between PS and PFDMS to be *ca.* 0.037 at 25 °C, and is similar to that for PS and PI.[266] The value of $\chi_{PI-PFEMS}$ has been estimated as 0.17.[267]

Self-assembled BCP thin films can be prepared by spin coating dilute solutions of the BCP onto surfaces. The orientation

of cylinder-forming self-assembled PFS BCP thin films can be controlled through manipulation of the film thickness.[268] When the films were thinner than the equilibrium periodicity of the microdomains, cylinders orientated themselves perpendicular to the substrate, whilst films with a thickness close to the equilibrium periodicity exhibited in-plane cylinders. Annealing conditions also affected the orientation of the cylindrical nanostructures.

PFS BCPs can form mesoscale dendritic structures when subjected to hybrid annealing conditions, where thermal and solvent annealing are implemented simultaneously, *via* dewetting phenomena.[269] These hybrid annealing conditions are essential to forming mesoscale morphologies, as using only one of these annealing methods does not lead to notable mesostructures. Alteration of film thickness and the solvent annealing time can lead to the formation of different types of mesostructure.

Blending of a PFS BCP with a different incompatible BCP has shown to allow the preparation of host–guest-type hybridised thin films that cannot be prepared with an individual PFS BCP on its own.[270] For example, blending of PS-*b*-PDMS and PS-*b*-PFDMS BCPs has afforded hexagonally perforated lamellae thin films with PFDMS "guest" spheres, coated in PS spheres in a PDMS "host" matrix. These kind of hybrid films are unattainable without blending of two BCPs.

The effects of confinement upon the self-assembly of PS-*b*-PFDMS diblock copolymer has been studied in order to understand how topographically patterned substrates affect the packing and morphology obtained.[271–274] PS-*b*-PFDMS thin films were assembled under confinement in etched nanochannels with differing widths (30–80 nm) followed by O_2 RIE.[274,275] When the row spacing of the diblock copolymer and the channel width were equal, spheres of PFDMS were formed. As the width of the nanochannels increased, thereby becoming incommensurate to the period of the BCP, elliptical domains were obtained due to distortion of the PFDMS spheres, as shown in Fig. 23. Once the nanochannel became wide enough to support a second row of spheres the ellipsoidal distortion was removed. Confinement in V-shaped grooves promoted the formation of a well-ordered face-centred cubic (fcc) close packed sphere morphology within the trough; this is in contrast to the body-centred cubic (bcc) packing that is obtained with the equilibrium bulk state. Studies into the topographical ordering of a statistical BCP PI-*b*-PFDMS-*stat*-PFEMS has also been reported.[276] These manipulations of the BCP morphologies using different substrates are seen as a useful route for the formation of new geometries and features *via* BCP lithography.

The effect of periodic 3D confinement on the behaviour of a PS-*b*-PFEMS in two different colloidal crystal (CC) templates was examined by TEM and energy-dispersive X-ray spectroscopy (EDX).[277,278] In the bulk state with no confinement a lamellar structure was observed. In the CC lattice consisting of air spheres in a silica matrix, concentric shells were obtained, whilst in a CC lattice composed of silica spheres in an air matrix, a lamellar structure oriented perpendicular to the silica spheres surface was observed.

5.1.2. Self-assembly of linear PFS triblock terpolymers to form phase-separated materials. Although diblock copolymers are the simplest and most well-studied BCPs for thin film self-assembly, they are mostly limited to simple line and dot pattern geometries which restricts their potential device applications.[201,204,279,280] By increasing the complexity of the system used, for example by using ABC triblock terpolymers or miktoarm star polymers, a host of previously unattainable morphologies become available with a diverse range of possible geometries and applications. For example, a polystyrene-*block*-polyferrocenylethylmethylsilane-*block*-poly(2-vinylpyridine) (PS-*b*-PFEMS-*b*-P2VP) triblock terpolymer was spin coated and annealed to give bulk and films under different solvent annealing conditions composed of a PS core/PFEMS shell cylinder morphology in a P2VP matrix perpendicular to the film (Fig. 24a).[230] Thin films of a polyisoprene-*block*-polysyrene-*block*-polyferrocenylethylmethylsilane

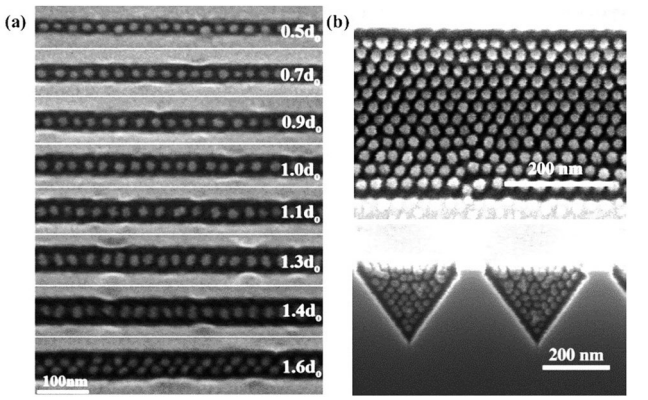

Fig. 23 SEM images of PS-*b*-PFDMS thin films following O_2 RIE in (a) channels of different confinement widths (b) and in V-shaped grooves. Reproduced with permission from ref. 274 and 275. Copyright 2006 American Chemical Society.

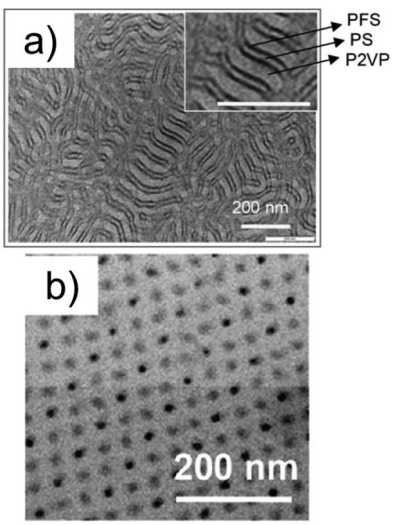

Fig. 24 Bright field TEM images of (a) the bulk morphology of PS-*b*-PFEMS-*b*-P2VP and (b) PI-*b*-PS-*b*-PFEMS triblock terpolymers. Reproduced with permission from ref. 230 (copyright 2009 American Chemical Society) and ref. 281 (copyright 2011 American Chemical Society).

(PI-*b*-PS-*b*-PFEMS) and PI-*b*-PS-*b*-PFEMS/PS homopolymer blend have been used to prepare nanosquare symmetrical arrays of PI and PFEMS cylinders in a PS matrix (Fig. 24b).[281] Both of these examples are unobtainable with simple AB diblock copolymers and demonstrate the complexity of the nanostructures that can be achieved with PFS BCPs.

Topographical studies of PFS triblock terpolymers have also been performed. The PI-*b*-PS-*b*-PFEMS/PS blend was also studied on silicon substrates with shallow grooves etched into the surface.[281,282] The orientation of the PFS cylindrical domains could be manipulated by treatment of the substrate with a PS brush whilst the periodicity of the square array templates could be controlled upon varying trench width. Increasing the thickness of the film allowed the formation of in-plane cylinders where the influence over their orientation once again could be controlled using a PS brush. Preferential wetting of the central PS block to the trench wall alters the lattice vector of the PFEMS square array from 90° to 45° with respect to the trench edge. In addition, the grain size of the square pattern could be greatly increased to several microns.[282] This was achieved through a combination of using brush layers, specific solvent annealing conditions and using templates composed of topographical sidewalls and posts.

5.1.3. Self-assembly of PFS star triblock terpolymers to form phase-separated materials. A miktoarm star polymer is a star polymer consisting of arms with different chemical composition originating from a central core. The simplest miktoarm star material with each arm with different composition is a μ-ABC miktoarm star, with one arm each composed of polymers A, B and C respectively. These materials have shown interesting bulk self-assembly with complex and novel morphologies,[283] such as Archimedean tiling patterns. However, until recently, the thin film behaviour of miktoarm star polymers and their use in nanolithography had not been investigated. Examples of these types of morphologies are shown in Fig. 25 for a range of polyisoprene-*arm*-polystyrene-*arm*-polyferrocenylethylmethylsilane (μ-ISF) miktoarm star terpolymers where different polymer block lengths afforded cylinders, lamellae and two different Archimedean tiling patterns.[247,267]

5.2. Applications of PFS BCP thin films

The incorporation of blocks containing inorganic elements together with complementary organic segments into BCPs is desirable as such materials typically have high χ values and greater etch selectivity when compared to all-organic materials.[284–289] The presence of iron and silicon atoms in the backbone of PFS means that it has a high resistance to reactive ion etching (RIE) when compared to organic polymers.[258] For example, PMMA has an O_2 RIE etching rate of 200 nm min^{-1}, whilst PFS has an etching rate of 4 nm min^{-1}.[198] Films containing PFS have shown the formation of an iron/silicon oxide layer at the film surface, in contrast to many organic polymers which are volatised and are removed from the surface. This allows the formation of nanopatterned surfaces derived from PFS after the removal of organic coblocks with a variety of uses and applications.[5,6,288,290,291]

5.2.1. PFS BCP thin films for carbon nanotube formation. Periodic PFS nanodomains have been shown to be converted

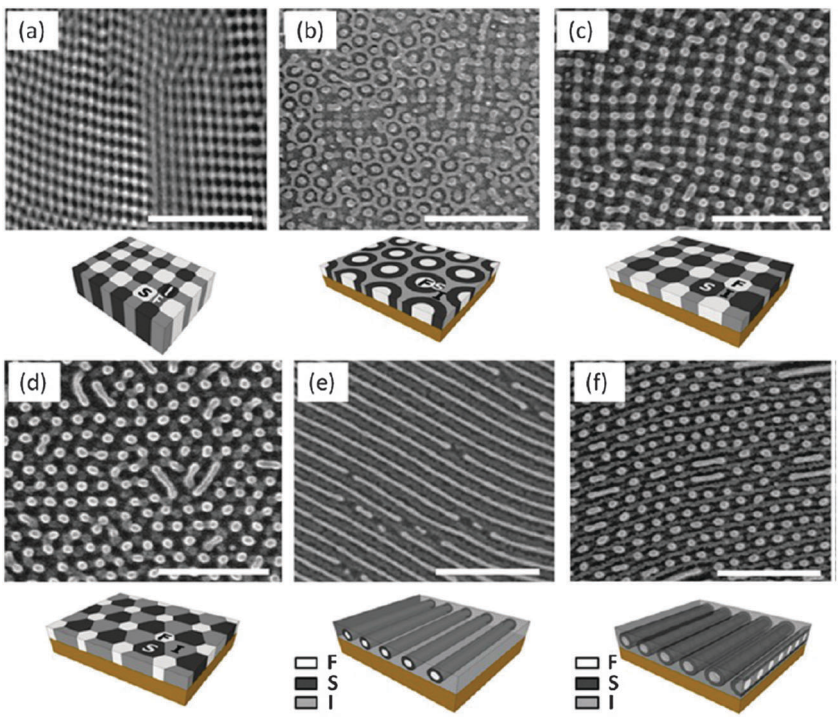

Fig. 25 Microscopy images and schematic representations of some of the obtained morphologies of μ-ISF; (a) TEM image of unblended bulk film; (b–d) SEM images of thin films blended with varying amounts of PS homopolymer on Si wafer; (e and f) SEM images of thin films blended with varying amounts of PS homopolymer on P2VP-coated surface. Scale bars are 200 nm. Reproduced with permission from ref. 267. Copyright 2013 American Chemical Society.

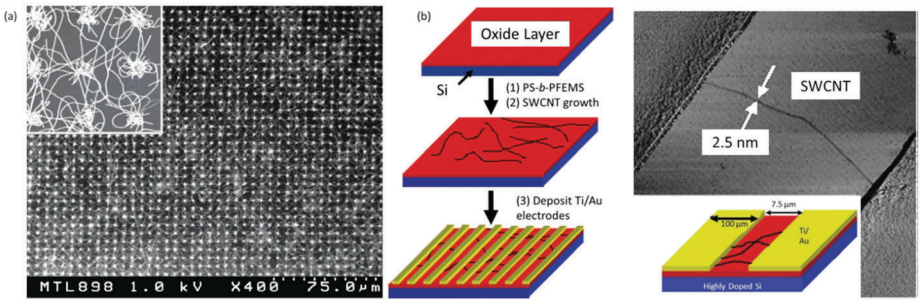

Fig. 26 (a) SEM images for single-walled carbon nanotubes (SWCNT) synthesised by chemical vapour deposition (CVD) with PS-*b*-PFEMS derived catalytic ceramic particles; (b) schematic and AFM height images of high throughput field effect transistors (FET) prepared from SWCNTs *via* PS-*b*-PFEMS derived catalytic ceramic particles. Reproduced with permission from ref. 294 (copyright 2005 American Chemical Society) and ref. 297 (copyright 2006 American Institute of Physics).

into iron-containing nanostructured ceramics that can be utilised as catalysts in the formation of single-walled carbon nanotubes (SWCNTs).[292–295] PS-*b*-PFEMS thin films were self-assembled and treated with UV-ozone to remove volatile organics and convert non-volatile inorganics into SiO_2 and Fe_2O_3. After pyrolysis, the films were used for chemical vapour deposition (CVD) growth of SWCNTs, which were subsequently characterised by scanning electron microscopy (SEM), atomic force microscopy (AFM), X-ray photoelectron spectroscopy (XPS) and Raman spectroscopy. Films with uniformly distributed SWCNTs were prepared where the growth density was easily and reproducibly controlled. Fig. 26a shows a SEM image of a SWCNT array prepared by CVD onto a PS-*b*-PFEMS film.[294] The ability of PFS BCP to generate catalytically-active Fe nanoparticles for the formation of SWCNTs is significantly greater than that shown by PFS homopolymers. This appears to be a consequence of the formation of smaller, higher surface area particles from confined PFS nanodomains.[296] Multi-walled carbon nanotubes (MWCNTs) have been grown off of PS-*b*-PFEMS films by an analogous method using a plasma treatment approach.[292]

The SWCNTs grown from PS-*b*-PFEMS films could then be used in high throughput individually addressable field-effect transistors (FETs) with high device yield (96%).[297] The schematic in Fig. 26b shows the method for the preparation of high throughput FETs from SWCNTs. Facile preparation of over 160 devices on a 15×15 mm^2 chip were achieved which are ideally suited to a variety of nanoscale sensing applications due to the excellent uniformity and dispersity of the SWCNT films. In a similar vein, self-assembled PS-*b*-PFEMS films have been used as a template for the generation of suspended SWCNTs across a large surface area.[298]

5.2.2. PFS BCP thin films for nanolithography and nanotemplating. The ability for BCPs to phase separate into a number of different morphologies has meant they have generated significant interest in nanolithographic applications.[204,288,299–305] BCPs with a metalloblock have garnered significant attention with respect to the formation of nanotemplates. One of the earliest examples involves the formation of arrays of tungsten-capped cobalt nanodots using a PS-*b*-PFDMS diblock copolymer thin film, which is outlined in the schematic in Fig. 27.[306] First, the diblock copolymer was spin-coated followed by O_2 and a subsequent CF_3H RIE, removing the PS matrix and underlying silica layer respectively. Further CF_4 + O_2 RIE and successive ashing allowed direct pattern transfer to the underlying tungsten layer. Finally an ion beam etch was used to form the desired tungsten-capped cobalt dots which has dimensions and whose pattern is inherent of that of the original PS-*b*-PFDMS film. These methodologies are promising for the preparation of high density materials for data storage.

Densely packed arrays of high aspect ratio (>200) single crystalline Si nanowires have been prepared using a similar combined approach of metal-assisted etching and BCP lithography.[307] Gratings were also used to show effective preparation of high aspect-ratio Si nanowires on topographical substrates which facilitate the application of these arrays as photonic and sensing devices.

Similar methods have been used for the preparation of a nanotextured Ag surface from a PS-*b*-PFEMS diblock copolymer.[308] Initially a thin film of the diblock copolymer was self-assembled into hexagonally close-packed standing cylinders of PFS in a PS matrix, followed by UV-ozonation to remove the matrix and convert the PFS into iron/silicon oxide nanocylinders. A thin layer of Ag was then sputtered over the cylinders to afford the nanotextured silver surface (Fig. 28). Such materials have great promise as Surface Enhanced Raman Spectroscopy (SERS) substrates. In this case, Raman spectroscopic analysis of adsorbed benzenethiol showed uniform enhancement factors of up to 10^6. Significantly, this system can be tailored effectively to change the size and spacing of the cylinders merely by changing BCP segment lengths, as well as allowing facile reproduction and fabrication of uniformly enhancing SERS-active substrates.

A sample of PS-*b*-PFEMS BCP that forms cylindrical domains of the metalloblock has been pyrolysed following self-assembly into a thin film with an orientation of the PFEMS cylinders perpendicular to the substrate. Crosslinking of the PS using UV-light followed by pyrolysis at 600 °C afforded arrays of magnetic ceramic cylinders that were characterised by magnetic force microscopy.[309]

A PS-*b*-PFiPMS BCP has been used to prepare wire grid polarisers with extremely high aspect ratios over cm^2 areas.[310] Firstly, an amorphous layer of silicon (α-Si) was deposited onto a fused silica substrate by plasma-enhanced chemical vapour

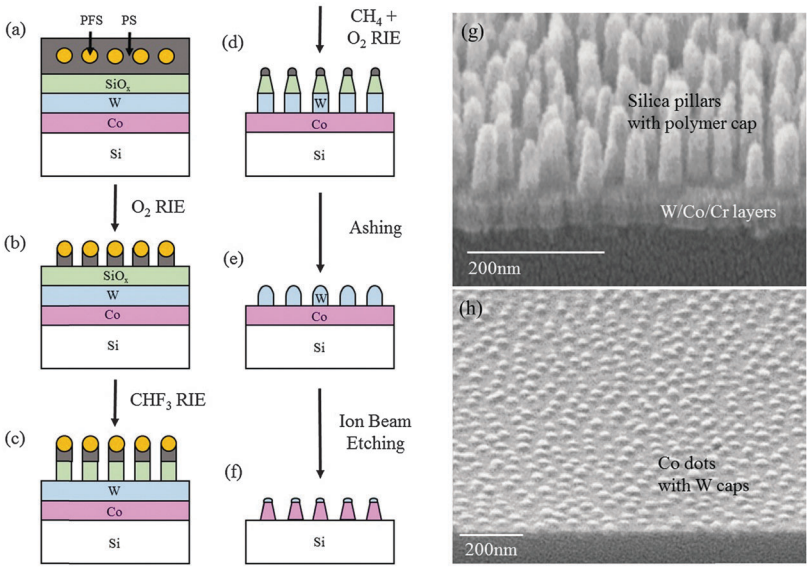

Fig. 27 Schematic (a–f) for the fabrication of W-capped Co nanodot arrays using PS-*b*-PFDMS thin film BCP lithography and TEM images for (g) the preparation of silica pillars with polymer cap and (h) Co nanodots with W caps. Reproduced with permission from ref. 306. Copyright 2001 John Wiley & Sons Inc.

deposition (PECVD). This was followed by spin coating a thin film of PS-*b*-PFiPMS which was shear aligned and the resulting PS domains were removed by O_2 RIE. Finally, the α-Si layer was deeply and anisotropically etched through the BCP mask layer by SF_6 using the Bosch process. The substrates were characterised by SEM, AFM and UV/visible spectroscopy, showing the formation of α-Si nanowire grids with widths of 15 nm and heights of 80 nm (see Fig. 29). These grids can be used as wire grid polarisers on UV-transparent substrates, with polarisation efficiencies as high as 90% for deep UV light (193 nm), significantly greater than for other reported compact transmission polarisers.

Using the same PS-*b*-PFiPMS diblock copolymer, large-area nanoscopic square arrays of distinct layers of the BCP were prepared that had been shear-aligned perpendicular to each other.[311] This in turn allowed the fabrication of dense, substrate-supported arrays of different nanostructures depending on the final step, as shown in Fig. 30. Initially the diblock copolymer was spin coated onto the substrate and film ordering was induced by shear alignment (Fig. 30a). The film was exposed to UV irradiation to cross-link the PS block (Fig. 30b). A second layer was subsequently spin-coated on top of the first layer and aligned with the same shearing conditions perpendicular to the directionality of the first shear, followed by removal of the PS matrix by O_2 RIE to give a nanosquare grid composed of PFiPMS residues (Fig. 30e). These domains' resistance to SF_6 RIE allowed the preparation of nanowells by deep Si etching *via* the Bosch process (Fig. 30f), giving wells up to 80 nm deep, which could potentially be used to contain individual biomolecules or as a master mould for nanoimprint lithography.

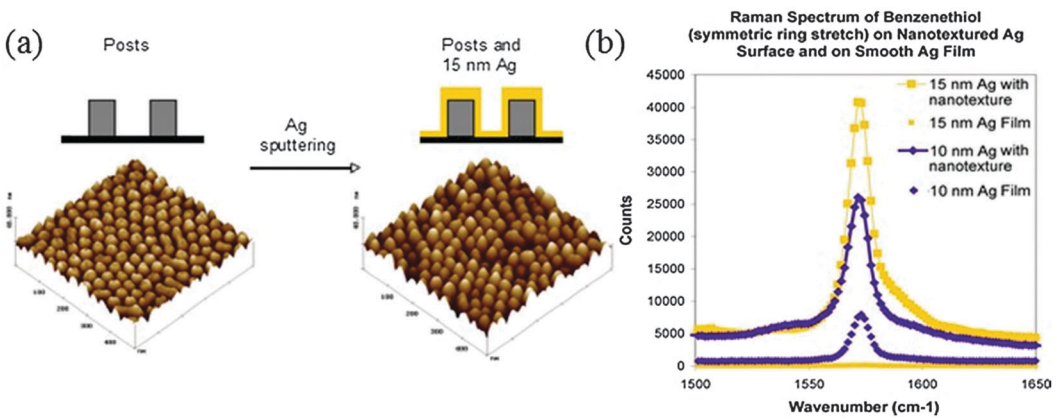

Fig. 28 (a) Schematic and corresponding AFM height images for the preparation of a silver nanotextured surface for SERS using a PS-*b*-PFEMS diblock copolymer thin film; (b) corresponding SERS of benzenethiol on nanotextured Ag films. Reproduced with permission from ref. 308. Copyright 2006 Institute of Physics Publishing.

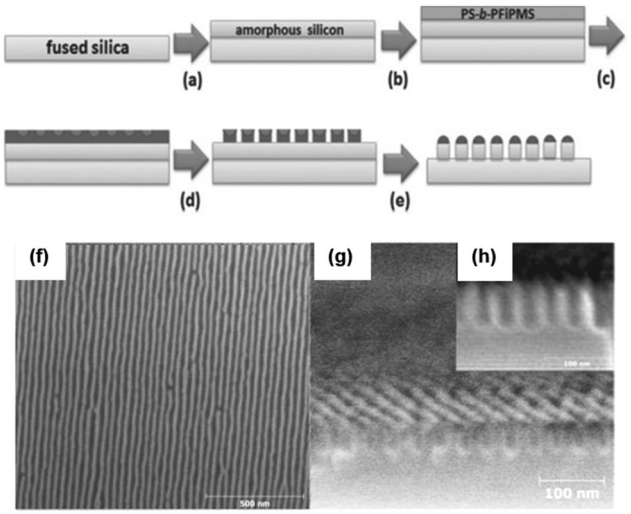

Fig. 29 (a–e) Schematic for fabrication of high aspect ratio wire grid polarisers formed from PS-*b*-PFiPMS diblock copolymer thin films; (f) SEM images of wire grid polarisers after Bosch etching and (g and h) of cross-sections formed by etching of α-Si layers. Reproduced with permission from ref. 310. Copyright 2014 American Chemical Society.

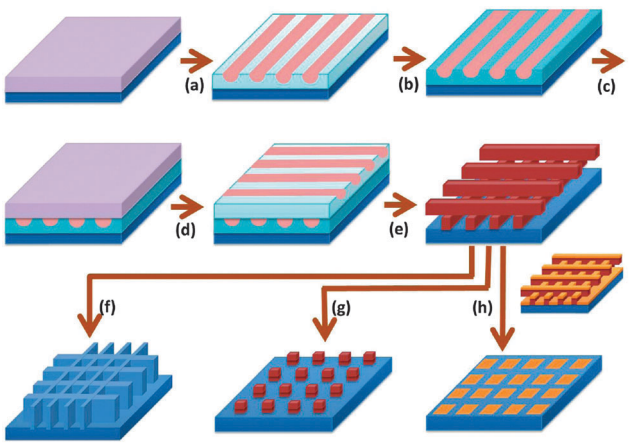

Fig. 30 (a–e) Schematic towards the preparation of a cross-pattern by sequential perpendicular shear alignment of PS-*b*-PFiPMS diblock copolymer thin films for the subsequent formation of (f) square nanowells, (g) square arrays of nanoposts and (h) metal nanodot arrays. Reproduced with permission from ref. 311. Copyright 2014 American Chemical Society.

Treatment by controlled wet etching with 5% HCl yielded a square array of nanoposts (Fig. 30g), which could be used to permit further patterning into the substrate. If the nanosquare grids are treated by metal evaporation and subsequent lift-off by sonication in 5% HCl, metal nanodot arrays are formed (Fig. 30h) which are of particular interest for high density magnetic storage and plasmonics. The pattern symmetry of these structures can easily be manipulated by changing the molecular weights of the BCPs and through controlling shear directions, allowing square, rectangular and rhombic structures to be formed.

Blending of a PFS BCP with a different incompatible BCP to form hybridised host–guest-type thin films has allowed

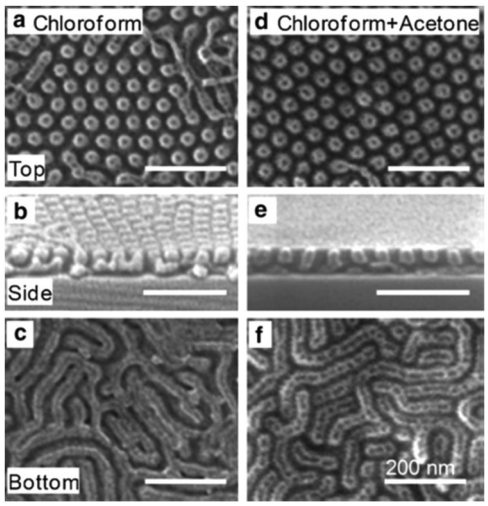

Fig. 31 SEM images of PS-*b*-PFEMS-*b*-P2VP triblock copolymer thin films after annealing in (a–c) chloroform and (d–f) a chloroform/acetone mixture for 4 h followed by O_2 RIE; (a and d) plane view, (b and e) side view, (c and f) bottom view. Scale bars are 200 nm. Reproduced with permission from ref. 230. Copyright 2009 American Chemical Society.

the preparation of hollow phase change memory devices.[312] A PS-*b*-PFDMS BCP, when blended with a PS-*b*-PDMS BCP, formed hexagonally perforated lamellae thin films with PS coated PFDMS spheres in a PDMS matrix. These systems were optimised to form dot-in-hole structures on $Ge_2Sb_2Te_5$/TiN/(Ti)W/SiO_2/Si phase-change memory substrates to allow formation of ring-shaped nanostructures through a combination of Pt evaporation and a pattern-reversal process. The high-density nanoring patterns exhibited a low switching current and could be effectively extended to other non-volatile memory device applications.

Nanoscale arrays of rings have been prepared from a PS-*b*-PFEMS-*b*-P2VP triblock terpolymer.[230] These are of particular interest in the fabrication of memories or sensors and in quantum devices. Spin-coating and annealing of the material gave a PS core/PFEMS shell-cylinder morphology in a P2VP matrix perpendicular to the film substrate with a period of 50 nm, as shown in Fig. 31. The PS and P2VP domains were removed by O_2 RIE, leaving partially oxidised PFS nanorings with a diameter and width of 33 nm and 11 nm respectively. The remaining PFS pattern could be used as a mold for pattern transfer and was imprinted into a PS layer, showing this is a useful system for self-assembled nanolithography.

Thin films of PI-*b*-PS-*b*-PFEMS and PI-*b*-PS-*b*-PFEMS/PS homopolymer blend have been used to prepare square symmetrical arrays.[281,282] Such a geometry is essential for furthering BCP lithography in areas such as developing array structures in integrated circuits. Square-packed cylinders of PI and PFEMS in a PS matrix were formed in thin films of both materials, however addition of PS homopolymer improved the long-range ordering of the morphology by allowing relaxation of the highly stretched triblock terpolymer chains by occupying volume between the PI and PFEMS cylinders. PI and PS domains were removed by O_2 RIE to give square-packed PFEMS cylinders with a 40.5 nm period. This pattern was transferred into a 30 nm

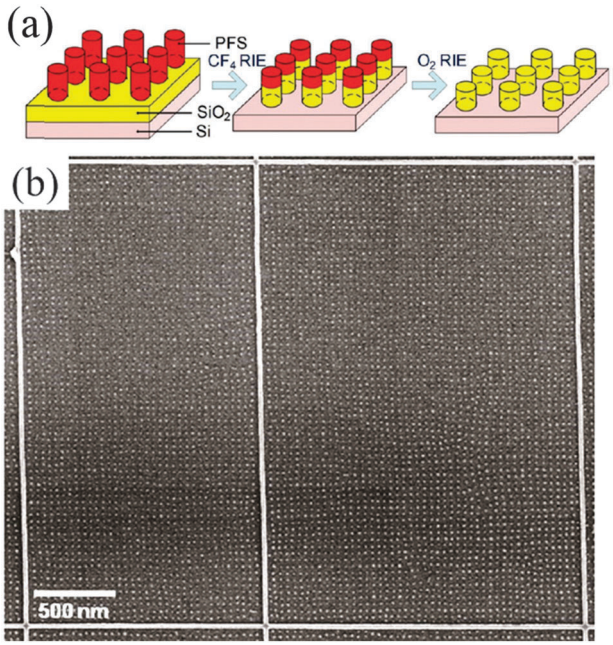

Fig. 32 (a) Schematic for formation of pattern transfer to prepare square arrays of silica posts from PI-*b*-PS-*b*-PFS diblock copolymer thin films; (b) corresponding SEM image showing highly-ordered square arrays of PFS microdomains within topographical HSQ sidewalls. Reproduced with permission from ref. 281 and 282 (copyright 2011 American Chemical Society).

thick silica film by successive CF_4 RIE and O_2 RIE (see Fig. 32), affording silica posts 30 nm in height and 20 nm in diameter with a greater aspect ratio than that of the original PFEMS posts.

Surface reconstruction of thin films of a PI-*b*-PS-*b*-PFEMS/PS blend resulted in either a positive pattern of PFEMS posts by O_2 RIE or a negative pattern of holes using a selective solvent for the PI block. Square arrays of posts, pits and inverted pyramids were fabricated in silicon substrates by dry and wet etching processes.[313] Coexisting post and hole patterns could also be formed.

The negative hole pattern described above has been exploited in the hierarchical templating of $BiFeO_3$–$CoFe_2O_4$ multiferroic vertical nanocomposites, which is outlined in the schematic in Fig. 33.[314] A thin film of a PI-*b*-PS-*b*-PFEMS/PS blend with the negative hole pattern was prepared on a Nb-doped $SrTiO_3$ (STO) substrate by surface reconstruction in hexane (a PI selective solvent). The residual polymer layer on the bottom of the holes was removed by a short O_2 RIE (Fig. 33, iii). The pattern was used as a mask to etch pits into the substrate by wet etching with aqua regia, followed by calcination to remove the polymer template. $CoFe_2O_4$ (CFO) nuclei were selectively grown into the patterned pits (Fig. 33, v) and a thin layer of $BiFeO_3$ (BFO) was deposited to cover the unetched area of the substrate. The $BiFeO_3$–$CoFe_2O_4$ thin film was then used as a guide to grow a thick layer of the nanocomposite, composed of $CoFe_2O_4$ pillars in a $BiFeO_3$ matrix (Fig. 33, vii). This hierarchical process whereby one self-assembling system templates the epitaxial growth of oxide nanocomposite films could allow the incorporation of multiferroic nanocomposite structures into magnetic memory or logic devices.

Thin film self-assembly of a PI-*b*-PS-*b*-PFEMS (μ-ISF) miktoarm star polymer blended with PS homopolymer was studied for the preparation of 2D Archimedean tiling patterns to be utilised in nanolithography.[267,315] Self-assembly was achieved by solvent vapour annealing in chloroform, and samples were characterised by SEM, TEM and AFM. A range of Archimedean tiling patterns were obtained, as shown in Fig. 25, and the morphology could be controlled by altering solvent annealing conditions, the amount of blended homopolymer and the substrate used. Pattern transfer from the tiling arrays was demonstrated following CF_4 and O_2 RIE to remove the PI and PS domains, leaving only oxidised PFEMS domains and the resulting pattern was effectively transferred into a silicon substrate. These kind of geometries are not obtainable through linear BCPs and can provide a toolset for the preparation of novel patterns for nanolithographic applications, as well as the potential to form surfaces with chemical heterogeneity that can be used in a host of nanoscale devices.

The self-assembly behaviour of the pure μ-ISF miktoarm polymer was studied, which yielded a novel morphology described as a "knitting pattern", which had been previously predicted from simulations (see Fig. 34).[316] Films were prepared by spin-coating onto silicon wafers followed by solvent vapour annealing in chloroform, giving films that showed extraordinary periodicity composed of undulating PFEMS lamellae and alternating PI and PS cylinders. The morphology of the knitting pattern could be controlled by altering the film thickness and the etching process. Interestingly some films showed sharp 90° bends and T-junction configurations

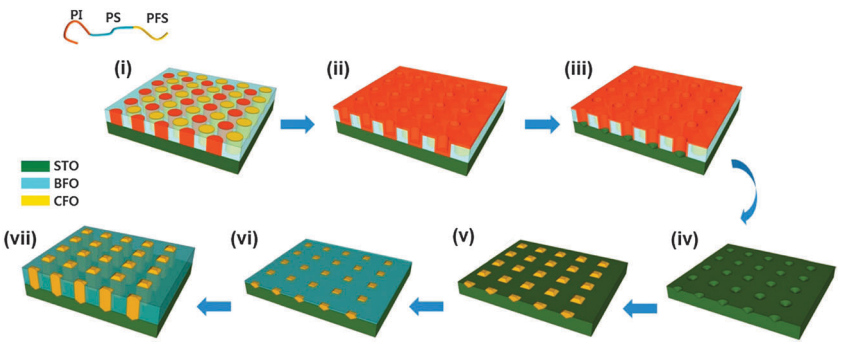

Fig. 33 (i–vii) Schematic for the fabrication of a templated $BiFeO_3$–$CoFe_2O_4$ nanocomposite thin film by thin film self-assembly of PI-*b*-PS-*b*-PFS/PS blend. Reproduced with permission from ref. 314. Copyright 2014 American Chemical Society.

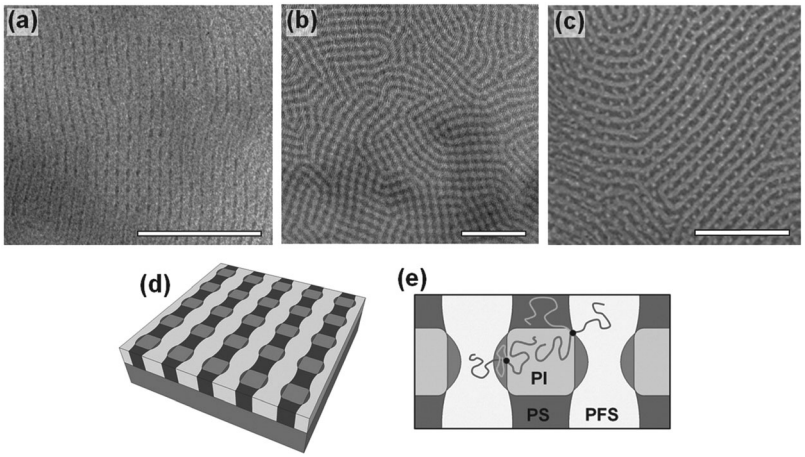

Fig. 34 TEM images of μ-ISF (a) before staining and (b) after staining with OsO_4; (c) SEM image of bottom interface of μ-ISF; schematics showing (d) thin film patter and (e) its chain conformation within the microdomain. Scale bars are 300 nm. Reproduced with permission from ref. 316. Copyright 2014 American Chemical Society.

which had only previously been observed with diblock copolymers by using topographical or chemical templates. Transfer of various patterns into silicon substrates was also possible by RIE of the films.

5.2.3. Redox-properties: fabrication of surface relief gratings and protein arrays. Stable surface-relief gratings (SRGs) can be written into complexes of phase-separated PFS block polyelectrolytes assembled with azobenzene-based surfactants.[317] The presence of the redox-active and etch-resistant PFS polymer allows the SRGs to be post-modified. For example, on oxidation, enhancement of the modulation depth occurs, allowing feature sizes to be tuned. In addition, as a result of their excellent etch resistance, the organic components can be removed leaving behind ceramic SRGs.

The controlled adsorption of the iron-containing cage protein ferritin to stimuli-responsive self-assembled PS-*b*-PFEMS BCP thin films has also been studied.[318] A thin film with an orientation of the PFEMS cylinders perpendicular to the substrate was prepared. To prevent any spontaneous protein adsorption on either block, the electrolyte pH was selected to leave the ferritin negatively charged, and the protein concentration and solution ionic strength were carefully tuned. Selective adsorption of ferritin on the PFS domains of the self-assembled thin films was triggered *in situ* by applying a positive potential, simultaneously oxidising the PFS and attracting the ferritin electrostatically.

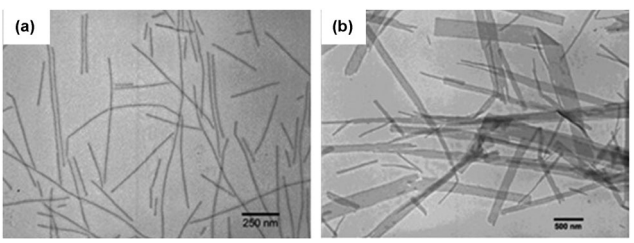

Fig. 35 TEM images for the micelles formed from (a) PI_{320}-*b*-$PFDMS_{53}$ (6 : 1) and (b) PI_{30}-*b*-$PFDMS_{60}$ (1 : 2) in hexane/THF (9 : 1) and (7 : 3) respectively. Reproduced with permission from ref. 221. Copyright 2002 American Chemical Society.

5.3. Self-assembly of PFS BCPs in solution

5.3.1. General considerations for PFS BCP solution phase self-assembly. The solution self-assembly of organic coil–coil BCPs has been very well studied. These materials self-assemble in block-selective solvents to form core–shell nanoparticles referred to as micelles.[208,209,319,320] It is well established that the increase in volume of the solvent-swollen corona relative to the dry state favours curvature of the core–corona interface. Generally, the effect causes phase diagrams of BCPs in selective solvents to be shifted so as to generate an expanded region of phase space corresponding to the spherical morphology relative to the analogous phase diagram in the bulk state. For BCPs with relatively short coronal chain lengths relative to those for the core-forming block an extraordinarily broad range of morphologies have been characterised. These are often difficult to predict in advance. The lack of predictability and increased complexity compared to self-assembly in the bulk state arises from two main factors. First, additional competing interactions between the different blocks and the solvent exist. Second, the low or negligible rates of unimer exchange for micelles formed by high molar mass amphiphiles leads to a high propensity to form kinetically-trapped rather than equilibrium structures.[321]

As anticipated based on the well-established behaviour of all-organic analogues, PFS BCPs also form micelles in selective solvents. The presence of PFS in the core or corona is attractive for a variety of applications based on the properties of the material established through the studies of the homopolymer (see Section 3). To date, the vast majority of the reported investigations have focused on micelles in which the PFS constitutes the solvophobic block that forms the micelle core to minimise enthalpically or entropically unfavourable interactions with solvent molecules. Colloidal stabilisation is provided by the swollen solvophilic corona formed by the complementary organic or inorganic solvophilic block.

As for the studies in bulk and thin films, many of the investigations of PFS BCPs in solution have aimed to exploit the inherent functionality provided by the PFS block. In addition, studies of the solution self-assembly of PFS BCPs have made an unexpected contribution to the broad field of polymer and colloidal science through the emergent discovery of a process termed "Living Crystallisation-Driven Self-Assembly (CDSA)". Living CDSA provides a route to nanomaterials with tailored complexity and dimensions that is of potentially broad significance and this method is discussed within the following sections below.

5.3.2. Crystallisation-driven self-assembly of PFS BCPs in solution. The overwhelming majority of the literature reports on BCP self-assembly in solution involve materials in which the core-forming block does not crystallise. Studies of the self-assembly of BCPs with an amorphous PFS core-forming block reveal behaviour that is broadly similar to that observed for the well-studied all-organic analogues. Nevertheless, the redox-activity of the PFS block has been utilised to create stimuli-responsive self-assembling systems that reversibly form micelles on oxidation and disassemble on reduction.[322] Redox-active vesicles with a cationic PFS polyelectrolyte as the corona have also been prepared.[323]

Investigations of BCPs with a short crystallisable PFDMS core-forming block in the late 1990s revealed highly unexpected results with a preference for the formation of micelles with lower mean curvature of the core–corona interface such as cylinders rather than spheres.[48] This subsequently led to the discovery that the crystalline cores at the micelle termini were able to elongate by the addition of further BCP.[324] The use of small seed micelles (generated by sonication of longer cylinders) as "initiators" led to a process that is analogous to a living covalent polymerisation of molecular monomers.[325] This process, termed "Living Crystallisation-Driven Self-Assembly (CDSA)", permits control of micelle dimensions, the formation of low length dispersity samples, and the formation of segmented or "block comicelles" (see the next Section 5.3.3).

BCPs with a PFS core-forming block that is symmetrically substituted at silicon (*e.g.* R = R′ = Me, PFDMS; R = R′ = Et, PFDES) and is able to crystallise can self-assemble in various solvents to produce a number of different micellar morphologies including cylinders,[255,256,326] tubes,[327–329] fibres,[330] platelets[221] and, if the core-forming block does not crystallise, usually spheres.[48,226,331] As an example, when a sample of $PFDMS_{50}$-*b*-$PDMS_{300}$, with a block ratio of 1 : 6, was heated and then cooled in a selective solvent for the PDMS block such as *n*-hexane, cylindrical micelles were obtained composed of a PFDMS core and a PDMS corona. These nanostructures are easily visualised by TEM because the PFDMS core is electron-rich, allowing effective contrast for imaging without the need for staining.[256] The crystallisation of the core-forming PFDMS was believed to be the driving force for the formation of a cylindrical rather than spherical morphology, and the ordered nature of the core and the chain packing has been explored by wide angle X-ray scattering (WAXS).[7,332]

Spherical micelles are obtainable in certain cases such as when cylindrical micelles are heated above the T_m of the PFS core-forming block and the solution is then rapidly cooled to prevent core-crystallisation or when an unsymmetrical PFS block, such as poly(ferrocenylethylmethylsilane) (PFEMS), is the core-forming block.[48,333,334] Unsymmetrically substituted PFS blocks generally cannot crystallise and, to date, have only been observed to form spherical micelles in solution. This implies that the crystallinity of the core-forming block is a key factor to the formation of one-dimensional micellar structures. BCPs with an amorphous core-forming PFS block can undergo redox-controlled micellisation due to an induced polarity change resulting from partial oxidation of the PFS block.[322,335] Spherical micelles that have been formed with a crystallisable PFS block in an amorphous state due to rapid precipitation[226] have been shown to transform into cylinders with a crystalline core after a maturation period in a corona-selective solvent over a period of weeks or months.[336]

The block ratio plays a key role in determining which morphology is obtained.[221] For example, PI_{320}-*b*-$PFDMS_{53}$ has a block ratio of 6 : 1 (PI : PFS) and self-assembles into cylindrical micelles in PI-selective hexanes, however PI_{30}-*b*-$PFDMS_{60}$, which has a block ratio of 1 : 2, forms tape-like platelet micelles (see Fig. 35). Although both materials have similar PFS block lengths, the significant difference in coronal block lengths has an obvious effect on the morphology formed. As the PI coronal block length increases, there are increased coronal repulsions which favours greater curvature at the core–corona interface, and cylindrical micelles are preferred.[48]

The effect of molar mass and solvent selectivity upon micellar morphologies and the transitions between these architectures has been investigated in detail.[337] Three PFDMS-*b*-P2VP BCPs were prepared with the same block ratio (1 : 6) but different molar masses and it was shown that sphere-to-cylinder transitions in isopropanol was greatly slowed by increasing the molar mass. Furthermore, increasing the content of THF (a common solvent for both blocks) improved the solvation of the PFS core-forming block, which allowed core crystallisation *via* a plasticisation effect. The morphologies obtained also changed from spheres to cylinders and then to narrow lenticular platelets as the THF content increased.[337]

Shape anisotropic nanoparticles with internal nanostructures have been reported by self-assembly of an amphiphilic PFS BCP in an aqueous mixed surfactant system.[338] Nanosheets with a hexagonal array of PFS cylinders in a P2VP matrix were formed when a PFDMS-*b*-P2VP BCP was self-assembled under neutral wetting conditions (Fig. 36a). Self-assembly of the PFS BCP with additional PFS homopolymer under the same conditions formed ellipsoidal particles with an axially stacked lamellar structure (Fig. 36b). These type of structures are in contrast to traditional PFS micelle systems as outlined previously. Spatial control over the distinct domains within the nanoparticles was exploited to demonstrate morphological transitions between the two structures.

Several amphiphilic PFS-containing BCPs have been shown to be able to self-assemble in water when hydrophilic blocks create the micelle corona.[339,340] $PFDMS_9$-*b*-$PDMAEMA_{50}$ was prepared as outlined earlier (see Section 4.1.2.1), and the PDMAEMA

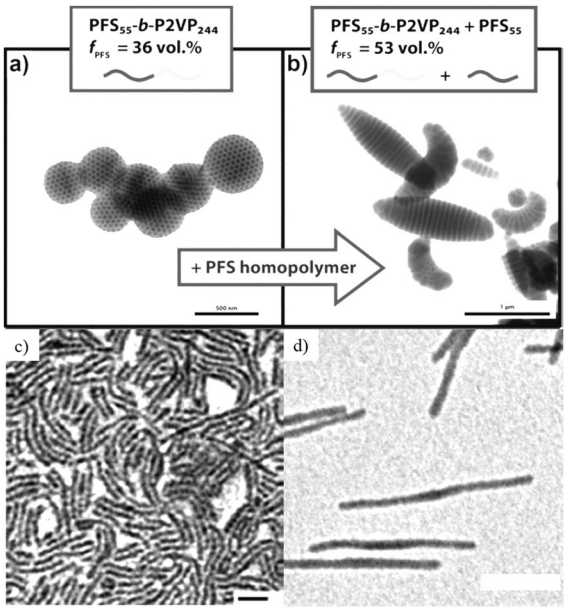

Fig. 36 (top) TEM images showing (a) nanosheets with a hexagonal packed cylinder structure and (b) ellipsoidal particles with an axially stacked lamellar structure formed from blending of PFS-*b*-P2VP and PFS homopolymer. (bottom) TEM images showing (c) irreversibly and (d) reversibly crosslinked PI-*b*-PFDMS micelles. Scale bars are 250 nm. Reproduced with permission from ref. 338 (copyright 2015 American Chemical Society), ref. 344 (copyright 2003 American Chemical Society), and ref. 349 (copyright 2011 American Chemical Society).

block quaternised with methyl iodide. Whilst a range of morphologies were obtained for the unquaternised $PFDMS_9$-*b*-$PDMAEMA_{50}$, including polydisperse spherical aggregates upon direct dissolution into water, the quaternised analogue was self-assembled into cylindrical micelles upon dissolution in alcoholic solvents. Dialysis of these micelle solutions against water was effective in the preparation of cylinders dispersed in water. The PFS core within the micelles surprisingly appeared to be amorphous by wide-angle X-ray scattering (WAXS). This was similar for PFDMS-*b*-PMMA BCPs[331] upon self-assembly in acetone where variable temperature ^{1}H NMR studies showed an amorphous core in a mobile state and solvent molecules could easily penetrate into the micelle core. It was deduced that the polar solvents used in both these cases were the driving forces for micellisation, with high interfacial energy caused by the exposure of hydrophobic PFS core to polar solvents, instead of the crystallisation of the core driving the formation of aggregates.

The introduction of functional groups into the micelle corona allows for the possibility of shell-crosslinking reactions which give rise to a marked increase in the stability for the self-assembled structures.[341–343] BCPs that have corona-forming blocks such as PI and PMVS with pendant vinyl groups within the polymer backbone have been shown to undergo Pt-catalysed hydrosilylation crosslinking with tetramethyldisiloxane and Karstedt's catalyst,[222,344–347] or by UV-initiated crosslinking.[35,348] As a result of this shell-crosslinking, the micellar structures are essentially "locked in" and are preserved even if they are transferred from a corona-selective solvent into a common solvent for both blocks.[222,344,346] For example, cylindrical micelles composed from PI_{320}-*b*-$PFDMS_{53}$ were self-assembled and the coronal chains were subsequently crosslinked. The micellar solution was dialysed against THF, which is a good solvent for both the PFS and PI blocks, but there was no discernible difference in structure after transferring into THF (see Fig. 36c).[344,346] Reversible cross-linking of PI-*b*-PFDMS BCPs has also been reported.[349] By using only Karstedt's catalyst in the absence of any silanes, crosslinking of the PI corona occurs through Pt(0)–olefin coordination which can be reversed through the addition of 2-bis(diphenylphosphine)-ethane (dppe) (see Fig. 36d).

5.3.3. Living CDSA of PFS BCPs. Control over the growth of PFS-containing cylindrical micelles has been demonstrated by using living CDSA approaches.

Initial studies into this area focused on the stability of PFDMS-*b*-PDMS cylindrical micelles. Upon ultrasonication of the preformed fiber-like structures, the formation of shorter cylinders through fragmentation of the micelles was observed without any apparent change in the micelle width.[326] This was also detected for PI-*b*-PFDMS cylindrical micelles. Significantly, it was found that addition of further unimer to these short micelles resulted in longer cylinders, with the preformed micelles essentially acting as "seeds" for further unimer nucleation.[324] The length of the micelles depended linearly on the unimer-to-seed ratio and was also found to be of low polydispersity. This demonstrated an analogy with a living covalent polymerisation of molecular monomers.[325] The micelles grown by this method were also shown to be stable with respect to a change in dimensions in the selective solvent at ambient temperature over a period of many months with no change in their average length or the length distribution. This implied that the micelles were kinetically-trapped in that the constituent BCP chains were resistant to significant dynamic exchange between micelles under these conditions. The micelles were stable to fusion in solution over long periods of time; the addition of BCP unimer in solution was found to be required for this process to occur.[350] In addition, when a corresponding diblock copolymer unimer with an amorphous PFS block (PFEMS-*b*-PMVS) was added, no growth was detected. This seeded growth method exploits the crystallisation of the PFDMS block and has been termed as "living" CDSA.[325] Cylindrical micelles with length dispersities of 1.01 and overall length greater than 2 μm have been prepared by this protocol (see Fig. 37).[324,325]

An alternative approach to length control of PFS BCP micelles, termed a "self-seeding" process, has also been reported for the preparation of monodisperse cylindrical architectures.[351–354] To facilitate the process, relatively short cylindrical micelles were prepared through ultrasonication of long, polydisperse PI-*b*-PFDMS cylinders. Within the PFDMS micelle core, regions of different crystallinity and therefore different melting points exist. When heated, the least crystalline domains dissolve first to give unimers. This leaves very short, more highly crystalline seeds. Upon cooling, the dissolved unimer will grow from the remaining seed micelle termini *via* epitaxial growth to a length that will depend inversely on temperature (Fig. 38).

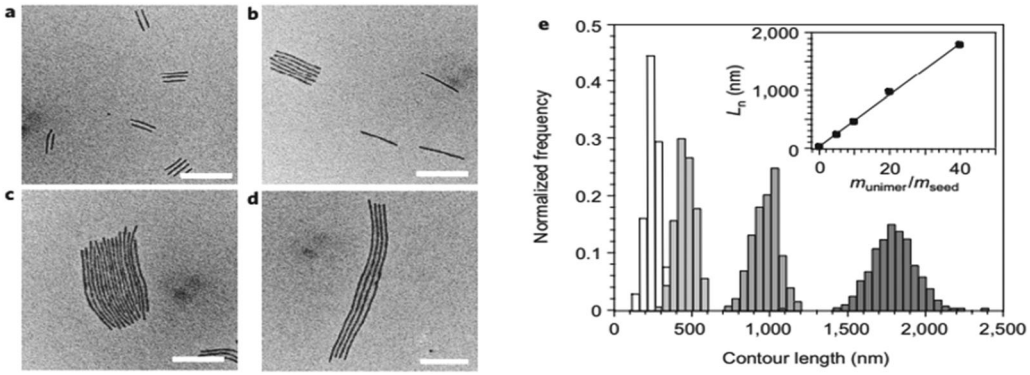

Fig. 37 (a–d) TEM images of monodisperse PFDMS-*b*-PDMS cylindrical micelles grown from uniform stub-like seed micelles with increasing amounts of unimer solution added; (e) histogram of the contour length distribution of the samples; scale bars are 500 nm. Reproduced with permission from ref. 325. Copyright 2010 Nature Publishing Group.

Block comicelles with spatially segregated regions of different chemistry in the corona can be readily prepared by the sequential addition of different PFS-containing diblock copolymer unimers to seeds.[324,349] For example, addition of PFDMS-*b*-PMVS to cylinders of PI-*b*-PFDMS created block comicelles with a central compartment with PI corona and end compartments with PMVS corona whilst having a continuous crystalline PFS core. Similar block comicelles were prepared using a PFDMS-*b*-P2VP BCPs, where cylindrical seeds were quaternised, and this was followed by the addition of neutral PFDMS-*b*-P2VP unimer to the seed termini. Composite nanostructures have been prepared from this kind of block comicelle through the aggregation of nanoparticles or quantum dots on the quaternised block of the comicelle.[356]

It has been shown that epitaxial growth of cylinder-forming PFS BCPs can also occur off of the edges of platelet micelles.[357] When the block ratio for a PI-*b*-PFDMS BCP is 1 : 1 (PI : PFS), platelet micelles are formed instead of cylinders when self-assembled in a solvent selective for the corona-forming block. These platelet micelles can also be fragmented using ultrasound to form small platelets in the same manner as that for cylindrical micelles, although with much less control over size and polydispersity. Addition of cylinder-forming unimer to the platelet seed micelles resulted in epitaxial growth from only two of the available six faces, forming hybrid "scarf-like" micelles with tassels of uniform length (see Fig. 39a). Hollow "scarf-like" micelles have been prepared in an analogous manner by dissolving out a PFDMS-*b*-PDMS platelet inside a surrounding layer of cross-linked PI-*b*-PFDMS diblock copolymer.[349]

Annealed PFS homopolymer films have been used to seed the growth of cylindrical micelles.[357] Unimer growth occurred at steps and ridges at the surface of the crystalline substrate corresponding to stacked layers of crystalline lamellae.

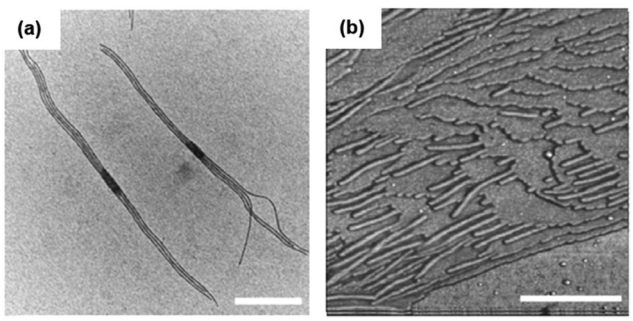

Fig. 39 (a) TEM images of "scarf"-like micelles and (b) AFM phase image of cylindrical micelles grown from a PFDMS thin film. Scale bars are 500 nm. Reproduced with permission from reference 357. Copyright 2009 Nature Publishing Group.

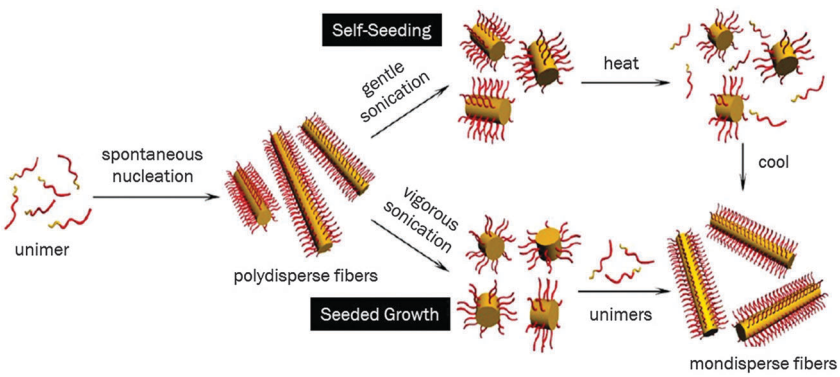

Fig. 38 Schematic for the preparation of monodisperse cylindrical micelles by (top) self-seeding and (bottom) seeded growth methods. Reproduced with permission from ref. 355. Copyright 2015 American Chemical Society.

The cylinders formed off the surface grew parallel to the surface giving a cylindrical micelle mat (see Fig. 39b). In addition, epitaxial growth from PFS nanocrystals was also demonstrated forming multi-armed micelles that possessed hierarchical "multipod" structures with monodisperse and controllable arm lengths.[358]

Heteroepitaxial growth, where unimer containing one core-forming block can grow off a seed micelle composed of a different core-forming block, has also been reported.[357] In principle, for this to occur, crystal lattice parameters with a mismatch of less than 15% in lattice spacing is required.[359,360] Poly(ferrocenyldimethylgermane) (PFDMG) BCPs, isostructural analogues to PFS BCPs, were studied because PFDMG has a layer spacing <5% larger than of PFS.[361] PFDMG BCP unimers were added to both PFS-containing monodisperse cylindrical micelles and platelets, resulting in the formation of composite nanostructures *via* heteroepitaxial growth. PFS BCP unimer was also effectively added to cylindrical micelles with ends composed of a PFDMG core.

Addition of BCPs with different composition and functionality can allow the preparation of a variety of discrete, well-defined micelle and block comicelle structures.[356,362–366] Branched micelles have been prepared by adding BCP unimer with a short PFS block to a preformed cylindrical micelle with a core composed of a longer PFS block.[355,367] For example, monodisperse cylindrical micelles were prepared by seeded growth of $PFDMS_{48}$-*b*-$P2VP_{414}$. A unimer solution of $PFDMS_{20}$-*b*-$P2VP_{140}$ was then added to the micelle solution, resulting in epitaxial growth usually of two branches from either end of the seed micelle, as shown in Fig. 40A–C. Due to the redox-activity of the core-forming block, one-dimensional arrays of Ag nanoparticles were prepared through *in situ* redox chemistry after shell-crosslinking of the P2VP corona. Branched micelles of various PFS-containing BCPs have been shown to form by living CDSA under kinetic control.[355] These branched-type micelles offer a promising scaffold for the preparation of more complex branched nanomaterials.

Living CDSA has been effective in the preparation of light-responsive micellar structures with a photocleavable junction at the core–corona interface.[364,368] PFDMS-ONB-P2VP BCPs (ONB: *o*-nitrobenzyl junction) were synthesised through a combination of living anionic polymerisation, reversible addition–fragmentation transfer (RAFT) polymerisation and "click" chemistry. The BCPs were self-assembled into monodisperse cylindrical micelles and the coronal chains removed by UV irradiation (see Fig. 40D). These materials could then be used effectively to form well-defined branched micelles, as well as P2VP nanotubes through crosslinking of the coronal chains.

Cylindrical micelles with "patchy" coronal structures have been prepared through the co-assembly of linear PFDMS-*b*-PMVS and brush PFDMS-*b*-PMVS diblock copolymers that had been functionalised with *n*-alkyl branches off of a PFDMS-*b*-PDMS cylindrical micelle (see Fig. 40E).[365] Previous attempts at preparing "patchy" architectures by co-assembly of non-brush BCPs had apparently been unsuccessful.[369] Co-assembly with brush BCPs was necessary because the increased steric bulk hindered micelle growth. Tapping-mode AFM showed that co-assembly afforded a gradient type structure with an initial bias for the assembly of the linear PFDMS-*b*-PMVS over the brush PFDMS-*b*-PMVS, which was reversed slowly as the linear BCP was consumed. A miktoarm-star PFS-containing polymer has also been shown to form phase-segregated "patchy"-type cylindrical micelles and comicelles.[370]

5.3.4. Non-centrosymmetric PFS block comicelles. As previously discussed, cylindrical micelles that have a corona with pendant vinyl groups are able to undergo shell-crosslinking reactions (see Section 5.3.2). Through a combination of selective micelle corona shell-crosslinking and living CDSA of PFS-containing block comicelles, non-centrosymmetric unidirectional micelles have been prepared (see schematic (a, b) in Fig. 41).[371] For example, symmetric ABA triblock comicelles with a central PFDMS-*b*-PDMS block and outer PI-*b*-PFDMS blocks can undergo selective shell-crosslinking of the PI corona (Fig. 41c and d). If the PI corona is sufficiently long, crosslinking can effectively cover the ends of the cylindrical micelle which inhibits the addition of further unimer. The central block can be removed through the addition of common solvent such as toluene to the micelle solution, leaving shell-crosslinked PI-*b*-PFDMS micelles with only one open face for unimer addition and solvated PFDMS-*b*-PDMS unimer in solution (Fig. 41e). Subsequent evaporation of toluene promoted PFDMS-*b*-PDMS unimer addition to the PI-*b*-PFDMS seeds, forming non-centrosymmetric AB diblock comicelles that grow selectively in one direction

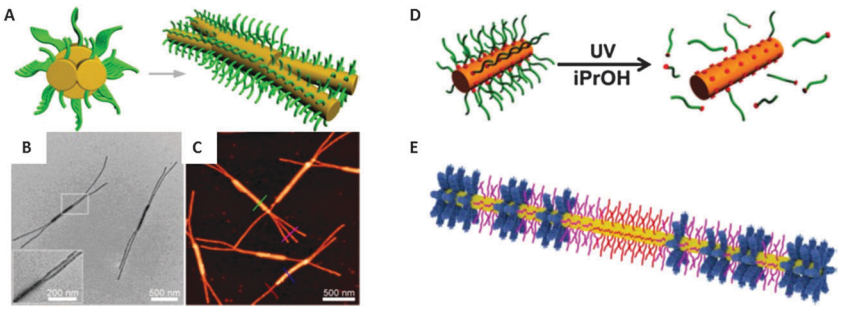

Fig. 40 (A) Schematic representation, (B) TEM image and (C) AFM height image of branched comicelles of PFDMS-*b*-P2VP; (D) schematic representation for coronal photocleavage of PFDMS-ONB-P2VP; (E) schematic representation of "patchy" cylindrical block comicelles from gradient CDSA. Reproduced with permission from ref. 364 (copyright 2015 American Chemical Society), ref. 365 (copyright 2014 American Chemical Society), and 355 (copyright 2013 American Chemical Society).

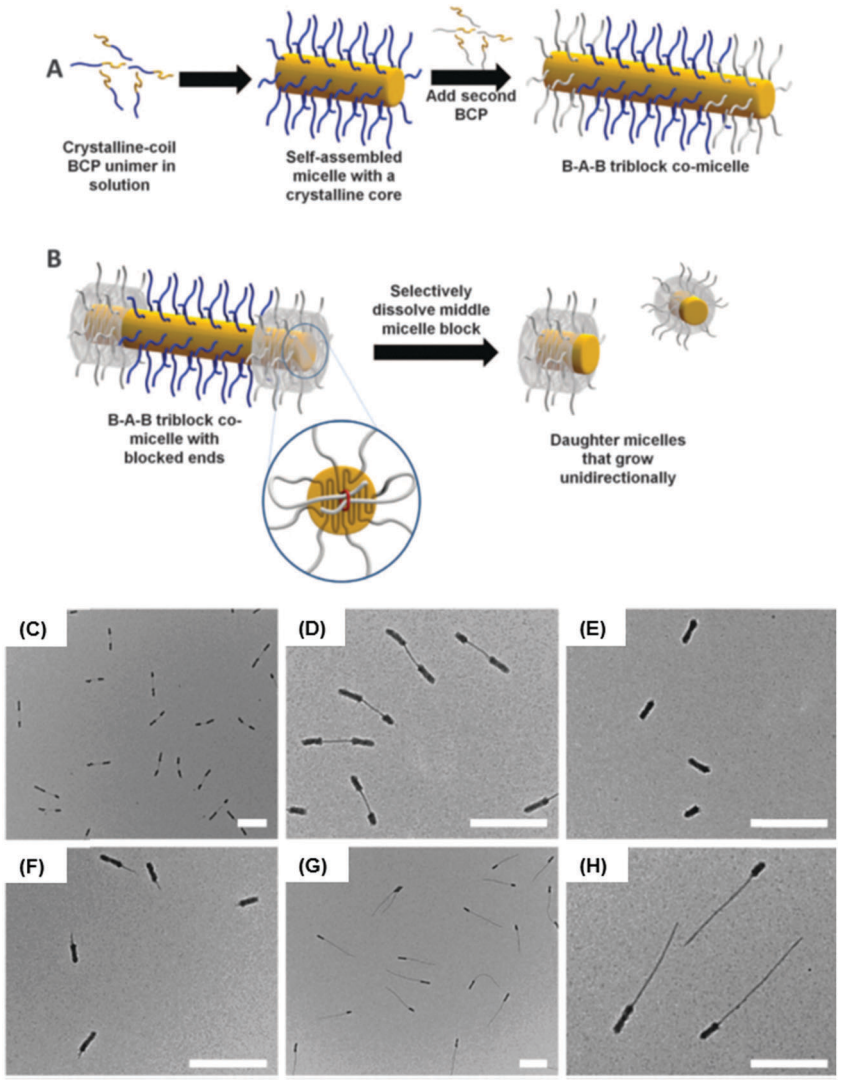

Fig. 41 Schematic (a and b) showing the preparation of unidirectional seed micelles; TEM images of (c and d) ABA triblock comicelles with crosslinked end blocks; (e) crosslinked unidirectional A block seed micelles after dissolution of the central block; (f) unidirectional AB diblock comicelles after removal of toluene; (g and h) unidirectional AB diblock comicelles after the addition of further unimer. Scale bars are 500 nm. Reproduced with permission from ref. 371. Copyright 2012 The American Association for the Advancement of Science.

from the singular open crystalline face of the micelle (Fig. 41f–h). Non-centrosymmetric diblock comicelles have also been prepared *via* self-assembly of BCP off PFDMS homopolymer nanocrystals.[358] A PI-*b*-PFDMS BCP unimer solution was added to PFDMS nanocrystals, which acted as a nucleation point for the BCP, to give cylindrical micelle arms off the central nanoparticle. The PI coronal chains were crosslinked, and a second PFDMS-*b*-PMVS unimer solution was added to afford non-centrosymmetric AB block comicelles, followed by a second crosslinking reaction for the PMVS coronal chains. Dissolution of the PFS homopolymer led to the release of non-centrosymmetric AB cylindrical diblock comicelles.

As an extension of this work, fluorescent non-centrosymmetric multi-compartment block comicelles have been prepared that can act as nanoscale pixels with fully tunable colour emissions.[348] A PFS-containing BCP with a random copolymer corona-forming block ($PFDMS_{62}$-*b*-[($PDMS_{605}$)/($PMVS_{21}$)]$_{626}$) was prepared through sequential living anionic polymerisation. The pendant vinyl groups on the PMVS components within the second block were then functionalised through a thiol–ene "click" reaction with a number of different fluorescent dye molecules to form red, blue and green fluorescent BCPs. Seeded growth of different ratios of these unimers enabled the preparation of monodisperse coassembled cylindrical micelles that emitted different colours depending on the amounts of each fluorescent unimer used. Individual imaging of each coloured micelle could be tracked with laser scanning confocal microscopy (LSCM), revealing that the luminescence was uniform throughout the micelle. Fluorescent BCP unimers were also added sequentially to a pre-formed PFDMS-*b*-PDMS cylindrical seed micelle, followed by a non-fluorescent PFDMS-*b*-PDMS BCP to act as a spacer between each fluorescent block in order to increase optical resolution. This allowed the formation of centrosymmetric 11-block comicelles where each colour represented along the micelle can be

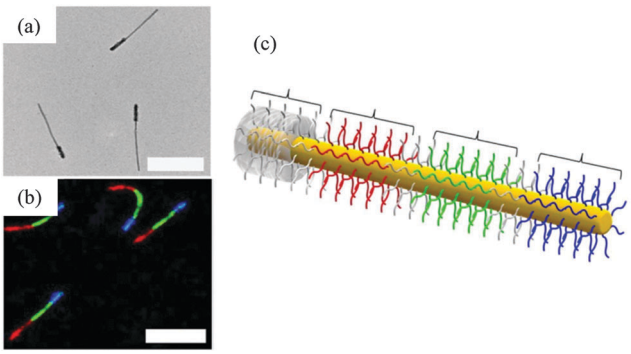

Fig. 42 (a) TEM image, (b) LSCM image and (c) schematic representation of non-centrosymmetric RGB "nanopixel" block comicelles. Scale bars are (a) 500 nm and (b) 2 μm. Reproduced with permission from ref. 348. Copyright 2014 Nature Publishing Group.

individually tuned. Furthermore, by using unidirectional cylindrical seed micelles, non-centrosymmetric 7-block comicelles could be prepared through the sequential addition of each fluorescent BCP followed by small segments of non-fluorescent BCP (see Fig. 42). The block comicelles are stable over long periods with no detected rearrangement of the fluorescent unimers along the length of the cylinders, which indicated that they exist as static, kinetically trapped structures.

5.3.5. Formation of PFS supermicelles by hierarchical self-assembly. It has been demonstrated that the level of control over the formation of individual micelles by living CDSA can allow the preparation of a variety of micron-sized superstructures with coronal nanodomains of different composition and functionality. For example, the ability to tailor PFS-containing block comicelles through the assembly of a variety of BCPs can allow the introduction of amphiphilicity. The resulting building blocks can be used for the preparation of complex hierarchical structures.[372–377]

For example, PFS homopolymer can be used to aggregate short BCP cylindrical micelles into networks.[350] End-to-end coupling of two or more micelles gave linear, linked or branched structures depending on the composition of the BCP micelle and the PFS polymer added.

Cylindrical non-centrosymmetric ABC triblock comicelles composed of two hydrophobic blocks (A and B) and a long hydrophilic block (C) have been shown to undergo hierarchical self-assembly in a selective solvent for the hydrophilic coronal block.[371] The block comicelles self-assembled into star-shaped supermicelles with a "core" composed of the hydrophobic blocks and a "corona" of the hydrophilic blocks.

The use of amphiphilic ABA triblock comicelles as building blocks for hierarchical self-assembly can allow the formation of a range of different supermicellar morphologies (see Fig. 43).[378] Block comicelles with a central hydrophobic PFDMS-*b*-PDMS block and terminal hydrophilic PFDMS-*b*-P2VP blocks can self-assemble upon dialysing the micellar solutions against isopropanol, a selective solvent for the terminal hydrophilic coronal blocks. Depending on the length of the central B block within the pre-formed micelles, the aggregation number,

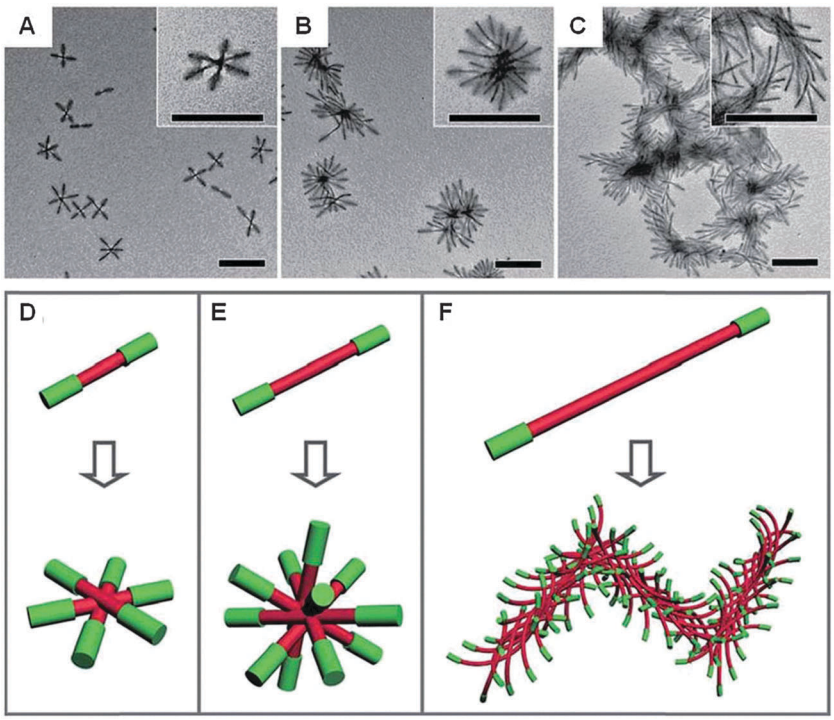

Fig. 43 (a–c) TEM images and (d–f) corresponding schematic representations of hierarchical self-assembly of ABA amphiphilic triblock comicelles with different B block lengths after dialysis against isopropanol. Scale bars are 500 nm. Reproduced with permission from ref. 378. Copyright 2012 John Wiley & Sons Inc.

morphology, packing and symmetry of the resulting supermicelles can be tuned to achieve crossed and elongated network structures.

As a continuation of this work on amphiphilic block comicelles, it was reported that the resulting micron-scale assemblies can be easily controlled through altering the structural features of the starting block comicelles.[379] Monodisperse BAB amphiphilic triblock comicelles with either hydrophilic or hydrophobic central or terminal corona-forming blocks were prepared. These structures were found to stack either side by side in non-solvents for the central block, or end to end in non-solvents for the terminal block, which allows the formation of a variety of 1D and 3D superlattice structures (see Fig. 44).[379] These aggregates possess multiple levels of structural hierarchy on length-scales that are normally only apparent in nature. In addition, the functionality of the micelle coronas is unchanged throughout the self-assembly process from the initial stages to the formation of superstructures. Therefore it is an effective way of incorporating function to these supermicelles, which is demonstrated by using BCPs tagged with fluorescent dyes, allowing fluorescent superstructures to be prepared.

Due to the size of many of these superstructures, they can be observed using optical microscopy techniques and can be efficiently manipulated in three dimensions using optical tweezers.[380] This can allow the fabrication of hierarchical chain-like superstructures *via* crosslinking of "arms" of multiple supermicelles and patterning of supermicelles into arrays by dynamic holographic assembly, which is outlined in Fig. 45.[380] These supermicelles are able to undergo further living CDSA processes and "grow" under flow conditions with a unimer-containing solution.

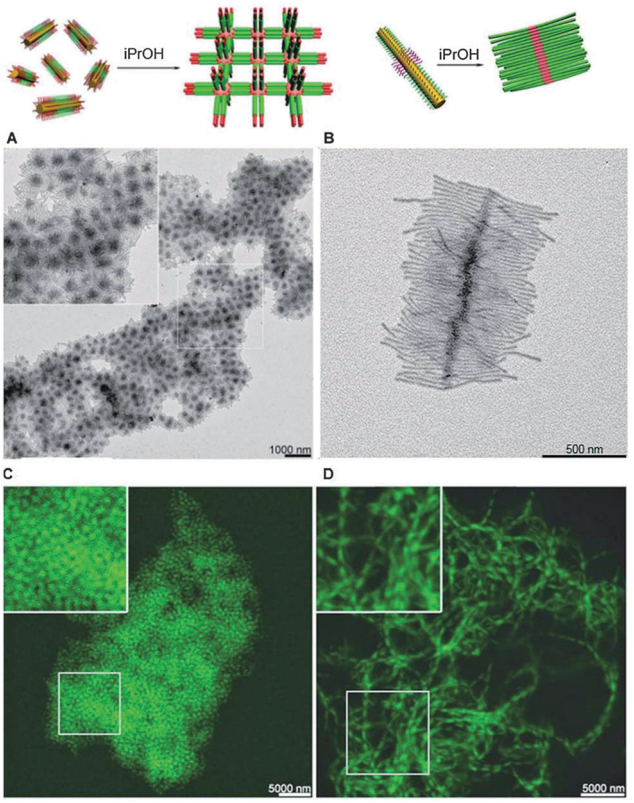

Fig. 44 (top) Schematic representations for the formation of 1D and 3D supermicelles and superlattices through stacking of ABA and BAB triblock comicelles; (a and b) corresponding TEM images and (c and d) LSCM images of 1D and 3D supermicelle aggregates. Reproduced with permission from ref. 379. Copyright 2015 The American Association for the Advancement of Science.

Supermicelles with complex architectures have also been prepared through a combination of solvophobic interactions and hydrogen bonding.[381] Amphiphilic block comicelles with a very short hydrophobic PFDMS-*b*-PMVS central block and long hydrophilic PFDMS-*b*-P2VP end blocks could self-assemble into cross-type structures after dialysing into a selective solvent for the terminal coronal blocks. Following crosslinking of the central PFDMS-*b*-PMVS blocks, PFDMS-*b*-PtBA (PtBA: poly-*tert*-butylacrylate) unimer was added to the cross arms, and the preceding PFDMS-*b*-P2VP blocks were crosslinked using Karstedt's catalyst. Secondly, PFDMS-*b*-P2VP blocks were grown off the cross arms and short stub-like seeds of PFDMS-*b*-PMVSOH (PMVSOH: hydroxyl-functionalised PMVS) were then added to the micellar solution. The seeds selectively hydrogen bonded with the uncrosslinked PFDMS-*b*-P2VP blocks of the cross superstructures and following addition of further PFDMS-*b*-PtBA unimer, intricate "windmill"-type supermicelles were formed (see Fig. 46). This approach shows an efficient methodology towards the fabrication of highly complex and potentially functional architectures through the use of a range of different non-covalent interactions.

5.3.6. Living CDSA of PFS BCPs in two dimensions. Despite the significant work on the formation of one-dimensional micellar aggregates from PFS-containing BCPs and the excellent control exhibited, the analogous creation of two-dimensional assemblies has proven more difficult. Early investigations into the influence of block ratio on self-assembly yielded two-dimensional platelet PFS BCP micelles when the block ratio between the two blocks is 1 : 1.[221] However, recently more systems forming 2D structures have been reported.

Lenticular platelets have been reported in recent years, however little to no control over their size was demonstrated.[337,382] Pointed oval platelets have been prepared through a living CDSA type method by the addition of PFDMS-*b*-PP BCP unimer (PP = polyphosphazene) to PFDMS-*b*-P2VP seed micelles.[383] It was shown that the use of monodisperse rather than polydisperse seed micelles led to ovals with a uniform shape and size by living CDSA. AFM analysis revealed 3D growth around the PFDMS-*b*-P2VP seed which occurs due to interplay of the relative growth rates in all three orthogonal directions. Additionally, these pointed oval micelles could be used as initiators for the growth of cylindrical micelles to yield hierarchical assemblies.

The formation of lenticular platelets and multicompartment 2D structures of controlled area has been reported.[384] A range of platelet-forming PFS BCPs were prepared and unimer solutions of these were added to short cylindrical seed micelles. The resulting 2D lenticular platelets were shown to be uniform in size and grew linearly with unimer-to-seed ratio and with narrow area polydispersity (<1.1).

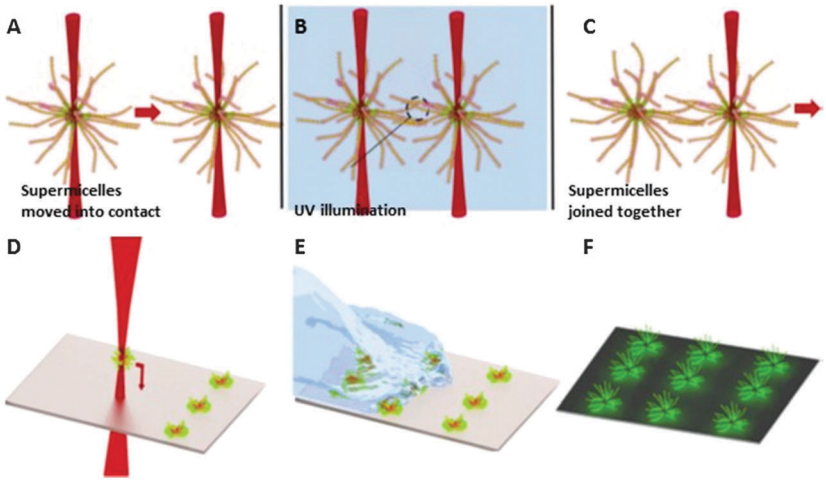

Fig. 45 (a–c) Schematic representation showing the assembly process of linking multiple supermicelles together; (d–f) schematic representation of patterned deposition and growth of supermicelle arrays. Reproduced with permission from ref. 380. Copyright 2015 Nature Publishing Group.

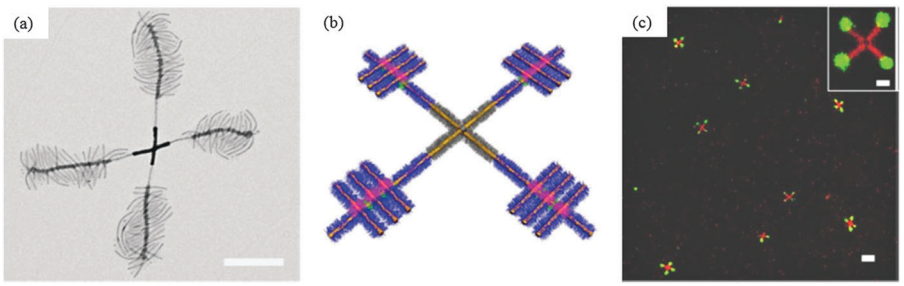

Fig. 46 (a) TEM image, (b) schematic representation and (c) LSCM image of "windmill"-like supermicelles. Scale bars are (a) 500 nm, (c) 5 μm and 1 μm (inset). Reproduced with permission from ref. 381. Copyright 2015 Nature Publishing Group.

Block comicelle platelet structures were also formed through the sequential addition of different PFS-containing platelet-forming BCP unimer. These concentric multicompartment aggregates were easily visualised by LSCM through the use of BCPs functionalised with red, green and blue fluorescent dyes (see Fig. 47). Single- and double-headed arrow- and spear-type architectures were also formed through using both unidirectional non-centrosymmetric and longer cylindrical seed micelles, respectively.[384]

Polydisperse two-dimensional structures have been prepared by the simple blending of cylinder-forming PFS-containing BCPs with lamellae-forming PFS homopolymer, where co-crystallisation plays a vital role in the structure obtained during micellisation. Self-assembly of the homopolymer and block copolymer blends leads to the formation of assemblies with elongated 2D cores and fibre-like protrusions from the core ends. The morphology obtained could be varied by changing the ratio of homopolymer

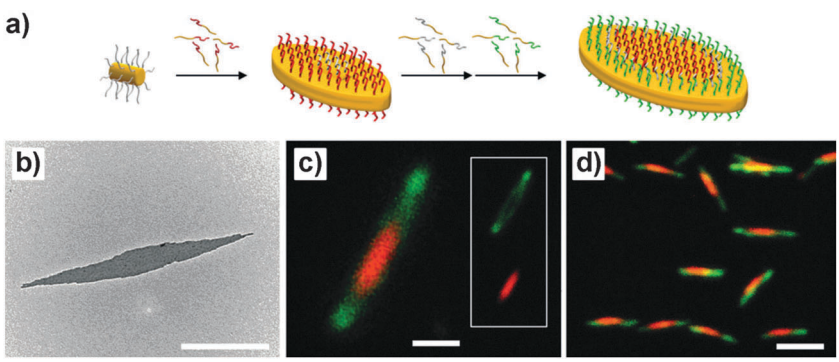

Fig. 47 (a) Schematic representation for the formation of uniform concentric 2D lenticular platelets; (b) TEM image and (c and d) LSCM images of lenticular platelet micelles showing their concentric structure. Scale bars are (b and c) 500 nm and (d) 2 μm. Reproduced with permission from ref. 384. Copyright 2014 Nature Publishing Group.

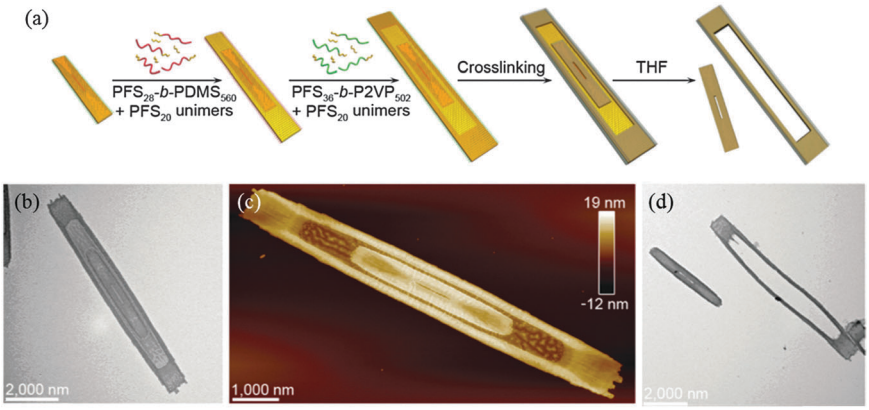

Fig. 48 (a) Schematic representation for the formation of uniform concentric and hollow rectangular platelet micelles; (b) TEM and (c) AFM images of a concentric rectangular micelle and (d) TEM image of a perforated rectangular platelet micelle and the corresponding rectangular ring platelet micelle after crosslinking and subsequent dissolution of the non-crosslinked segment. Reproduced with permission from ref. 386. Copyright 2016 The American Association for the Advancement of Science.

to block copolymer, as well as the molecular weight of the homopolymer.[385] The use of a seeded growth approach allows the preparation of well-defined platelet micelles, including segmented structures (see Fig. 48). Perforated and hollow rectangular micelles can be prepared by spatially selective crosslinking and dissolution procedures.[386]

5.3.7. Hybrid mesostructures from PFS-containing materials. Synthetic approaches towards hierarchical materials have to overcome significant challenges.[387–389] As a result of recent developments, a number of hybrid mesostructures have been prepared with PFS-based BCPs and micelles.

Controlled hybrid architectures have been reported by anchoring PFDMS-*b*-P2VP seed micelles onto the surface of silica nanoparticles (see Fig. 49A). The adsorbed seed micelles were active towards living CDSA and addition of further PFDMS-*b*-P2VP unimer afforded "sunflower"-type assemblies.[390] Following the same rationale, when using silica-coated Ni-nanorods, "butterfly"-type architectures were formed. Furthermore, when quaternised unimer was added to the seed micelles, the structures could be functionalised with Au nanoparticles, showing that the hybrid mesostructures are robust enough to undergo post-modifications.

In a similar procedure, PFDMS-*b*-P2VP seeds have been shown to adsorb onto the surface of PS nanobeads which can allow the formation of fibre-basket polymersomes *via* corona-crosslinking of the micelles (see Fig. 49B).[391] The PS scaffold acted as a sacrificial template, affording hollow vesicular assemblies which can be efficiently post-functionalised both at the micelle cores and corona.

Hybrid "shish kebab"-type mesostructures have also been prepared through the functionalisation of carbon nanotubes with PFS-containing materials.[392] PFS homopolymer crystals were attached to multi-walled carbon nanotubes which could subsequently act as nucleation sites for PFS-containing BCPs, yielding the aforementioned hybrid assemblies (see Fig. 49C). After crosslinking of the surrounding micelles, these architectures could then be used as scaffolds for the growth of Ag nanoparticles within the micelle cores.

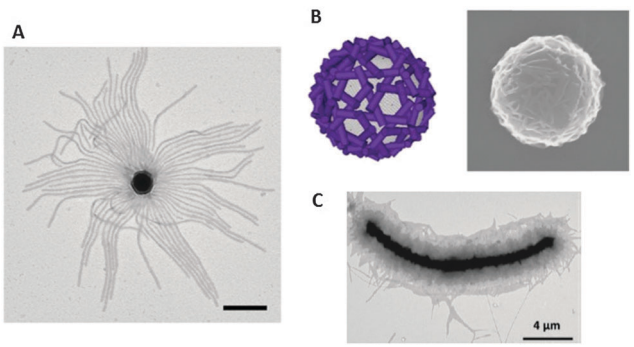

Fig. 49 Images showing hybrid mesostructures possible with PFS-containing materials; (A) TEM image of "sunflower"-type assembly *via* seeded growth off a silica nanoparticle; (B) schematic representation and SEM image of fibre-basket polymersome by crosslinking of PFDMS-*b*-P2VP seed micelles on the surface of a PS bead; (C) TEM image of PFS–carbon nanotube hybrid structure. Scale bar is (A) 500 nm. Reproduced with permission from ref. 390 (copyright 2014 Nature Publishing Group), ref. 391 (copyright 2014 American Chemical Society), and ref. 392 (copyright 2015 American Chemical Society).

5.4. Applications of PFS BCP micelles

Crosslinking of PFS-containing micelles has been shown to be necessary for certain applications of cylindrical and nanotube morphologies. Crosslinking is essential for accessing one-dimensional PFS nanoceramics in high yield.[222,344,346] Pyrolysis of the shell-crosslinked micelles occurs upon heating to 600 °C which results in ceramics with excellent shape retention. Uncrosslinked micelles were also pyrolysed however this lead to the destruction of the micellar core. Shell-crosslinked micelles have also been aligned and patterned on silicon substrates by microfluidic techniques, which may have interesting applications as magnetic memory materials or catalysts after pyrolysis.[292–294]

PFS shell-crosslinked nanotubes have potential for encapsulation of guest particles or compounds within the hollow centre of the nanotube *via in situ* redox-reactions using PFS as a reductant.[345,347,367] Silver nanoparticles were prepared within the nanotubes through reaction with $Ag[PF_6]$. Partial pre-oxidation

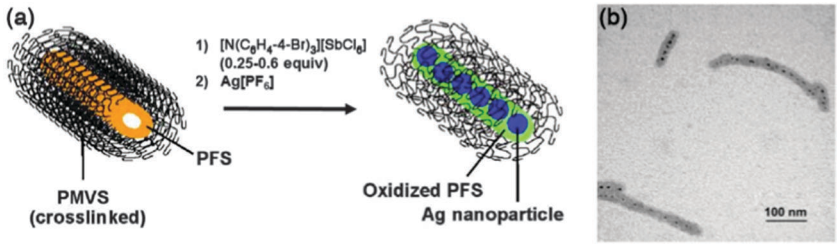

Fig. 50 (a) Scheme for the generation of Ag nanoparticles within self-assembled PFDMS-*b*-PMVS nanotube micelles and (b) TEM images with Ag nanoparticles within micelle cores. Reproduced with permission from ref. 345. Copyright 2005 American Chemical Society.

of the PFS domains with an organic oxidant is needed for efficient formation of one-dimensional arrays of nanoparticles within the nanotube (see Fig. 50). Redox-controlled self-assembling PFS BCP systems and redox-active vesicles have also been studied.[322,323]

Cylindrical PFS BCP micelles have possible applications as nanolithographic etch resists for semiconducting substrates like GaAs or Si with potential for the fabrication of magnetic or semiconducting nanoscopic patterns.[54,393] Cylindrical micelles have been deposited onto a GaAs surface by capillary forces into grooves etched out by electron beam patterning and, following plasma etching, generated connected ceramic lines with reduced size.

PFS BCPs with a polypeptide corona-forming block have been found to form thermally reversible gels.[394] PFDMS-*b*-PBLG materials are soluble in hot toluene but upon cooling to room temperature they form amber, optically transparent gels. The critical concentration for gelation was dependant on the PBLG block length and the block ratio. However when the block ratio became greater than 1 : 3 (PFS : PBLG), incomplete gelation was observed.

Functional electrodes composed of glucose oxidase and cross-linkable PI-*b*-PFDMS nanostructures including nanoparticles and cylinders have been shown to be effective as biosensors.[395] The morphology of the PFS BCP was shown to have a key role in affecting the electrochemical properties and the catalytic activities of the enzyme integrated electrodes. The biosensing ability of optimised electrodes showed good sensitivity at the physiological concentration of glucose in blood, and could be applicable to other types of nanostructured enzymatic biofuel cells.

Shape anisotropic PFS BCP nanoparticles have been shown to exhibit both morphological transitions and shape changes upon either exposure to selective solvents, or redox agents such as $FeCl_3$, respectively.[338] This opens up applications as stimuli-responsive materials. Fluorescent multiblock comicelles present a novel approach towards the preparation of encoded nanomaterials with potential applications in high density data storage materials and biological diagnostics.[348]

6. Summary and future work

Since the first syntheses of high molar mass examples were reported in the early 1990s, PFS materials have developed into a large class of metal-containing organosilicon hybrid polymers. Living anionic ROP methods have allowed the preparation of well-defined main chain metallopolymers with controlled architectures such as end-functionalised homopolymers and PFS BCPs. As is clear from this detailed review, PFS homopolymers and BCPs have attracted much attention as a result of their interesting properties and functions.

Although many further advances in the area of functional PFS materials that exploit their unique combination of easy processing and unusual physical and chemical properties are anticipated, the development of these polymers has clearly led to an even broader scientific impact. For example, the phenomenon "living crystallisation-driven self-assembly" discovered for PFS BCPs has also now been transposed to other organic BCP systems.[396–398] In addition, PFS materials represent a key new class of readily accessible metallopolymer[399] and their development has provided an excellent illustration of the potential of this very broad and vibrant field.[1] Thus, analogues of PFS with other elements in the spacer or containing different metals to iron (in some cases in combination with alternative π-hydrocarbon ligands) have been prepared and their formation by ROP has been successfully demonstrated in a growing number of cases. This provides a route to new and fascinating metallopolymers with modified properties,[223,400–406] and studies of these materials are likely to constitute a broad new area of future research.

The development of PFS materials has also helped stimulate further development of other polymer systems with metallocene side groups, such as poly(vinylferrocene), poly(ferrocenylmethacrylates), and related materials,[407,408] and also side chain polycobaltocenes.[409] Important advances in these areas with respect to living polymerisation, self-assembly, and applications have been recently reported. Overall, these considerations all suggest that the prospects for various polymer classes containing metallocene units appear to be very bright.

References

1 G. R. Whittell, M. D. Hager, U. S. Schubert and I. Manners, *Nat. Mater.*, 2011, **10**, 176–188.
2 I. Manners, *Polyhedron*, 1996, **15**, 4311–4329.
3 E. W. Neuse and H. Rosenberg, *J. Macromol. Sci., Polym. Rev.*, 1970, **4**, 1–145.
4 I. Manners, *Chem. Commun.*, 1999, 857–865.
5 V. Bellas and M. Rehahn, *Angew. Chem., Int. Ed.*, 2007, **46**, 5082–5104.
6 D. A. Rider and I. Manners, *Polym. Rev.*, 2007, **47**, 165–195.

7 K. Kulbaba and I. Manners, *Macromol. Rapid Commun.*, 2001, **22**, 711–724.
8 I. Manners, *Synthetic Metal-Containing Polymers*, John Wiley & Sons, Ltd., Chichester, 2004.
9 A. Osborne and R. Whiteley, *J. Organomet. Chem.*, 1975, **101**, C27–C28.
10 I. R. Butler and W. R. Cullen, *Organometallics*, 1986, **5**, 2537–2542.
11 I. R. Butler, W. R. Cullen, J. Ni and S. J. Rettig, *Organometallics*, 1985, **4**, 2196–2201.
12 J. J. Bishop, A. Davison, M. L. Katcher, D. W. Lichtenberg, R. E. Merrill and J. C. Smart, *J. Organomet. Chem.*, 1971, **27**, 241–249.
13 R. A. Musgrave, A. D. Russell and I. Manners, *Organometallics*, 2013, **32**, 5654–5667.
14 A. B. Fischer, J. B. Kinney, R. H. Staley and M. S. Wrighton, *J. Am. Chem. Soc.*, 1979, **101**, 6501–6506.
15 R. A. Musgrave, A. D. Russell, G. R. Whittell, M. F. Haddow and I. Manners, *Organometallics*, 2015, **34**, 897–907.
16 P. Nguyen, G. Stojcevic, K. Kulbaba, M. J. MacLachlan, X.-H. Liu, A. J. Lough and I. Manners, *Macromolecules*, 1998, **31**, 5977–5983.
17 F. Jäkle, E. Vejzovic, K. N. Power-Billard, M. J. MacLachlan, A. J. Lough and I. Manners, *Organometallics*, 2000, **19**, 2826–2828.
18 Y. Hatanaka, S. Okada, T. Minami, M. Goto and K. Shimada, *Organometallics*, 2005, **24**, 1053–1055.
19 S. C. Bourke, F. Jäkle, E. Vejzovic, K.-C. Lam, A. L. Rheingold, A. J. Lough and I. Manners, *Chem. – Eur. J.*, 2003, **9**, 3042–3054.
20 M. J. MacLachlan, A. J. Lough, W. E. Geiger and I. Manners, *Organometallics*, 1998, **17**, 1873–1883.
21 A. Berenbaum, F. Jäkle, A. J. Lough and I. Manners, *Organometallics*, 2001, **20**, 834–843.
22 D. A. Foucher, B. Z. Tang and I. Manners, *J. Am. Chem. Soc.*, 1992, **114**, 6246–6248.
23 J. K. Pudelski, D. A. Foucher, C. H. Honeyman, A. J. Lough, I. Manners, S. Barlow and D. O'Hare, *Organometallics*, 1995, **14**, 2470–2479.
24 J. C. Green, *Chem. Soc. Rev.*, 1998, **27**, 263–272.
25 J.-J. Wang, L. Wang, T. Chen, X.-J. Wang, C.-L. Wang, X.-C. Dong and J.-H. Yang, *Eur. Polym. J.*, 2006, **42**, 843–848.
26 J.-J. Wang, L. Wang, X.-J. Wang, T. Chen, H.-J. Yu, W. Wang and C.-L. Wang, *Mater. Lett.*, 2006, **60**, 1416–1419.
27 G. Calleja, F. Carré, G. Cerveau, P. Labbé and L. Coche-Guérente, *Organometallics*, 2001, **20**, 4211–4215.
28 D. L. Zechel, K. C. Hultzsch, R. Rulkens, D. Balaishis, Y. Ni, J. K. Pudelski, A. J. Lough, I. Manners and D. A. Foucher, *Organometallics*, 1996, **15**, 1972–1978.
29 J. K. Pudelski and I. Manners, *J. Am. Chem. Soc.*, 1995, **117**, 7265–7266.
30 J. K. Pudelski, D. A. Foucher, C. H. Honeyman, P. M. Macdonald, I. Manners, S. Barlow and D. O'Hare, *Macromolecules*, 1996, **29**, 1894–1903.
31 F. Jäkle, R. Rulkens, G. Zech, J. A. Massey and I. Manners, *J. Am. Chem. Soc.*, 2000, **122**, 4231–4232.
32 T. Baumgartner, F. Jäkle, R. Rulkens, G. Zech, A. J. Lough and I. Manners, *J. Am. Chem. Soc.*, 2002, **124**, 10062–10070.
33 Y. Ni, R. Rulkens, J. K. Pudelski and I. Manners, *Macromol. Rapid Commun.*, 1995, **16**, 637–641.
34 N. P. Reddy, H. Yamashita and M. Tanaka, *J. Chem. Soc., Chem. Commun.*, 1995, 2263–2264.
35 P. W. Cyr, D. A. Rider, K. Kulbaba and I. Manners, *Macromolecules*, 2004, **37**, 3959–3961.
36 K. N. Power-Billard and I. Manners, *Macromolecules*, 2000, **33**, 26–31.
37 K. Temple, S. Dziadek and I. Manners, *Organometallics*, 2002, **21**, 4377–4384.
38 K. Temple, F. Jäkle, J. B. Sheridan and I. Manners, *J. Am. Chem. Soc.*, 2001, **123**, 1355–1364.
39 P. Gómez-Elipe, R. Resendes, P. M. Macdonald and I. Manners, *J. Am. Chem. Soc.*, 1998, **120**, 8348–8356.
40 C. A. Jaska, A. Bartole-Scott and I. Manners, *Dalton Trans.*, 2003, 4015–4021.
41 A. Bartole-Scott, R. Resendes and I. Manners, *Macromol. Chem. Phys.*, 2003, **204**, 1259–1268.
42 H. Tang, Y. Liu, X. Chen, J. Qin, M. Inokuchi, M. Kinoshita, X. Jin, Z. Wang and B. Xu, *Macromolecules*, 2004, **37**, 9785–9792.
43 J. Rasburn, R. Petersen, R. Jahr, R. Rulkens, I. Manners and G. J. Vancso, *Chem. Mater.*, 1995, **7**, 871–877.
44 J. Rasburn, D. A. Foucher, W. F. Reynolds and G. J. Vancso, *Chem. Commun.*, 1998, 843–844.
45 R. Rulkens, Y. Ni and I. Manners, *J. Am. Chem. Soc.*, 1994, **116**, 12121–12122.
46 Y. Ni, R. Rulkens and I. Manners, *J. Am. Chem. Soc.*, 1996, **118**, 4102–4114.
47 R. G. H. Lammertink, M. A. Hempenius, I. Manners and G. J. Vancso, *Macromolecules*, 1998, **31**, 795–800.
48 J. A. Massey, K. Temple, L. Cao, Y. Rharbi, J. Raez, M. A. Winnik and I. Manners, *J. Am. Chem. Soc.*, 2000, **122**, 11577–11584.
49 D. A. Rider, K. A. Cavicchi, K. N. Power-Billard, T. P. Russell and I. Manners, *Macromolecules*, 2005, **38**, 6931–6938.
50 C. Acikgoz, M. A. Hempenius, G. J. Vancso and J. Huskens, *Nanotechnology*, 2009, **20**, 135304.
51 J. Gwyther and I. Manners, *Polymer*, 2009, **50**, 5384–5389.
52 K. N. Power-Billard, P. Wieland, M. Schäfer, O. Nuyken and I. Manners, *Macromolecules*, 2004, **37**, 2090–2095.
53 C. Kloninger and M. Rehahn, *Macromolecules*, 2004, **37**, 1720–1727.
54 J. A. Massey, M. A. Winnik, I. Manners, V. Z.-H. Chan, J. M. Ostermann, R. Enchelmaier, J. P. Spatz and M. Möller, *J. Am. Chem. Soc.*, 2001, **123**, 3147–3148.
55 M. Zhang, P. A. Rupar, C. Feng, K. Lin, D. J. Lunn, A. Oliver, A. Nunns, G. R. Whittell, I. Manners and M. A. Winnik, *Macromolecules*, 2013, **46**, 1296–1304.
56 X.-S. Wang, M. A. Winnik and I. Manners, *Macromol. Rapid Commun.*, 2002, **23**, 210–213.
57 M. Tanabe and I. Manners, *J. Am. Chem. Soc.*, 2004, **126**, 11434–11435.
58 M. Tanabe, G. W. M. Vandermeulen, W. Y. Chan, P. W. Cyr, L. Vanderark, D. A. Rider and I. Manners, *Nature Mater.*, 2006, **5**, 467–470.

59 W. Y. Chan, A. J. Lough and I. Manners, *Chem. – Eur. J.*, 2007, **13**, 8867–8876.
60 G. S. Smith, S. K. Patra, L. Vanderark, S. Saithong, J. P. H. Charmant and I. Manners, *Macromol. Chem. Phys.*, 2010, **211**, 303–312.
61 W. Y. Chan, A. J. Lough and I. Manners, *Organometallics*, 2007, **26**, 1217–1225.
62 Z. Wang, G. Masson, F. C. Peiris, G. A. Ozin and I. Manners, *Chem. – Eur. J.*, 2007, **13**, 9372–9383.
63 M. Erhard, K. Lam, M. Haddow, G. R. Whittell, W. E. Geiger and I. Manners, *Polym. Chem.*, 2014, **5**, 1264–1274.
64 L. Chabanne, I. Matas, S. K. Patra and I. Manners, *Polym. Chem.*, 2011, **2**, 2651–2660.
65 W. Y. Chan, A. J. Lough and I. Manners, *Angew. Chem., Int. Ed.*, 2007, **46**, 9069–9072.
66 D. E. Herbert, J. B. Gilroy, W. Y. Chan, L. Chabanne, A. Staubitz, A. J. Lough and I. Manners, *J. Am. Chem. Soc.*, 2009, **131**, 14958–14968.
67 D. E. Herbert, M. Tanabe, S. C. Bourke, A. J. Lough and I. Manners, *J. Am. Chem. Soc.*, 2008, **130**, 4166–4176.
68 Z. Cheng, B. Ren, D. Zhao, X. Liu and Z. Tong, *Macromolecules*, 2009, **42**, 2762–2766.
69 Z. Wang, A. Lough and I. Manners, *Macromolecules*, 2002, **35**, 7669–7677.
70 M. A. Hempenius, N. S. Robins, R. G. H. Lammertink and G. J. Vancso, *Macromol. Rapid Commun.*, 2001, **22**, 30–33.
71 M. A. Hempenius, F. F. Brito and G. J. Vancso, *Macromolecules*, 2003, **36**, 6683–6688.
72 F. Jäkle, Z. Wang and I. Manners, *Macromol. Rapid Commun.*, 2000, **21**, 1291–1296.
73 S. Hilf, P. W. Cyr, D. A. Rider, I. Manners, T. Ishida and Y. Chujo, *Macromol. Rapid Commun.*, 2005, **26**, 950–954.
74 X.-H. Liu, D. W. Bruce and I. Manners, *J. Organomet. Chem.*, 1997, **548**, 49–56.
75 L. Chabanne, S. Pfirrmann, D. J. Lunn and I. Manners, *Polym. Chem.*, 2013, **4**, 2353–2360.
76 S. B. Clendenning and I. Manners, *Macromol. Symp.*, 2003, **196**, 71–76.
77 W. Y. Chan, S. B. Clendenning, A. Berenbaum, A. J. Lough, S. Aouba, H. E. Ruda and I. Manners, *J. Am. Chem. Soc.*, 2005, **127**, 1765–1772.
78 G. Masson, P. Beyer, P. W. Cyr, A. J. Lough and I. Manners, *Macromolecules*, 2006, **39**, 3720–3730.
79 A. Presa Soto, L. Chabanne, J. Zhou, J. B. Gilroy and I. Manners, *Macromol. Rapid Commun.*, 2012, **33**, 592–596.
80 J. A. Massey, K. Kulbaba, M. A. Winnik and I. Manners, *J. Polym. Sci. Part B: Polym. Phys.*, 2000, **38**, 3032–3041.
81 D. A. Foucher, R. Ziembinski, B. Z. Tang, P. M. Macdonald, J. Massey, C. R. Jaeger, G. J. Vancso and I. Manners, *Macromolecules*, 1993, **26**, 2878–2884.
82 D. Foucher, R. Ziembinski, R. Petersen, J. Pudelski, M. Edwards, Y. Ni, J. Massey, C. R. Jaeger, G. J. Vancso and I. Manners, *Macromolecules*, 1994, **27**, 3992–3999.
83 K. Kulbaba, M. J. MacLachlan, C. E. B. Evans and I. Manners, *Macromol. Chem. Phys.*, 2001, **202**, 1768–1775.
84 G. R. Whittell, J. B. Gilroy, I. Grillo, I. Manners and R. M. Richardson, *J. Polym. Sci., Part A: Polym. Chem.*, 2013, **51**, 4011–4020.
85 Y. Xiong, G. Wang, J. Qin and H. Tang, *J. Inorg. Organomet. Polym.*, 2015, **25**, 91–97.
86 V. A. Du and I. Manners, *Macromolecules*, 2013, **46**, 4742–4753.
87 P. Nguyen, P. Gómez-Elipe and I. Manners, *Chem. Rev.*, 1999, **99**, 1515–1548.
88 M. A. Hempenius, R. G. H. Lammertink and G. J. Vancso, *Macromol. Symp.*, 1998, **127**, 161–163.
89 K. O'Driscoll and R. A. Sanayei, *Macromolecules*, 1991, **24**, 4479–4480.
90 J. Xu, V. Bellas, B. Jungnickel, B. Stühn and M. Rehahn, *Macromol. Chem. Phys.*, 2010, **211**, 1261–1271.
91 S. Barlow, A. L. Rohl, S. Shi, C. M. Freeman and D. O'Hare, *J. Am. Chem. Soc.*, 1996, **118**, 7578–7592.
92 K. H. Pannell, V. V. Dementiev, H. Li, F. Cervantes-Lee, M. T. Nguyen and A. F. Diaz, *Organometallics*, 1994, **13**, 3644–3650.
93 R. Rulkens, A. J. Lough, I. Manners, S. R. Lovelace, C. Grant and W. E. Geiger, *J. Am. Chem. Soc.*, 1996, **118**, 12683–12695.
94 V. S. Papkov, M. V. Gerasimov, I. I. Dubovik, S. Sharma, V. V. Dementiev and K. H. Pannell, *Macromolecules*, 2000, **33**, 7107–7115.
95 Z. Chen, M. D. Foster, W. Zhou, H. Fong, D. H. Reneker, R. Resendes and I. Manners, *Macromolecules*, 2001, **34**, 6156–6158.
96 J.-J. Wang, L.-X. Dai, Q. Gao, P.-F. Wu and X.-B. Wang, *Eur. Polym. J.*, 2008, **44**, 602–607.
97 K. Kulbaba, P. M. Macdonald and I. Manners, *Macromolecules*, 1999, **32**, 1321–1324.
98 W. D. Luke and A. Streitwieser, *J. Am. Chem. Soc.*, 1981, **103**, 3241–3243.
99 K. Kulbaba, I. Manners and P. M. Macdonald, *Macromolecules*, 2002, **35**, 10014–10025.
100 J. Rasburn, F. Seker, K. Kulbaba, P. G. Klein, I. Manners, G. J. Vancso and P. M. Macdonald, *Macromolecules*, 2001, **34**, 2884–2891.
101 H. Dislich, *Angew. Chem., Int. Ed.*, 1979, **18**, 49–59.
102 D. W. Mosley, K. Auld, D. Conner, J. Gregory, X.-Q. Liu, A. Pedicini, D. Thorsen, M. Wills, G. Khanarian and E. S. Simon, *Proc. SPIE*, 2008, **6910**, 691017–691018.
103 R. A. Gaudiana and R. A. Minns, *J. Macromol. Sci., Pure Appl. Chem.*, 1991, **28**, 831–842.
104 C.-J. Yang and S. A. Jenekhe, *Chem. Mater.*, 1995, **7**, 1276–1285.
105 C. Lu and B. Yang, *J. Mater. Chem.*, 2009, **19**, 2884–2901.
106 W. Caseri, *Macromol. Rapid Commun.*, 2000, **21**, 705–722.
107 S. D. Bhagat, J. Chatterjee, B. Chen and A. E. Stiegman, *Macromolecules*, 2012, **45**, 1174–1181.
108 J.-G. Liu and M. Ueda, *J. Mater. Chem.*, 2009, **19**, 8907–8919.
109 C. Paquet, P. W. Cyr, E. Kumacheva and I. Manners, *Chem. Commun.*, 2004, 234–235.
110 C. Paquet, P. W. Cyr, E. Kumacheva and I. Manners, *Chem. Mater.*, 2004, **16**, 5205–5211.

111 L. I. Espada, M. Shadaram, J. Robillard and K. H. Pannell, *J. Inorg. Organomet. Polym.*, 2000, **10**, 169–176.
112 D. A. Foucher, C. H. Honeyman, J. M. Nelson, B. Z. Tang and I. Manners, *Angew. Chem., Int. Ed.*, 1993, **32**, 1709–1711.
113 M. T. Nguyen, A. F. Diaz, V. V. Dement'ev and K. H. Pannell, *Chem. Mater.*, 1994, **6**, 952–954.
114 X. J. Wang, L. Wang and J. J. Wang, *J. Polym. Sci., Part B: Polym. Phys.*, 2004, **42**, 2245–2253.
115 F. Barrière, N. Camire, W. E. Geiger, U. T. Mueller-Westerhoff and R. Sanders, *J. Am. Chem. Soc.*, 2002, **124**, 7262–7263.
116 M. Péter, M. A. Hempenius, E. S. Kooij, T. A. Jenkins, S. J. Roser, W. Knoll and G. J. Vancso, *Langmuir*, 2004, **20**, 891–897.
117 W. Shi, S. Cui, C. Wang, L. Wang, X. Zhang, X. Wang and L. Wang, *Macromolecules*, 2004, **37**, 1839–1842.
118 S. Zou, I. Korczagin, M. A. Hempenius, H. Schönherr and G. J. Vancso, *Polymer*, 2006, **47**, 2483–2492.
119 W. Shi, M. I. Giannotti, X. Zhang, M. A. Hempenius, H. Schönherr and G. J. Vancso, *Angew. Chem., Int. Ed.*, 2007, **46**, 8400–8404.
120 H. J. Chung, J. Song and G. J. Vancso, *Appl. Surf. Sci.*, 2009, **255**, 6995–6998.
121 R. Rulkens, R. Resendes, A. Verma, I. Manners, K. Murti, E. Fossum, P. Miller and K. Matyjaszewski, *Macromolecules*, 1997, **30**, 8165–8171.
122 K. H. Pannell, V. I. Imshennik, Y. V. Maksimov, M. N. Il'ina, H. K. Sharma, V. S. Papkov and I. P. Suzdalev, *Chem. Mater.*, 2005, **17**, 1844–1850.
123 L. Bakueva, E. H. Sargent, R. Resendes, A. Bartole and I. Manners, *J. Mater. Sci.: Mater. Electron.*, 2001, **12**, 21–25.
124 L. Espada, K. H. Pannell, V. Papkov, L. Leites, S. Bukalov, I. Suzdalev, M. Tanaka and T. Hayashi, *Organometallics*, 2002, **21**, 3758–3761.
125 M. T. Nguyen, A. F. Diaz, V. V. Dement'ev and K. H. Pannell, *Chem. Mater.*, 1993, **5**, 1389–1394.
126 M. I. Giannotti, H. Lv, Y. Ma, M. P. Steenvoorden, A. R. Overweg, M. Roerdink, M. A. Hempenius and G. J. Vancso, *J. Inorg. Organomet. Polym.*, 2005, **15**, 527–540.
127 F. Ciminale, L. Lopez, G. M. Farinola and S. Sportelli, *Tetrahedron Lett.*, 2001, **42**, 5685–5687.
128 A. C. Arsenault, H. Míguez, V. Kitaev, G. A. Ozin and I. Manners, *Adv. Mater.*, 2003, **15**, 503–507.
129 P. W. Cyr, M. Tzolov, I. Manners and E. H. Sargent, *Macromol. Chem. Phys.*, 2003, **204**, 915–921.
130 P. W. Cyr, M. Tzolov, M. A. Hines, I. Manners, E. H. Sargent and G. D. Scholes, *J. Mater. Chem.*, 2003, **13**, 2213–2219.
131 R. Resendes, A. Berenbaum, G. Stojevic, F. Jäkle, A. Bartole, F. Zamanian, G. Dubois, C. Hersom, K. Balmain and I. Manners, *Adv. Mater.*, 2000, **12**, 327–330.
132 L. Thomi, P. Schaefer, K. Landfester and F. R. Wurm, *Macromolecules*, 2016, **49**, 105–109.
133 M. A. C. Stuart, W. T. S. Huck, J. Genzer, M. Müller, C. Ober, M. Stamm, G. B. Sukhorukov, I. Szleifer, V. V. Tsukruk, M. Urban, F. Winnik, S. Zauscher, I. Luzinov and S. Minko, *Nat. Mater.*, 2010, **9**, 101–113.
134 X. Sui, X. Feng, M. A. Hempenius and G. J. Vancso, *J. Mater. Chem. B*, 2013, **1**, 1658–1672.
135 M. J. MacLachlan, A. J. Lough and I. Manners, *Macromolecules*, 1996, **29**, 8562–8564.
136 J. J. McDowell, N. S. Zacharia, D. Puzzo, I. Manners and G. A. Ozin, *J. Am. Chem. Soc.*, 2010, **132**, 3236–3237.
137 D. P. Puzzo, A. C. Arsenault, I. Manners and G. A. Ozin, *Angew. Chem., Int. Ed.*, 2009, **121**, 961–965.
138 A. C. Arsenault, V. Kitaev, I. Manners, G. A. Ozin, A. Mihi and H. Miguez, *J. Mater. Chem.*, 2005, **15**, 133–138.
139 A. C. Arsenault, D. P. Puzzo, I. Manners and G. A. Ozin, *Nat. Photonics*, 2007, **1**, 468–472.
140 M. A. Hempenius, C. Cirmi, F. L. Savio, J. Song and G. J. Vancso, *Macromol. Rapid Commun.*, 2010, **31**, 772–783.
141 B. Zoetebier, M. A. Hempenius and G. J. Vancso, *Chem. Commun.*, 2015, **51**, 636–639.
142 M. A. Hempenius, C. Cirmi, J. Song and G. J. Vancso, *Macromolecules*, 2009, **42**, 2324–2326.
143 X. Sui, L. van Ingen, M. A. Hempenius and G. J. Vancso, *Macromol. Rapid Commun.*, 2010, **31**, 2059–2063.
144 X. Sui, X. Feng, A. Di Luca, C. A. van Blitterswijk, L. Moroni, M. A. Hempenius and G. J. Vancso, *Polym. Chem.*, 2013, **4**, 337–342.
145 E. Kutnyanszky, M. A. Hempenius and G. J. Vancso, *Polym. Chem.*, 2014, **5**, 771–783.
146 X. Sui, M. A. Hempenius and G. J. Vancso, *J. Am. Chem. Soc.*, 2012, **134**, 4023–4025.
147 K. Zhang, X. Feng, X. Sui, M. A. Hempenius and G. J. Vancso, *Angew. Chem., Int. Ed.*, 2014, **53**, 13789–13793.
148 D. Janczewski, J. Song, E. Csanyi, L. Kiss, P. Blazso, R. L. Katona, M. A. Deli, G. Gros, J. Xu and G. J. Vancso, *J. Mater. Chem.*, 2012, **22**, 6429–6435.
149 J. Bill and F. Aldinger, *Adv. Mater.*, 1995, **7**, 775–787.
150 P. Colombo, G. Mera, R. Riedel and G. D. Sorarù, *J. Am. Ceram. Soc.*, 2010, **93**, 1805–1837.
151 M. Ginzburg, M. J. MacLachlan, S. M. Yang, N. Coombs, T. W. Coyle, N. P. Raju, J. E. Greedan, R. H. Herber, G. A. Ozin and I. Manners, *J. Am. Chem. Soc.*, 2002, **124**, 2625–2639.
152 B.-Z. Tang, R. Petersen, D. A. Foucher, A. Lough, N. Coombs, R. Sodhi and I. Manners, *J. Chem. Soc., Chem. Commun.*, 1993, 523–525.
153 R. Petersen, D. A. Foucher, B.-Z. Tang, A. Lough, N. P. Raju, J. E. Greedan and I. Manners, *Chem. Mater.*, 1995, **7**, 2045–2053.
154 S. W. Hong, J. Xu, J. Xia, Z. Lin, F. Qiu and Y. Yang, *Chem. Mater.*, 2005, **17**, 6223–6226.
155 M. J. MacLachlan, M. Ginzburg, N. Coombs, T. W. Coyle, N. P. Raju, J. E. Greedan, G. A. Ozin and I. Manners, *Science*, 2000, **287**, 1460–1463.
156 Q. Sun, J. W. Y. Lam, K. Xu, H. Xu, J. A. K. Cha, P. C. L. Wong, G. Wen, X. Zhang, X. Jing, F. Wang and B. Z. Tang, *Chem. Mater.*, 2000, **12**, 2617–2624.
157 M. Häußler, Q. Sun, K. Xu, J. W. Y. Lam, H. Dong and B. Tang, *J. Inorg. Organomet. Polym. Mater.*, 2005, **15**, 67–81.
158 Q. Sun, K. Xu, H. Peng, R. Zheng, M. Häussler and B. Z. Tang, *Macromolecules*, 2003, **36**, 2309–2320.

159 Y. Gou, X. Tong, Q. Zhang, B. Wang, Q. Shi, H. Wang, Z. Xie and Y. Wang, *Ceram. Int.*, 2016, **42**, 681–689.
160 Y. Gou, X. Tong, Q. Zhang, H. Wang, B. Wang, S. Xie and Y. Wang, *J. Mater. Sci.*, 2015, **50**, 7975–7984.
161 A. Berenbaum, M. Ginzburg-Margau, N. Coombs, A. J. Lough, A. Safa-Sefat, J. E. Greedan, G. A. Ozin and I. Manners, *Adv. Mater.*, 2003, **15**, 51–55.
162 K. Liu, S. B. Clendenning, L. Friebe, W. Y. Chan, X. Zhu, M. R. Freeman, G. C. Yang, C. M. Yip, D. Grozea, Z.-H. Lu and I. Manners, *Chem. Mater.*, 2006, **18**, 2591–2601.
163 W. Y. Chan, A. Y. Cheng, S. B. Clendenning and I. Manners, *Macromol. Symp.*, 2004, **209**, 163–176.
164 (*a*) S. B. Clendenning, S. Han, N. Coombs, C. Paquet, M. S. Rayat, D. Grozea, P. M. Broderson, R. A. S. Sodhi, C. M. Yip, Z.-H. Lu and I. Manners, *Adv. Mater.*, 2004, **16**, 291–296; (*b*) K. R. Thomas, A. Ionescu, J. Gwyther, I. Manners, C. H. W. Barnes, U. Steiner and E. Sivaniah, *J. Appl. Phys.*, 2011, **109**, 073904.
165 M. J. MacLachlan, P. Aroca, N. Coombs, I. Manners and G. A. Ozin, *Adv. Mater.*, 1998, **10**, 144–149.
166 M. J. MacLachlan, M. Ginzburg, N. Coombs, N. P. Raju, J. E. Greedan, G. A. Ozin and I. Manners, *J. Am. Chem. Soc.*, 2000, **122**, 3878–3891.
167 R. Tong, Y. Zhao, L. Wang, H. Yu, F. Ren, M. Saleem and W. A. Amer, *J. Organomet. Chem.*, 2014, **755**, 16–32.
168 L. Wang, J. Huo, H. Yu, T. Chen and L. Deng, *J. Inorg. Organomet. Polym.*, 2007, **17**, 121–125.
169 K. Kulbaba, A. Cheng, A. Bartole, S. Greenberg, R. Resendes, N. Coombs, A. Safa-Sefat, J. E. Greedan, H. D. H. Stöver, G. A. Ozin and I. Manners, *J. Am. Chem. Soc.*, 2002, **124**, 12522–12534.
170 K. Kulbaba, R. Resendes, A. Cheng, A. Bartole, A. Safa-Sefat, N. Coombs, H. Stöver, J. Greedan, G. Ozin and I. Manners, *Adv. Mater.*, 2001, **13**, 732–736.
171 X. Sui, L. Shui, J. Cui, Y. Xie, J. Song, A. van den Berg, M. A. Hempenius and G. J. Vancso, *Chem. Commun.*, 2014, **50**, 3058–3060.
172 G. Decher and J. D. Hong, *Ber. Bunsen-Ges.*, 1991, **95**, 1430–1434.
173 G. Decher and J.-D. Hong, *Makromol. Chem., Macromol. Symp.*, 1991, **46**, 321–327.
174 M. Ginzburg, J. Galloro, F. Jäkle, K. N. Power-Billard, S. Yang, I. Sokolov, C. N. C. Lam, A. W. Neumann, I. Manners and G. A. Ozin, *Langmuir*, 2000, **16**, 9609–9614.
175 J. Halfyard, J. Galloro, M. Ginzburg, Z. Wang, N. Coombs, I. Manners and G. A. Ozin, *Chem. Commun.*, 2002, 1746–1747.
176 M. A. Hempenius and G. J. Vancso, *Macromolecules*, 2002, **35**, 2445–2447.
177 M. A. Hempenius, M. Péter, N. S. Robins, E. S. Kooij and G. J. Vancso, *Langmuir*, 2002, **18**, 7629–7634.
178 E. S. Kooij, Y. Ma, M. A. Hempenius, G. J. Vancso and B. Poelsema, *Langmuir*, 2010, **26**, 14177–14181.
179 Y. Ma, W.-F. Dong, E. S. Kooij, M. A. Hempenius, H. Möhwald and G. J. Vancso, *Soft Matter*, 2007, **3**, 889–895.
180 X. Feng, A. Cumurcu, X. Sui, J. Song, M. A. Hempenius and G. J. Vancso, *Langmuir*, 2013, **29**, 7257–7265.
181 A. Cumurcu, X. Feng, L. D. Ramos, M. A. Hempenius, P. Schön and G. J. Vancso, *Nanoscale*, 2014, **6**, 12089–12095.
182 Y. Ma, W.-F. Dong, M. A. Hempenius, H. Möhwald and G. J. Vancso, *Angew. Chem., Int. Ed.*, 2007, **46**, 1702–1705.
183 J. Song, D. Jańczewski, Y. Ma, M. Hempenius, J. Xu and G. J. Vancso, *J. Colloid Interface Sci.*, 2013, **405**, 256–261.
184 J. Song, D. Jańczewski, Y. Ma, M. Hempenius, J. Xu and G. J. Vancso, *J. Mater. Chem. B*, 2013, **1**, 828–834.
185 J. Song, D. Jańczewski, Y. Guo, J. Xu and G. J. Vancso, *Nanoscale*, 2013, **5**, 11692–11698.
186 S. Zou, Y. Ma, M. A. Hempenius, H. Schönherr and G. J. Vancso, *Langmuir*, 2004, **20**, 6278–6287.
187 M. Péter, R. G. H. Lammertink, M. A. Hempenius and G. J. Vancso, *Langmuir*, 2005, **21**, 5115–5123.
188 J. Song and G. J. Vancso, *Langmuir*, 2011, **27**, 6822–6829.
189 X. Feng, X. Sui, M. A. Hempenius and G. J. Vancso, *J. Am. Chem. Soc.*, 2014, **136**, 7865–7868.
190 X. Sui, X. Feng, J. Song, M. A. Hempenius and G. J. Vancso, *J. Mater. Chem.*, 2012, **22**, 11261–11267.
191 L. Dos Ramos, S. de Beer, M. A. Hempenius and G. J. Vancso, *Langmuir*, 2015, **31**, 6343–6350.
192 F. Fleischhaker, A. C. Arsenault, Z. Wang, V. Kitaev, F. C. Peiris, G. von Freymann, I. Manners, R. Zentel and G. A. Ozin, *Adv. Mater.*, 2005, **17**, 2455–2458.
193 Z. Wang, M. E. Calvo, G. Masson, A. C. Arsenault, F. Peiris, M. Mamak, H. Míguez, I. Manners and G. A. Ozin, *Adv. Mater. Interfaces*, 2014, **1**, 1300051.
194 Y. Ma, W.-F. Dong, M. A. Hempenius, H. Möhwald and G. Julius Vancso, *Nature Mater.*, 2006, **5**, 724–729.
195 C. Acikgoz, B. Vratzov, M. A. Hempenius, G. J. Vancso and J. Huskens, *ACS Appl. Mater. Interfaces*, 2009, **1**, 2645–2650.
196 C. Acikgoz, X. Y. Ling, I. Y. Phang, M. A. Hempenius, D. N. Reinhoudt, J. Huskens and G. J. Vancso, *Adv. Mater.*, 2009, **21**, 2064–2067.
197 X. Y. Ling, C. Acikgoz, I. Y. Phang, M. A. Hempenius, D. N. Reinhoudt, G. J. Vancso and J. Huskens, *Nanoscale*, 2010, **2**, 1455–1460.
198 R. G. H. Lammertink, M. A. Hempenius, V. Z. H. Chan, E. L. Thomas and G. J. Vancso, *Chem. Mater.*, 2001, **13**, 429–434.
199 K. Y. Suh, Y. S. Kim and H. H. Lee, *Adv. Mater.*, 2001, **13**, 1386–1389.
200 I. Korczagin, H. Xu, M. A. Hempenius and G. J. Vancso, *Eur. Polym. J.*, 2008, **44**, 2523–2528.
201 F. S. Bates and G. H. Fredrickson, *Phys. Today*, 1999, **52**, 32–38.
202 I. Manners, *J. Opt. A: Pure Appl. Opt.*, 2002, **4**, S221–S223.
203 A.-V. Ruzette and L. Leibler, *Nature Mater.*, 2005, **4**, 19–31.
204 R. A. Segalman, *Mater. Sci. Eng., R*, 2005, **48**, 191–226.
205 C. J. Hawker and K. L. Wooley, *Science*, 2005, **309**, 1200–1205.
206 I. Manners, *Angew. Chem., Int. Ed.*, 2007, **46**, 1565–1568.
207 T. Smart, H. Lomas, M. Massignani, M. V. Flores-Merino, L. R. Perez and G. Battaglia, *Nano Today*, 2008, **3**, 38–46.

208 Y. Mai and A. Eisenberg, *Chem. Soc. Rev.*, 2012, **41**, 5969–5985.
209 F. H. Schacher, P. A. Rupar and I. Manners, *Angew. Chem., Int. Ed.*, 2012, **51**, 7898–7921.
210 J. Zhou, G. R. Whittell and I. Manners, *Macromolecules*, 2014, **47**, 3529–3543.
211 Y. Ni, R. Rulkens, J. K. Pudelski and I. Manners, *Macromol. Rapid Commun.*, 1995, **16**, 637–641.
212 P. Gómez-Elipe, P. M. Macdonald and I. Manners, *Angew. Chem., Int. Ed.*, 1997, **36**, 762–764.
213 R. Resendes, J. A. Massey, H. Dorn, K. N. Power, M. A. Winnik and I. Manners, *Angew. Chem., Int. Ed.*, 1999, **38**, 2570–2573.
214 M. Szwarc, *Nature*, 1956, **178**, 1168–1169.
215 O. W. Webster, *Science*, 1991, **251**, 887–893.
216 M. Szwarc, *J. Polym. Sci., Part A: Polym. Chem.*, 1998, **36**, IX–XV.
217 T. Gädt, F. H. Schacher, N. McGrath, M. A. Winnik and I. Manners, *Macromolecules*, 2011, **44**, 3777–3786.
218 K. Temple, J. Massey, Z. Chen, N. Vaidya, A. Berenbaum, M. D. Foster and I. Manners, *J. Inorg. Organomet. Polym.*, 1999, **9**, 189–198.
219 J.-C. Eloi, D. A. Rider, J.-Y. Wang, T. P. Russell and I. Manners, *Macromolecules*, 2008, **41**, 9474–9479.
220 I. Manners, *J. Polym. Sci., Part A: Polym. Chem.*, 2002, **40**, 179–191.
221 L. Cao, I. Manners and M. A. Winnik, *Macromolecules*, 2002, **35**, 8258–8260.
222 X. S. Wang, M. A. Winnik and I. Manners, *Angew. Chem., Int. Ed.*, 2004, **43**, 3703–3707.
223 T. J. Peckham, J. A. Massey, C. H. Honeyman and I. Manners, *Macromolecules*, 1999, **32**, 2830–2837.
224 X. S. Wang, M. A. Winnik and I. Manners, *Macromolecules*, 2002, **35**, 9146–9150.
225 I. Korczagin, M. A. Hempenius and G. J. Vancso, *Macromolecules*, 2004, **37**, 1686–1690.
226 H. Wang, M. A. Winnik and I. Manners, *Macromolecules*, 2007, **40**, 3784–3789.
227 N. McGrath, F. H. Schacher, H. Qiu, S. Mann, M. A. Winnik and I. Manners, *Polym. Chem.*, 2014, **5**, 1923–1929.
228 A. Natalello, A. Alkan, A. Friedel, I. Lieberwirth, H. Frey and F. R. Wurm, *ACS Macro Lett.*, 2013, **2**, 313–316.
229 C. Kloninger and M. Rehahn, *Macromol. Chem. Phys.*, 2007, **208**, 833–840.
230 V. P. Chuang, C. A. Ross, J. Gwyther and I. Manners, *Adv. Mater.*, 2009, **21**, 3789–3793.
231 U. Datta and M. Rehahn, *Macromol. Rapid Commun.*, 2004, **25**, 1615–1622.
232 K. T. Kim, G. W. M. Vandermeulen, M. A. Winnik and I. Manners, *Macromolecules*, 2005, **38**, 4958–4961.
233 G. Molev, Y. Lu, K. S. Kim, I. C. Majdalani, G. Guerin, S. Petrov, G. Walker, I. Manners and M. A. Winnik, *Macromolecules*, 2014, **47**, 2604–2615.
234 Y. Wang, S. Zou, K. T. Kim, I. Manners and M. A. Winnik, *Chem. – Eur. J.*, 2008, **14**, 8624–8631.
235 G. W. M. Vandermeulen, K. T. Kim, Z. Wang and I. Manners, *Biomacromolecules*, 2006, **7**, 1005–1010.
236 S. Tangbunsuk, G. R. Whittell, M. G. Ryadnov, G. W. Vandermeulen, D. N. Woolfson and I. Manners, *Chem. – Eur. J.*, 2012, **18**, 2524–2535.
237 M. Roerdink, T. S. van Zanten, M. A. Hempenius, Z. Zhong, J. Feijen and G. J. Vancso, *Macromol. Rapid Commun.*, 2007, **28**, 2125–2130.
238 X. S. Wang, M. A. Winnik and I. Manners, *Macromol. Rapid Commun.*, 2003, **24**, 403–407.
239 T. Chen, L. Wang, G. Jiang, J. Wang, X. Wang, J. Zhou and W. Wang, *Eur. Polym. J.*, 2006, **42**, 687–693.
240 J.-H. Li, L. Wang, H.-J. Yu, Q.-H. Tan, L.-B. Deng and J. Huo, *Des. Monomers Polym.*, 2007, **10**, 193–205.
241 V. Bellas and M. Rehahn, *Macromol. Rapid Commun.*, 2007, **28**, 1415–1421.
242 A. P. Soto and I. Manners, *Macromolecules*, 2009, **42**, 40–42.
243 H. R. Allcock, J. M. Nelson, S. D. Reeves, C. H. Honeyman and I. Manners, *Macromolecules*, 1997, **30**, 50–56.
244 H. R. Allcock, S. D. Reeves, J. M. Nelson, C. A. Crane and I. Manners, *Macromolecules*, 1997, **30**, 2213–2215.
245 B. Wang, E. Rivard and I. Manners, *Inorg. Chem.*, 2002, **41**, 1690–1691.
246 R. K. Iha, K. L. Wooley, A. M. Nyström, D. J. Burke, M. J. Kade and C. J. Hawker, *Chem. Rev.*, 2009, **109**, 5620–5686.
247 A. Nunns, C. A. Ross and I. Manners, *Macromolecules*, 2013, **46**, 2628–2635.
248 M. Tanabe, G. W. M. Vandermeulen, W. Y. Chan, P. W. Cyr, L. Vanderark, D. A. Rider and I. Manners, *Nature Mater.*, 2006, **5**, 467–470.
249 D. E. Herbert, U. F. J. Mayer, J. B. Gilroy, M. J. López-Gómez, A. J. Lough, J. P. H. Charmant and I. Manners, *Chem. – Eur. J.*, 2009, **15**, 12234–12246.
250 S. K. Patra, G. R. Whittell, S. Nagiah, C.-L. Ho, W.-Y. Wong and I. Manners, *Chem. – Eur. J.*, 2010, **16**, 3240–3250.
251 R. Ahmed, S. K. Patra, I. W. Hamley, I. Manners and C. F. J. Faul, *J. Am. Chem. Soc.*, 2013, **135**, 2455–2458.
252 J. B. Gilroy, S. K. Patra, J. M. Mitchels, M. A. Winnik and I. Manners, *Angew. Chem., Int. Ed.*, 2011, **50**, 5851–5855.
253 L. Chabanne, I. Matas, S. K. Patra and I. Manners, *Polym. Chem.*, 2011, **2**, 2651–2660.
254 D. J. Lunn, C. E. Boott, K. E. Bass, T. A. Shuttleworth, N. G. McCreanor, S. Papadouli and I. Manners, *Macromol. Chem. Phys.*, 2013, **214**, 2813–2820.
255 F. Wurm, S. Hilf and H. Frey, *Chem. – Eur. J.*, 2009, **15**, 9068–9077.
256 J. A. Massey, K. N. Power, M. A. Winnik and I. Manners, *Adv. Mater.*, 1998, **10**, 1559–1562.
257 C. Kloninger and M. Rehahn, *Macromolecules*, 2004, **37**, 8319–8324.
258 R. G. H. Lammertink, M. A. Hempenius, J. E. van den Enk, V. Z. H. Chan, E. L. Thomas and G. J. Vancso, *Adv. Mater.*, 2000, **12**, 98–103.
259 R. G. H. Lammertink, M. A. Hempenius, E. L. Thomas and G. J. Vancso, *J. Polym. Sci., Part B: Polym. Phys.*, 1999, **37**, 1009–1021.
260 K. Temple, K. Kulbaba, K. N. Power-Billard, I. Manners, K. A. Leach, T. Xu, T. P. Russell and C. J. Hawker, *Adv. Mater.*, 2003, **15**, 297–300.

261 J. Gwyther, G. Lotze, I. Hamley and I. Manners, *Macromol. Chem. Phys.*, 2011, **212**, 198–201.
262 L. Leibler, *Macromolecules*, 1980, **13**, 1602–1617.
263 R. G. H. Lammertink, M. A. Hempenius and G. J. Vancso, *Langmuir*, 2000, **16**, 6245–6252.
264 J. Xu, V. Bellas, B. Jungnickel, B. Stühn and M. Rehahn, *Macromol. Chem. Phys.*, 2010, **211**, 2276–2285.
265 H. B. Eitouni and N. P. Balsara, *J. Am. Chem. Soc.*, 2004, **126**, 7446–7447.
266 H. B. Eitouni, N. P. Balsara, H. Hahn, J. A. Pople and M. A. Hempenius, *Macromolecules*, 2002, **35**, 7765–7772.
267 K. Aissou, H. K. Choi, A. Nunns, I. Manners and C. A. Ross, *Nano Lett.*, 2013, **13**, 835–839.
268 M. Ramanathan, E. Nettleton and S. B. Darling, *Thin Solid Films*, 2009, **517**, 4474–4478.
269 M. Ramanathan and S. B. Darling, *Soft Matter*, 2009, **5**, 4665–4671.
270 W. I. Park, Y. Kim, J. W. Jeong, K. Kim, J. K. Yoo, Y. H. Hur, J. M. Kim, E. L. Thomas, A. Alexander-Katz and Y. S. Jung, *Sci. Rep.*, 2013, **3**, 3190.
271 J. Y. Cheng, C. A. Ross, E. L. Thomas, H. I. Smith and G. J. Vancso, *Adv. Mater.*, 2003, **15**, 1599–1602.
272 J. Y. Cheng, A. M. Mayes and C. A. Ross, *Nature Mater.*, 2004, **3**, 823–828.
273 J. Y. Cheng, F. Zhang, H. I. Smith, G. J. Vancso and C. A. Ross, *Adv. Mater.*, 2006, **18**, 597–601.
274 J. Y. Cheng, F. Zhang, V. P. Chuang, A. M. Mayes and C. A. Ross, *Nano Lett.*, 2006, **6**, 2099–2103.
275 V. P. Chuang, J. Y. Cheng, T. A. Savas and C. A. Ross, *Nano Lett.*, 2006, **6**, 2332–2337.
276 M. Roerdink, M. A. Hempenius, U. Gunst, H. F. Arlinghaus and G. J. Vancso, *Small*, 2007, **3**, 1415–1423.
277 A. C. Arsenault, D. A. Rider, N. Tétreault, J.-I. L. Chen, N. Coombs, G. A. Ozin and I. Manners, *J. Am. Chem. Soc.*, 2005, **127**, 9954–9955.
278 D. A. Rider, J. I. L. Chen, J.-C. Eloi, A. C. Arsenault, T. P. Russell, G. A. Ozin and I. Manners, *Macromolecules*, 2008, **41**, 2250–2259.
279 W. Zheng and Z.-G. Wang, *Macromolecules*, 1995, **28**, 7215–7223.
280 Y. Bohbot-Raviv and Z.-G. Wang, *Phys. Rev. Lett.*, 2000, **85**, 3428–3431.
281 V. P. Chuang, J. Gwyther, R. A. Mickiewicz, I. Manners and C. A. Ross, *Nano Lett.*, 2009, **9**, 4364–4369.
282 J. G. Son, J. Gwyther, J.-B. Chang, K. K. Berggren, I. Manners and C. A. Ross, *Nano Lett.*, 2011, **11**, 2849–2855.
283 T. Gemma, A. Hatano and T. Dotera, *Macromolecules*, 2002, **35**, 3225–3237.
284 A. S. Abd-El-Aziz, *Macromol. Rapid Commun.*, 2002, **23**, 995–1031.
285 I. Manners, *Science*, 2001, **294**, 1664–1666.
286 U. S. Schubert and C. Eschbaumer, *Angew. Chem., Int. Ed.*, 2002, **41**, 2892–2926.
287 G. R. Whittell and I. Manners, *Adv. Mater.*, 2007, **19**, 3439–3468.
288 A. Nunns, J. Gwyther and I. Manners, *Polymer*, 2013, **54**, 1269–1284.
289 J. Zhang, K. Cao, X. S. Wang and B. Cui, *Chem. Commun.*, 2015, **51**, 17592–17595.
290 M. Ramanathan, Y.-C. Tseng, K. Ariga and S. B. Darling, *J. Mater. Chem. C*, 2013, **1**, 2080.
291 I. Korczagin, R. G. H. Lammertink, M. A. Hempenius, S. Golze and G. J. Vancso, *Adv. Polym. Sci.*, 2006, **200**, 91–117.
292 C. Hinderling, Y. Keles, T. Stöckli, H. F. Knapp, T. de los Arcos, P. Oelhafen, I. Korczagin, M. A. Hempenius, G. J. Vancso, R. Pugin and H. Heinzelmann, *Adv. Mater.*, 2004, **16**, 876–879.
293 S. Lastella, Y. J. Jung, H. Yang, R. Vajtai, P. M. Ajayan, C. Y. Ryu, D. A. Rider and I. Manners, *J. Mater. Chem.*, 2004, **14**, 1791.
294 J. Q. Lu, T. E. Kopley, N. Moll, D. Roitman, D. Chamberlin, Q. Fu, J. Liu, T. P. Russell, D. A. Rider and I. Manners, *Chem. Mater.*, 2005, **17**, 2227–2231.
295 J. Q. Lu, D. A. Rider, E. Onyegam, H. Wang, M. A. Winnik, I. Manners, Q. Cheng, Q. Fu and J. Liu, *Langmuir*, 2006, **22**, 5174–5179.
296 S. Lastella, H. Yang, D. Rider, I. Manners, P. M. Ajayan and C. Y. Ryu, *J. Polym. Sci., Part B: Polym. Phys.*, 2007, **45**, 758–765.
297 S. Lastella, G. Mallick, R. Woo, S. P. Karna, D. A. Rider, I. Manners, Y. J. Jung, C. Y. Ryu and P. M. Ajayan, *J. Appl. Phys.*, 2006, **99**, 024302.
298 J. Lu, T. Kopley, D. Dutton, J. Liu, C. Qian, H. Son, M. Dresselhaus and J. Kong, *J. Phys. Chem. B*, 2006, **110**, 10585–10589.
299 I. W. Hamley, *Nanotechnology*, 2003, **14**, R39.
300 C. J. Hawker and T. P. Russell, *MRS Bull.*, 2005, **30**, 952–966.
301 M. P. Stoykovich and P. F. Nealey, *Mater. Today*, 2006, **9**, 20–29.
302 J. Y. Cheng, C. A. Ross, H. I. Smith and E. L. Thomas, *Adv. Mater.*, 2006, **18**, 2505–2521.
303 J. Bang, U. Jeong, D. Y. Ryu, T. P. Russell and C. J. Hawker, *Adv. Mater.*, 2009, **21**, 4769–4792.
304 C. M. Bates, M. J. Maher, D. W. Janes, C. J. Ellison and C. G. Willson, *Macromolecules*, 2014, **47**, 2–12.
305 C. Cummins, T. Ghoshal, J. D. Holmes and M. A. Morris, *Adv. Mater.*, 2016, DOI: 10.1002/adma.201503432.
306 J. Y. Cheng, C. A. Ross, V. Z.-H. Chan, E. L. Thomas, R. G. H. Lammertink and G. J. Vancso, *Adv. Mater.*, 2001, **13**, 1174–1178.
307 S.-W. Chang, V. P. Chuang, S. T. Boles, C. A. Ross and C. V. Thompson, *Adv. Funct. Mater.*, 2009, **19**, 2495–2500.
308 J. Lu, D. Chamberlin, D. A. Rider, M. Liu, I. Manners and T. P. Russell, *Nanotechnology*, 2006, **17**, 5792–5797.
309 D. A. Rider, K. Liu, J.-C. Eloi, L. Vanderark, L. Yang, J.-Y. Wang, D. Grozea, Z.-H. Lu, T. P. Russell and I. Manners, *ACS Nano*, 2008, **2**, 263–270.
310 S. Y. Kim, J. Gwyther, I. Manners, P. M. Chaikin and R. A. Register, *Adv. Mater.*, 2014, **26**, 791–795.
311 S. Y. Kim, A. Nunns, J. Gwyther, R. L. Davis, I. Manners, P. M. Chaikin and R. A. Register, *Nano Lett.*, 2014, **14**, 5698–5705.
312 W. I. Park, J. M. Kim, J. W. Jeong, Y. H. Hur, Y. J. Choi, S.-H. Kwon, S. Hong, Y. Yin, Y. S. Jung and K. H. Kim, *Chem. Mater.*, 2015, **27**, 2673–2677.

313 H. K. Choi, J. Gwyther, I. Manners and C. A. Ross, *ACS Nano*, 2012, **6**, 8342–8348.
314 H. K. Choi, N. M. Aimon, D. H. Kim, X. Y. Sun, J. Gwyther, I. Manners and C. A. Ross, *ACS Nano*, 2014, **8**, 9248–9254.
315 K. Aissou, A. Nunns, I. Manners and C. A. Ross, *Small*, 2013, **9**, 4077–4084.
316 H. K. Choi, A. Nunns, X. Y. Sun, I. Manners and C. A. Ross, *Adv. Mater.*, 2014, **26**, 2474–2479.
317 R. Ahmed, A. Priimagi, C. F. J. Faul and I. Manners, *Adv. Mater.*, 2012, **24**, 926–931.
318 J.-C. Eloi, S. E. W. Jones, V. Poór, M. Okuda, J. Gwyther and W. Schwarzacher, *Adv. Funct. Mater.*, 2012, **22**, 3273–3278.
319 I. W. Hamley, *Block Copolymers in Solution: Fundamentals and Applications*, John Wiley & Sons, Ltd, Chichester, 2005.
320 J. Qian, M. Zhang, I. Manners and M. A. Winnik, *Trends Biotechnol.*, 2010, **28**, 84–92.
321 R. C. Hayward and D. J. Pochan, *Macromolecules*, 2010, **43**, 3577–3584.
322 J.-C. Eloi, D. A. Rider, G. Cambridge, G. R. Whittell, M. A. Winnik and I. Manners, *J. Am. Chem. Soc.*, 2011, **133**, 8903–8913.
323 K. N. Power-Billard, R. J. Spontak and I. Manners, *Angew. Chem., Int. Ed.*, 2004, **43**, 1260–1264.
324 X. Wang, G. Guerin, H. Wang, Y. Wang, I. Manners and M. A. Winnik, *Science*, 2007, **317**, 644–647.
325 J. B. Gilroy, T. Gädt, G. R. Whittell, L. Chabanne, J. M. Mitchels, R. M. Richardson, M. A. Winnik and I. Manners, *Nature Chem.*, 2010, **2**, 566–570.
326 J. Massey, K. N. Power, I. Manners and M. A. Winnik, *J. Am. Chem. Soc.*, 1998, **120**, 9533–9540.
327 J. Raez, I. Manners and M. A. Winnik, *J. Am. Chem. Soc.*, 2002, **124**, 10381–10395.
328 D. J. Frankowski, J. Raez, I. Manners, M. A. Winnik, S. A. Khan and R. J. Spontak, *Langmuir*, 2004, **20**, 9304–9314.
329 X. Wang, H. Wang, D. J. Frankowski, P. G. Lam, P. M. Welch, M. A. Winnik, J. Hartmann, I. Manners and R. J. Spontak, *Adv. Mater.*, 2007, **19**, 2279–2285.
330 J. Raez, I. Manners and M. A. Winnik, *Langmuir*, 2002, **18**, 7229–7239.
331 I. Korczagin, M. A. Hempenius, R. G. Fokkink, M. A. Cohen Stuart, M. Al-Hussein, P. H. H. Bomans, P. M. Frederik and G. J. Vancso, *Macromolecules*, 2006, **39**, 2306–2315.
332 J. B. Gilroy, P. A. Rupar, G. R. Whittell, L. Chabanne, N. J. Terrill, M. A. Winnik, I. Manners and R. M. Richardson, *J. Am. Chem. Soc.*, 2011, **133**, 17056–17062.
333 P. Cai, C. Wang, J. Ye, Z. Xie and C. Wu, *Macromolecules*, 2004, **37**, 3438–3443.
334 T. Chen, L. Wang, G. Jiang, J. Wang, J. Wang and J. Zhou, *Polymer*, 2005, **46**, 5773–5777.
335 D. A. Rider, M. A. Winnik and I. Manners, *Chem. Commun.*, 2007, 4483–4485.
336 L. Shen, H. Wang, G. Guerin, C. Wu, I. Manners and M. A. Winnik, *Macromolecules*, 2008, **41**, 4380–4389.
337 M.-S. Hsiao, S. F. M. Yusoff, M. A. Winnik and I. Manners, *Macromolecules*, 2014, **47**, 2361–2372.
338 B. V. K. J. Schmidt, J. Elbert, D. Scheid, C. J. Hawker, D. Klinger and M. Gallei, *ACS Macro Lett.*, 2015, **4**, 731–735.
339 J. F. Gohy, B. G. Lohmeijer, A. Alexeev, X. S. Wang, I. Manners, M. A. Winnik and U. S. Schubert, *Chem. – Eur. J.*, 2004, **10**, 4315–4323.
340 X. Wang, M. A. Winnik and I. Manners, *Macromolecules*, 2005, **38**, 1928–1935.
341 K. B. Thurmond, T. Kowalewski and K. L. Wooley, *J. Am. Chem. Soc.*, 1996, **118**, 7239–7240.
342 K. B. Thurmond, T. Kowalewski and K. L. Wooley, *J. Am. Chem. Soc.*, 1997, **119**, 6656–6665.
343 V. Bütün, A. B. Lowe, N. C. Billingham and S. P. Armes, *J. Am. Chem. Soc.*, 1999, **121**, 4288–4289.
344 X.-S. Wang, A. Arsenault, G. A. Ozin, M. A. Winnik and I. Manners, *J. Am. Chem. Soc.*, 2003, **125**, 12686–12687.
345 X.-S. Wang, H. Wang, N. Coombs, M. A. Winnik and I. Manners, *J. Am. Chem. Soc.*, 2005, **127**, 8924–8925.
346 X. Wang, K. Liu, A. C. Arsenault, D. A. Rider, G. A. Ozin, M. A. Winnik and I. Manners, *J. Am. Chem. Soc.*, 2007, **129**, 5630–5639.
347 H. Wang, X. Wang, M. A. Winnik and I. Manners, *J. Am. Chem. Soc.*, 2008, **130**, 12921–12930.
348 Z. M. Hudson, D. J. Lunn, M. A. Winnik and I. Manners, *Nat. Commun.*, 2014, **5**, 3372.
349 P. A. Rupar, G. Cambridge, M. A. Winnik and I. Manners, *J. Am. Chem. Soc.*, 2011, **133**, 16947–16957.
350 S. F. Mohd Yusoff, J. B. Gilroy, G. Cambridge, M. A. Winnik and I. Manners, *J. Am. Chem. Soc.*, 2011, **133**, 11220–11230.
351 J. Qian, G. Guerin, G. Cambridge, I. Manners and M. A. Winnik, *Macromol. Rapid Commun.*, 2010, **31**, 928–933.
352 J. Qian, G. Guerin, Y. Lu, G. Cambridge, I. Manners and M. A. Winnik, *Angew. Chem., Int. Ed.*, 2011, **50**, 1622–1625.
353 J. Qian, Y. Lu, G. Cambridge, G. Guerin, I. Manners and M. A. Winnik, *Macromolecules*, 2012, **45**, 8363–8372.
354 J. Qian, Y. Lu, A. Chia, M. Zhang, P. A. Rupar, N. Gunari, G. C. Walker, G. Cambridge, F. He, G. Guerin, I. Manners and M. A. Winnik, *ACS Nano*, 2013, **7**, 3754–3766.
355 H. Qiu, Y. Gao, V. A. Du, R. Harniman, M. A. Winnik and I. Manners, *J. Am. Chem. Soc.*, 2015, **137**, 2375–2385.
356 H. Wang, W. Lin, K. P. Fritz, G. D. Scholes, M. A. Winnik and I. Manners, *J. Am. Chem. Soc.*, 2007, **129**, 12924–12925.
357 T. Gädt, N. S. Ieong, G. Cambridge, M. A. Winnik and I. Manners, *Nature Mater.*, 2009, **8**, 144–150.
358 H. Qiu, G. Cambridge, M. A. Winnik and I. Manners, *J. Am. Chem. Soc.*, 2013, **135**, 12180–12183.
359 J. C. Wittmann and B. Lotz, *J. Polym. Sci., Polym. Phys. Ed.*, 1981, **19**, 1837–1851.
360 J. C. Wittmann, A. M. Hodge and B. Lotz, *J. Polym. Sci., Polym. Phys. Ed.*, 1983, **21**, 2495–2509.
361 T. J. Peckham, J. A. Massey, M. Edwards, I. Manners and D. A. Foucher, *Macromolecules*, 1996, **29**, 2396–2403.
362 F. He, T. Gädt, I. Manners and M. A. Winnik, *J. Am. Chem. Soc.*, 2011, **133**, 9095–9103.
363 H. Wang, A. J. Patil, K. Liu, S. Petrov, S. Mann, M. A. Winnik and I. Manners, *Adv. Mater.*, 2009, **21**, 1805–1808.

364 Y. Gao, H. Qiu, H. Zhou, X. Li, R. Harniman, M. A. Winnik and I. Manners, *J. Am. Chem. Soc.*, 2015, **137**, 2203–2206.
365 J. R. Finnegan, D. J. Lunn, O. E. C. Gould, Z. M. Hudson, G. R. Whittell, M. A. Winnik and I. Manners, *J. Am. Chem. Soc.*, 2014, **136**, 13835–13844.
366 Z. M. Hudson, J. Qian, C. E. Boott, M. A. Winnik and I. Manners, *ACS Macro Lett.*, 2015, **4**, 187–191.
367 H. Qiu, V. A. Du, M. A. Winnik and I. Manners, *J. Am. Chem. Soc.*, 2013, **135**, 17739–17742.
368 H. Zhou, Y. Lu, H. Qiu, G. Guerin, I. Manners and M. A. Winnik, *Macromolecules*, 2015, **48**, 2254–2262.
369 G. Cambridge, G. Guerin, I. Manners and M. A. Winnik, *Macromol. Rapid Commun.*, 2010, **31**, 934–938.
370 A. Nunns, G. R. Whittell, M. A. Winnik and I. Manners, *Macromolecules*, 2014, **47**, 8420–8428.
371 P. A. Rupar, L. Chabanne, M. A. Winnik and I. Manners, *Science*, 2012, **337**, 559–562.
372 Z. Nie, D. Fava, E. Kumacheva, S. Zou, G. C. Walker and M. Rubinstein, *Nature Mater.*, 2007, **6**, 609–614.
373 P. Y. Keng, B. Y. Kim, I.-B. Shim, R. Sahoo, P. E. Veneman, N. R. Armstrong, H. Yoo, J. E. Pemberton, M. M. Bull, J. J. Griebel, E. L. Ratcliff, K. G. Nebesny and J. Pyun, *ACS Nano*, 2009, **3**, 3143–3157.
374 Q. Chen, S. C. Bae and S. Granick, *Nature*, 2011, **469**, 381–384.
375 A. H. Gröschel, F. H. Schacher, H. Schmalz, O. V. Borisov, E. B. Zhulina, A. Walther and A. H. E. Müller, *Nat. Commun.*, 2012, **3**, 710.
376 Y. Wang, A. D. Hollingsworth, S. K. Yang, S. Patel, D. J. Pine and M. Weck, *J. Am. Chem. Soc.*, 2013, **135**, 14064–14067.
377 H. Cui, Z. Chen, S. Zhong, K. L. Wooley and D. J. Pochan, *Science*, 2007, **317**, 647–650.
378 H. Qiu, G. Russo, P. A. Rupar, L. Chabanne, M. A. Winnik and I. Manners, *Angew. Chem., Int. Ed.*, 2012, **51**, 11882–11885.
379 H. Qiu, Z. M. Hudson, M. A. Winnik and I. Manners, *Science*, 2015, **347**, 1329–1332.
380 O. E. C. Gould, H. Qiu, D. J. Lunn, J. Rowden, R. L. Harniman, Z. M. Hudson, M. A. Winnik, M. J. Miles and I. Manners, *Nat. Commun.*, 2015, **6**, 10009.
381 X. Li, Y. Gao, C. E. Boott, M. A. Winnik and I. Manners, *Nat. Commun.*, 2015, **6**, 8127.
382 S. F. Mohd Yusoff, M.-S. Hsiao, F. H. Schacher, M. A. Winnik and I. Manners, *Macromolecules*, 2012, **45**, 3883–3891.
383 A. P. Soto, J. B. Gilroy, M. A. Winnik and I. Manners, *Angew. Chem., Int. Ed.*, 2010, **49**, 8220–8223.
384 Z. M. Hudson, C. E. Boott, M. E. Robinson, P. A. Rupar, M. A. Winnik and I. Manners, *Nature Chem.*, 2014, **6**, 893–898.
385 G. Cambridge, M. J. Gonzalez-Alvarez, G. Guerin, I. Manners and M. A. Winnik, *Macromolecules*, 2015, **48**, 707–716.
386 H. Qiu, Y. Gao, C. E. Boott, O. E. C. Gould, R. L. Harniman, M. J. Miles, S. E. D. Webb, M. A. Winnik and I. Manners, *Science*, 2016, **352**, 697–701.
387 J. Ge, J. Lei and R. N. Zare, *Nature Nanotechnol.*, 2012, **7**, 428–432.
388 R. Shrestha, M. Elsabahy, H. Luehmann, S. Samarajeewa, S. Florez-Malaver, N. S. Lee, M. J. Welch, Y. Liu and K. L. Wooley, *J. Am. Chem. Soc.*, 2012, **134**, 17362–17365.
389 J. Zhu, S. Zhang, F. Zhang, K. L. Wooley and D. J. Pochan, *Adv. Funct. Mater.*, 2013, **23**, 1767–1773.
390 L. Jia, G. Zhao, W. Shi, N. Coombs, I. Gourevich, G. C. Walker, G. Guerin, I. Manners and M. A. Winnik, *Nat. Commun.*, 2014, **5**, 3882.
391 L. Jia, L. Tong, Y. Liang, A. Petretic, G. Guerin, I. Manners and M. A. Winnik, *J. Am. Chem. Soc.*, 2014, **136**, 16676–16682.
392 L. Jia, A. Petretic, G. Molev, G. Guerin, I. Manners and M. A. Winnik, *ACS Nano*, 2015, **9**, 10673–10685.
393 L. Cao, J. A. Massey, M. A. Winnik, I. Manners, S. Riethmüller, F. Banhart, J. P. Spatz and M. Möller, *Adv. Funct. Mater.*, 2003, **13**, 271–276.
394 K. T. Kim, C. Park, G. W. M. Vandermeulen, D. A. Rider, C. Kim, M. A. Winnik and I. Manners, *Angew. Chem., Int. Ed.*, 2005, **44**, 7964–7968.
395 J. Lee, H. Ahn, I. Choi, M. Boese and M. J. Park, *Macromolecules*, 2012, **45**, 3121–3128.
396 J. Schmelz, A. E. Schedl, C. Steinlein, I. Manners and H. Schmalz, *J. Am. Chem. Soc.*, 2012, **134**, 14217–14225.
397 J. Qian, X. Li, D. J. Lunn, J. Gwyther, Z. M. Hudson, E. Kynaston, P. A. Rupar, M. A. Winnik and I. Manners, *J. Am. Chem. Soc.*, 2014, **136**, 4121–4124.
398 L. Sun, A. Pitto-Barry, N. Kirby, T. L. Schiller, A. M. Sanchez, M. A. Dyson, J. Sloan, N. R. Wilson, R. K. O'Reilly and A. P. Dove, *Nat. Commun.*, 2014, **5**, 5746.
399 Y. Ni, I. Manners, J. B. Sheridan and R. T. Oakley, *J. Chem. Educ.*, 1998, **75**, 766.
400 C. H. Honeyman, D. A. Foucher, F. Y. Dahmen, R. Rulkens, A. J. Lough and I. Manners, *Organometallics*, 1995, **14**, 5503–5512.
401 M. Tamm, A. Kunst, T. Bannenberg, E. Herdtweck, P. Sirsch, C. J. Elsevier and J. M. Ernsting, *Angew. Chem., Int. Ed.*, 2004, **43**, 5530–5534.
402 U. F. J. Mayer, J. B. Gilroy, D. O'Hare and I. Manners, *J. Am. Chem. Soc.*, 2009, **131**, 10382–10383.
403 H. Braunschweig and T. Kupfer, *Acc. Chem. Res.*, 2010, **43**, 455–465.
404 S. Baljak, A. D. Russell, S. C. Binding, M. F. Haddow, D. O'Hare and I. Manners, *J. Am. Chem. Soc.*, 2014, **136**, 5864–5867.
405 H. Bhattacharjee and J. Müller, *Coord. Chem. Rev.*, 2016, **314**, 114–133.
406 D. E. Herbert, U. F. J. Mayer and I. Manners, *Angew. Chem., Int. Ed.*, 2007, **46**, 5060–5081.
407 M. Gallei, *Macromol. Chem. Phys.*, 2014, **215**, 699–704.
408 A. Alkan, L. Thomi, T. Gleede and F. R. Wurm, *Polym. Chem.*, 2015, **6**, 3617–3624.
409 Y. Yan, P. Pageni, M. P. Kabir and C. Tang, *Synlett*, 2016, 984–1005.